Spring 7-23-2015

Techniques for Capturing Force Interactions in Reinforced Concrete Wall-Frame Systems Under Seismic Excitation

Travis A. Marcilla
University of Colorado at Boulder, travis.marcilla@gmail.com

Techniques for Capturing Force Interactions in Reinforced Concrete Wall-Frame Systems under Seismic Excitation

by

Travis A. Marcilla

University of Colorado, 2015

A thesis submitted to the

Faculty of the Graduate School of the

University of Colorado in fulfillment

of the requirement for the degree of

Master of Science

Department of Civil, Environmental, and Architectural Engineering

2015

This thesis entitled:

Techniques for Capturing Force Interactions in Reinforced Concrete Wall-Frame Systems under Seismic Excitation

written by Travis A. Marcilla

has been approved for the Department of Civil, Environmental, and Architectural Engineering

_____

Abbie Liel

_____

Petros Sideris

*Date*_____

The final copy of this thesis has been examined by the signatories, and we find that both the content and the form meet acceptable presentation standards of scholarly work in the above mentioned discipline.

Travis A. Marcilla (B.S/M.S., Architectural and Civil Engineering)

Techniques for Capturing Force Interactions in Reinforced Concrete Wall-Frame Systems under Seismic Excitation

Thesis directed by Associate Professor Abbie Liel

Abstract

Estimating the lateral yielding strength of a multi-story RC wall coupled with a moment resisting RC frame is complex due to the interaction forces that occur between the two systems. The interaction force is perpetually changing corresponding with a time varying load, such as seismic excitation, and depending on nonlinearities, such as concrete cracking and rebar yielding, occurring throughout the structure. In addition, yielding drift varies among different structures and is dependent on the composition of the wall, the size of the foundation and the soil interaction.

This thesis is motivated by the ATC 78 (ATC 78, 2014) project, in which the team members are designing a method that requires quick and accurate analysis of yielding strength and drift for RC wall-frame systems. By identifying the correct yield strength and drift, then the effective period of the structure can be determined. Effective period is a variable that is necessary to determine the seismic demand on the structure using the ATC 78 (2014) method. The overall goal of the ATC 78 project is to develop simplified hand calculations, which consider nonlinearities and use probabilistic approaches, as a way to effectively and efficiently "rate" the seismic performance of reinforced concrete buildings on a unified rating system. In doing so, the new methodology will be able locate "killer buildings", which were built before

modern seismic building codes and may be particularly dangerous for building occupants and the public.

Results show a linear relation between total strength of a wall-frame system from pushover analysis and the summation of simplified hand calculations for flexural strength of a RC wall and the existing ATC 78 methodology for calculating flexural strength of RC frames. This linear relation is used to develop a new engineering parameter β that can be used to relate simplified hand calculations to the actual strength of a wall-frame system. Proposals are made to describe how this engineering parameter β can be used to develop the new procedure that incorporates RC walls into the existing frame methodology. In addition, future studies that need to be conducted in order to complete the framework are identified.

Dedication

I dedicate this thesis work to my loving and supportive mother Holly, her incredible boyfriend Bruce, to my badass sister Tara, and to my dearly departed father Arthur; you went too early man and you are missing all the good stuff. Also, dedication and special thanks to the best structural engineering research professor in the entire country and possibly the world, Abbie; the research work and team you have allowed me to be part of and the fortuity of higher education you have made available, are by far the best opportunities I have ever had in this life and I am eternally grateful. Finally, to the best darn research group there ever was. Sarah, Cody, Rob, Juan, Derya, and Orlando, you guys are the best and I look forward to more wonderful years of saving lives through earthquake engineering research!

Table of Contents

List of Tables

List of Figures

List of Equations

1. Introduction

The objective of this work is to develop a new hand analysis method which considers RC wall-frame structures and accurately calculates their lateral yielding strength and drift as well as their effective period. These parameters are necessary in order to determine the seismic demand of RC wall-frame structures through the methods developed by ATC 78 project. The ATC 78 project uses a probabilistic approach to determine the collapse risk of RC structures located in highly seismic regions. The information presented in this thesis discusses the non-linear modeling approach that has been selected for analysis, some of the investigations that have helped to develop the new proposed method, and a detailed outline of the newly proposed hand calculation method, along with a description of the future works that well be needed in order for the procedure to include all RC structures.

1.1. Scope of Study

This study analyzes the interaction forces between reinforced concrete buildings that have both walls and frames in the lateral force resisting system. Buildings of 3, 6 and 9 stories, and varying in terms of the relative strength of the wall and the frame are considered.
The bulk of the analyses in this thesis are conducted considering only capacity and failure mechanisms in a wall and frame resulting from flexure. The systems are analyzed using finite element, fiber-based models and hand calculations. The most interesting parameter is the strength change in the wall as the wall-to-frame strength index ratio changes, due to wall-frame interaction.

1.2. Arrangement of the Thesis

Chapter 2: Literature Review. A literature review is conducted to best understand how other researchers and structural engineers are modeling RC walls. Four different modeling approaches are researched and discussed. Based on the modeling needs of the wall-frame interaction studies contained in this thesis, and based on the findings of the literature review, two models are selected for a comparison study.

Chapter 3: Model Comparison. A RC wall modeling comparison study is conducted between a Layered Shell Section model, a finite element modeling approach, and a Fiber Beam-Column element model, a fiber-based modeling approach. Based on the findings of the comparison study, the author determined that the Fiber Beam-Column element model is best suited for the rest of the research presented in this thesis.

Chapter 4: Lateral Strength of Wall-Frame Systems. Nine different wall-frame structures are modeled in *OpenSees* and analyzed using pushover analysis to determine their system strengths and their individual component strengths when disaggregated from the system. Then, walls and frames of identical composition are analyzed separately as both a pure wall and a pure frame. These pure wall and pure frame analyses simulate simplified hand calculations that will be used in the ATC 78 procedure. Using these parameters, a detailed investigation is conducted which considers various approaches for approximating wall strength when coupled with a frame system. A series of simplified approaches are presented, but found to be unsuitable for calculating strength, despite the desire for the simple method. In addition, a method developed by MacLeod (1972) is closely analyzed and is shown to have potential.

Unfortunately, the MacLeod (1972) method is much more complicated than the procedure desired by the ATC 78 committee.

Chapter 5: Effective Period of Wall-Frame Systems. The pushover results from the study in Chapter 3 are analyzed using bilinear approximation according to a procedure outlined in FEMA 356 (2000). The bilinear approximation is used to determine the secant stiffness of the structure. Secant stiffness provides an estimate of effective period that can be compared to the estimates from the ATC 78 methodology. Analytical equations for period are compared from various documents (FEMA 356, ASCE 41, ASCE 7-10, and ATC 78) and also to measured periods from instrumented buildings (Chopra, 1998).

Chapter 6: Hand-Calculations for Building Strength. The first part of this chapter contains a detailed description for a new β parameter, which will ultimately be used to develop a simplified relationship to characterize building strength. This analysis is based on the original nine structures described in Chapter 4. The rest of the chapter fully develops β values for the 3, 6, and 9 story structures. Thirty-seven wall-frame structures are analyzed for strength using pushover analysis in *OpenSees*. Wall and frame strengths and drifts are disaggregated from the system and compared to pure wall and pure frame strengths analyzed independently. Next, β is used for T_e calculations and comparisons are presented.

Chapter 7: Conclusions, Limitations and Future Work. A new procedure for adding RC walls to the existing ATC 78 methodology, and further studies needed to complete the framework are outlined.

2. Literature Review

Non-linear computer modeling allows the modern engineer to move past the rigors of repetition and detail of hand calculations and study a greater range of global behaviors that take more finite local details into account. However, different types of non-linear models are based on different assumptions and, as such, may lead to different results, and it is up to the engineer to determine the required level of accuracy acceptable for the project at hand and show that the assumptions used and values obtained are reasonable.

Sources of nonlinearities in buildings are either material or geometric (Saouma, 2014). Geometric nonlinearities arise in the analysis of skeletal structures in the form of instability or buckling, P-Δ effects, or P-δ effects (Saouma, 2014) and represent the impacts of changing geometry (or large deformations) on the analysis. Buckling calculations in concrete members can vary greatly because of imperfections in the material. This becomes a concern when attempting to model slender and lightly reinforced concrete walls, which are susceptible to spalling and rebar buckling (Royal Commission, 2012). Older buildings are especially prone to concrete imperfections such as the presence of other than specified concrete strengths, non-homogeneity, honeycombing, and more. Buckling strength can also change due to nonlinearities in the reinforcing bars, such as corrosion or de-bonding. The P-Δ effect is a global structural effect that accounts for the effect of axial load on equilibrium, which can influence the internal forces of a member and nodal displacements. This is accounted for in modeling by including the geometric stiffness matrix in analysis (Saouma, 2014).

Each nonlinearity considered in a structural analysis of a single member is defined by using a separate term or by adding complexity to an existing term contained within a single

differential equation. The geometric stiffness matrix would be an example of a separate term within the construct of the differential equation used to describe a member. Structural analysis of the building as a whole aims to incrementally solve the accumulation of all the differential equations (members) in the entire structure. To incrementally solve a differential equation is either to consider a step displacement that yields a force, or to consider step force that yields a displacement. Each additional nonlinearity that is considered and the step size used, adds to the computational expense of each differential equation and to the model as a whole. Thus, convergence becomes increasingly timely and difficult to achieve.

Reaching convergence for models is a matter of approximating the solutions to the differential equations using explicit, implicit, or both explicit and implicit solutions. An explicit solution is an exact solution to the differential equation. This does not mean that there is no error in the structural analysis because there is error in the terms used to describe the member behavior. It just means that there is no error in the approximation of the solution to the differential equation. It is rarely possible to be able to use only explicit solutions for complex systems since, by definition, an explicit solution with respect to the dependent variable is an exact solution which is solved solely in terms of the independent variable (Hafiz, 2011). Complex systems may have multiple dependent and/or independent variables, and therefore, implicit approaches must be used to approximate the answer. These implicit approximation methods/algorithms introduce error to the solution of the differential equation and increase the overall error to the analysis of the structure. The quantity of error in analysis will depend heavily on the algorithm used to achieve convergence and the loading or displacement step size.

Some of the common solution algorithms in *OpenSees* are the Linear, Newton, Modified Newton, and the Krylov-Newton methods. Building an analysis modeling tool from scratch and

then comparing, proving, validating and justifying its performance is difficult and time intensive, and as such, relying on a modeling tools built by previous researchers, such as *OpenSees* software, becomes extremely important.

This literature review investigates various *OpenSees* tools available for modeling walls in an effort to determine the optimal option for the studies in this thesis based on runtime, accuracy, ease of programming, and the ability to reproduce similar results using simplified hand calculations. The *OpenSees* software is used here because it is an open source platform with advanced wall models available for investigating nonlinear seismic performance.

When using *OpenSees* software, there are four techniques commonly used to model concrete walls: Lumped Plasticity, Fiber Beam-Column elements, MVLEM (Multiple Vertical Line Element Model), and a Layered Shell Fiber model. The lumped plasticity and MVLEM models are spring type models that aggregate nonlinear behavior in springs. For all of the springs used in this thesis it is the concrete material property definition that produces nonlinear behavior in compression, and the reinforcement quantity, layout and strength definition that produces the nonlinear behavior in tension (Yassin, 1994). The Fiber Nonlinear Beam-Column element model is one of a class of fiber models where nonlinearities are captured through finite element analysis across the quantity of fibers specified in the model (Taucer, Spacone, & Filippou, 1991). The Layered Shell Fiber Model is the most modern tool available for *OpenSees* and is a highbred version of a Layered Fiber Model combined with a Shell model (Lu, 2015).

2.1. Lumped Plasticity Spring Model

The most basic modeling approach that can be used in *OpenSees* for simulating wall behavior is built using Lumped Plasticity (springs) and Elastic Beam-Column elements. This

modeling technique is comprised of Elastic Beam-Column elements at the wall's centroidal axis, axial springs at the top of each story, and rotational springs at each level. In this approach, all of the nonlinear behavior is concentrated in the response of the springs. This is a common modeling approach used to model concrete walls (Orakcal & Wallace, 2004). An illustration of the modeling geometry is presented in Figure 1.

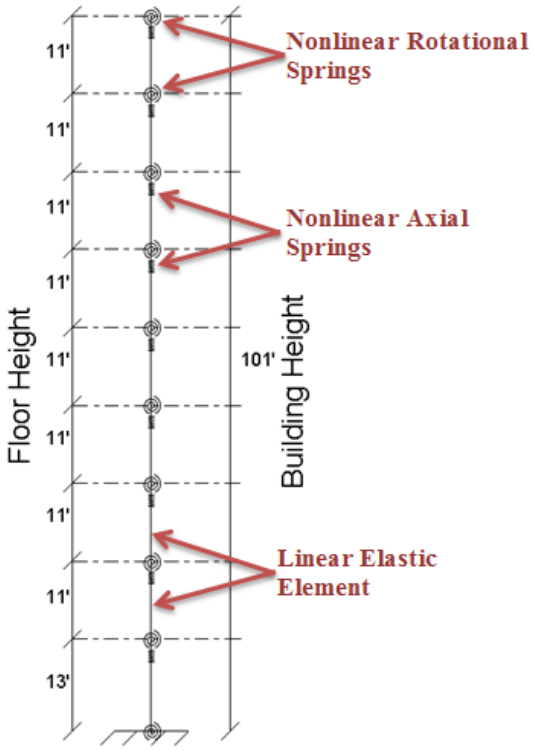

Figure 1: Example of Lumped Plasticity Spring Model

The advantage to using lumped plasticity springs is that the models run very quickly since all of the nonlinear behavior is defined in the springs. The difficulty is in the definition of the spring model response and parameters, and then redefining these parameters for any changes to the wall dimensions and/or reinforcement layout that may be desired for different analyses. The backbone of the spring depends on the concrete and reinforcement property definitions of the RC concrete member, which is based on experimental results (Orakcal & Wallace, 2004), but

ultimately this method of calibration leaves substantial room for error and differences due to judgment and simplifications.

In addition to these complications, a major limitation to using springs is the assumption that rotations occur about the centroidal axis of the wall (Orakcal & Wallace, 2004). In reality this does not happen because the compression strength is different than the tensile strength of the wall, and cracking will cause the rocking point to move horizontally along the bottom of the wall. Another aspect of the model which decreases the accuracy of the results is that lumped plasticity spring models are unable to account for the changing location of the inflection point over the height of the wall. The inflection point is constantly changing in the vertical direction during each iterative step of a pushover analysis (Arteta, Parra, & Moehle, 2015). In a multi-story building, it will be unknown where the inelastic action will occur which is important for estimating the non-linear behavior (Lowes, Lehman, & Pugh, 1996).

Beyond that, another disadvantage is that lumped plasticity springs are not able to capture some of the other important behaviors that more complex models are able to capture. Basically, all of the behavior is represented phenomenology by one spring which does not account for toe crushing at one end of the wall and rebar yielding at the other end of the wall. These nonlinearities can be calibrated into some additional complicated flexural springs or into additional springs that would need to be added to the model to work with the flexural springs. Each of these options adds to the difficulty in calibrating and recalibrating the springs for each different wall analyzed.

Figure 2 shows an example of a layout that would be difficult to model with lumped plasticity springs because they do not account for real space and only represent a wall's centroidal axis. Notice that the entire length of the RC walls must be replaced with a point in the

center, and rigid links are employed to transfer force and displacement information to the location that beams would be connected in a real building. The problem that arises from this issue is that the force transfer mechanisms between the wall and the other elements are hard to represent realistically. For the many limitations, difficulties in calibration, and crudeness of the spring shear-wall model it is not used for any of the modeling in this thesis.

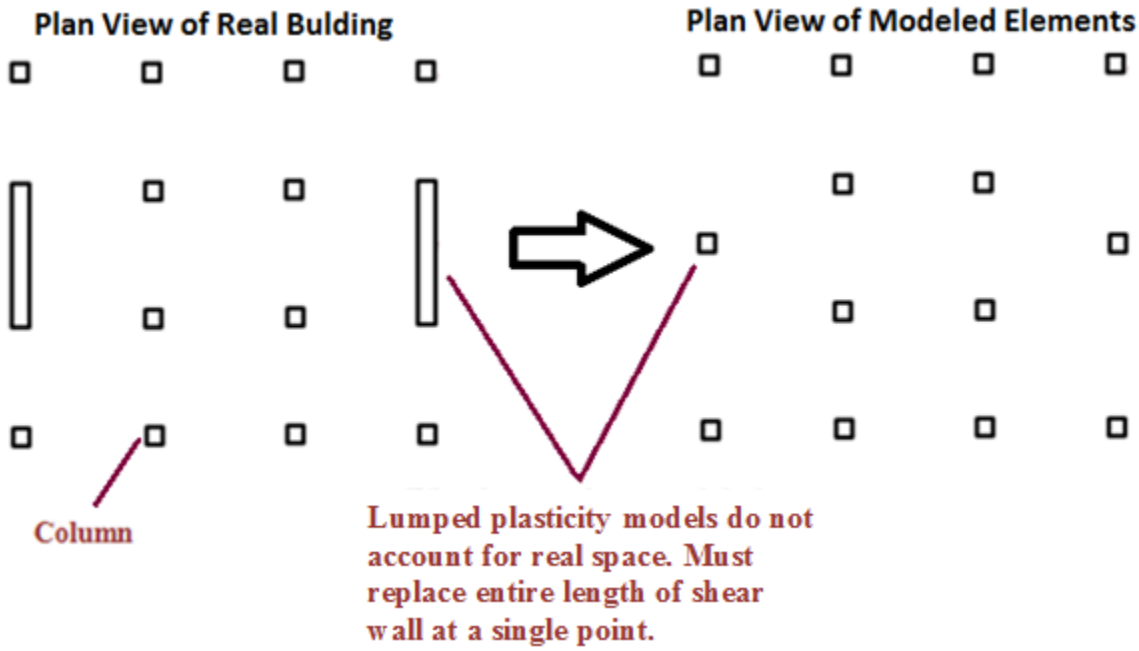

Figure 2: Example of Building Layout that is Difficult to Model Using Lumped Plasticity

2.2. Fiber Beam-Column Model

The fiber model is potentially the easiest RC wall model to build and change in *OpenSees* in the fact that "they do not require definitions of member stiffness, strength, or deformation capacity, as these effects are inherently captured in the model through the material properties" (Moehle, Mahin, & Yousef, 2010). Fiber models were first developed by Fabio Taucer, Enrico Spacone and Filip Filippou. They use a relation of force-deformation, which is derived by integration of the stress-strain relation theory between each of the fibers. The key advantages are

that they capture axial-flexure interaction in column sections and complex hysteretic behavior while remaining computationally stable and robust (Taucer, Spacone, & Filippou, 1991). The key aspects of the model to be defined are the member composition, which is defined in the fiber section, and the building geometry, which is defined by using a finite length of the fiber section integrated at a specified number of points along the height of the member.

An illustration of how we built this model is presented in Figure 3. Working from top to bottom, the 1st section is an example of what the actual wall section would look like. The green is the concrete and the red is the reinforcing bars that run vertically in the wall. The 2nd section is a simplification of the reinforcement. The reinforcement is treated like a single plate that has equivalent area of steel as the 1st section. The 3rd section is an example of how the section is dissected in to individual fibers. The image to the right shows how the Fiber Beam-Column elements, which are comprised of the sections, are built into the model.

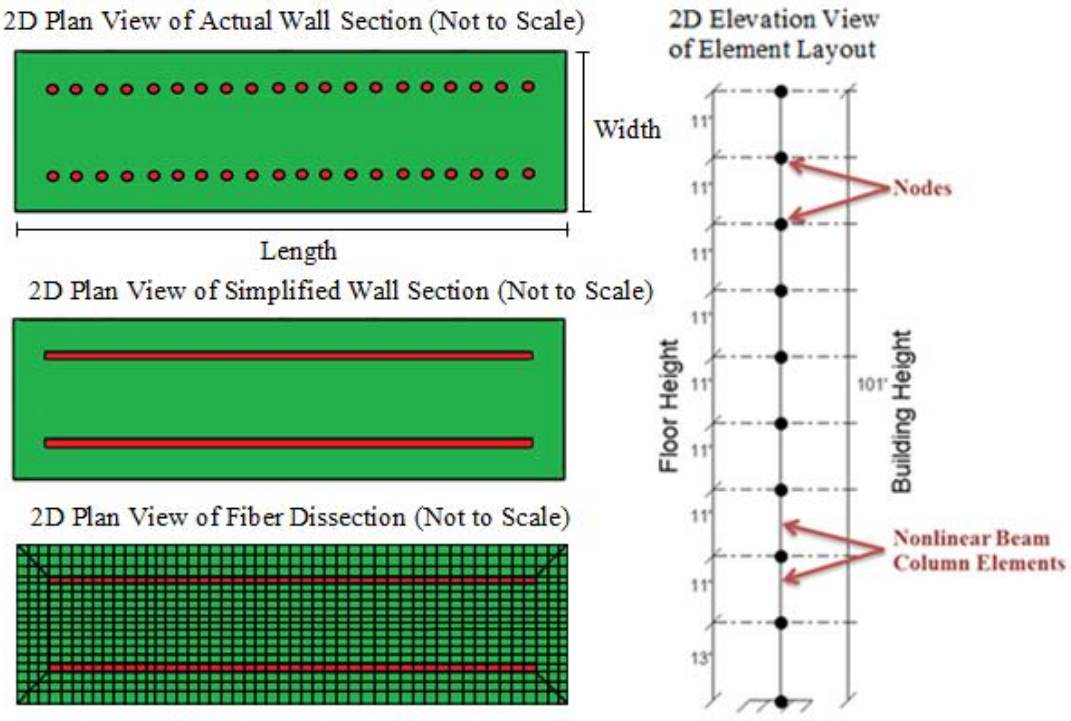

Figure 3: Example of Nonlinear Fiber Beam-Column Element Model

The benefits of using Fiber Beam-Column elements in *OpenSees* are that they are easy to build, which reduces the human error aspect, and they are computationally efficient (Taucer, Spacone, & Filippou, 1991). Additionally, the results can be readily post-processed and interpreted (Martinelli & Filippou, 2009). "Since the nonlinear behavior of most well-designed and detailed RC walls with an aspect ratio greater than 3 are dominated by flexure, it is expected that the simplicity of the element does not sacrifice accuracy" (Martinelli & Filippou, 2009). The modeling approach also enables accurate simulation of vertical strain distribution along the height of the member (Lowes, Lehman, & Pugh, 1996).

The construction of the sections allows concrete crushing and rebar yielding to be captured, unlike the lumped plasticity spring model. Using a Fiber Beam-Column element is ideal to meet a short time frame available for analysis, because after a typical section is built then the element aspect has the ability to model response with a single element definition (Martinelli & Filippou, 2009). This saves construct and computational time and makes Fiber Nonlinear Beam-Columns a desirable model to use considering the abundance of simulations that will need to be run in the later studies.

A disadvantage of this model is that it is designed to analyze columns, and flexure-dominated section, and the extension to long walls is not straightforward. This is a problem because the underlying assumptions that were used to build the model are that deformations are small and that plane sections remain plane during the loading history (Taucer, Spacone, & Filippou, 1991). These assumptions are acceptable for smaller members such as columns, but when using the model to simulate a long wall these assumptions lead to greater error in the results (Lowes, Lehman, & Pugh, 1996). Similar to the lumped plasticity spring models, the Fiber Beam-Column elements are not able to account for real space in a model despite the fact

that they account for the true geometry within the sections that the elements are comprised of. For most global building performance investigations, this is a suitable approach to modeling shear wall and frame interaction, however, Lu, the developer of the layered shell model, suggests that the "fiber model is incapable of simulating complex mechanical behaviors of various types of shear walls" (Lu, 2015).

2.3. MVLEM model

The MVLEM (Multiple Vertical Line Element Model) consists of a series of many springs strategically placed along the length of the bottom of the wall in order to capture the different behaviors that are happening within the wall at different locations. Essentially, this model uses multiple lumped plasticity springs centered between rigid elements which are arranged in a vertical direction to simulate the behavior of a wall in the axial, flexure and shear responses.

An illustration of a typical MVLEM model built by Haselton & Wallace (2009) is demonstrated in Figure 4. The vertical springs capture flexural response and the horizontal spring captures shear response. The material definition of the flexural springs are able to capture concrete compressive strength, tensile strength, and tension softening as described in detail in later in Section 3.2. The backbone to the shear spring uses a pinching limit state material definition which fails abruptly when critical shear stress is reached (Kakavand, 2007). The benefit of this model over the Fiber Beam-Column element model is that it is able to couple the shear and flexural response components (Orakcal, Massone, & Wallace, 2007). If desired it is possible to use multiple integration points over the height of each story (Haselton & Wallace, 2009). This is done by recording the moment force along the rigid member and allows the

changing inflection point of the moment force to be determined at each step, which can then updated for the next iteration. Generally, more iteration points will improve the accuracy of the results, but the computational time will be increased. A balance between time and accuracy must be compromised.

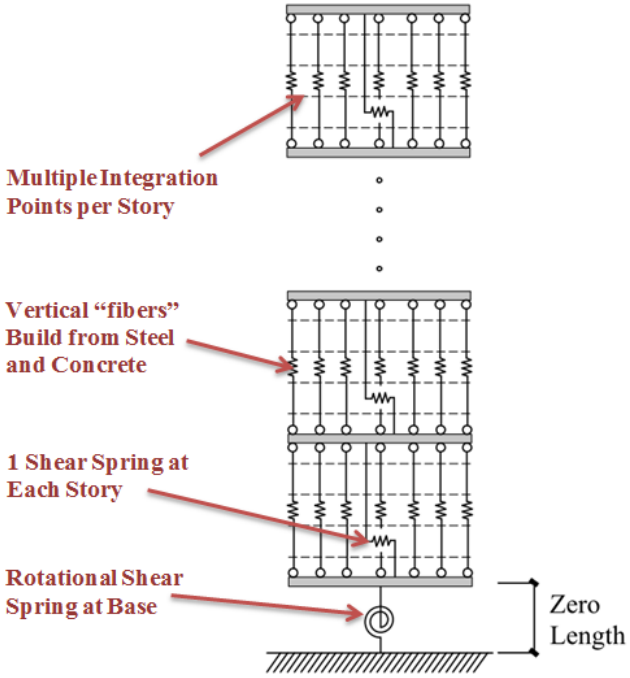

Figure 4: Example of MLVEM Model Designed by (Haselton & Wallace, 2009)

The benefits are that the MVLEM model does occupy real space and model parameters can be calibrated to capture specific behaviors of either real building failure data or shake table results with acute accuracy. To calibrate the model, the analyst needs to adjust the local behaviors of each individual vertical spring to mimic the desired global behavior of the entire wall. For example, if the damage that a real structure experienced during an earthquake is trying to be modeled, and destructive testing showed that concrete strength was not uniform along the length of the wall, then each spring can be calibrated to reproduce the exact strength from the destructive testing.

Haselton & Wallace (2009) used the MVLEM model to simulate collapse of a 12-Story reinforced concrete core building, identifying a number of the capabilities and limitations. In particular, this model is more difficult to build than the fiber model and takes longer to run. In addition, one of the more difficult challenges to using MVLEM models is accurately calibrating the properties of all the springs without experimental data to calibrate. This difficulty increases when multiple iterations of a wall design are desired for analysis. The characteristics of the multiple springs makes this model better suited to reproduce experimental data, but not as well suited for theoretical wall-frame simulations, as is the basis for the studies used in this thesis. The Fiber Beam-Column and MVLEM models are able to produce the similar results (Arteta, Parra, & Moehle, 2015). Ongoing comparison research by Arteta et al. (2015) shows that there is little if no advantage to building the MVLEM model over the Fiber model for the global analyses that will be conducted in this research.

2.4. Layered Shell Fiber Model

The most recent shear wall model that is available to use in *OpenSees* is the Layered Shell Fiber model, which is a finite element type model that has been developed by Lu (2015). Figure 5 illustrates the basic geometry of the Layered Shell Fiber model.

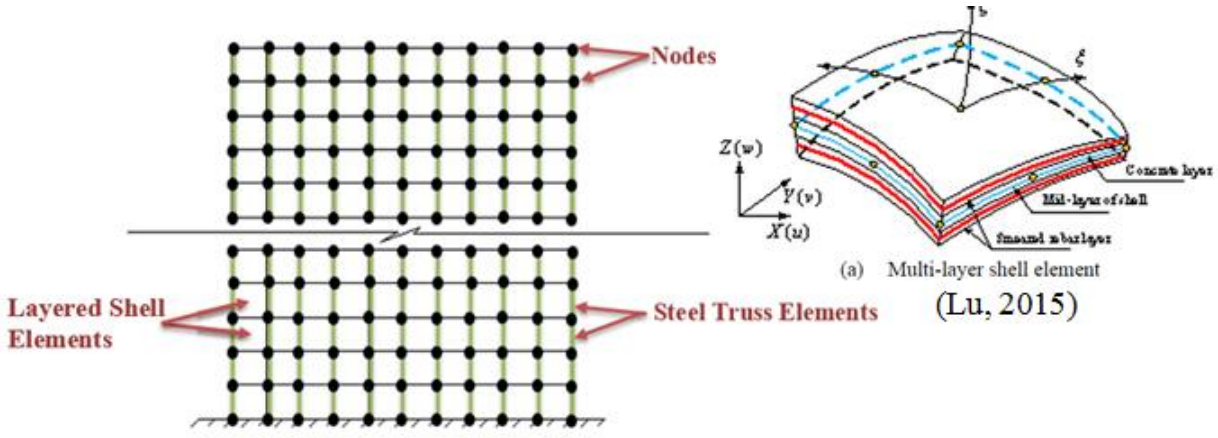

Figure 5: Example of Layered Shell Shear Wall Model

The Layered Shell Fiber model attempts to capture out of plane behavior that the Fiber Beam-Column, MVLEM and Lumped Plasticity models are unable to capture (Lu, 2015). The shell elements use the theory of mixed interpolation of tensorial components (Lu, 2015). Basically, finite element analysis is performed first within each layered shell element, and second across each node (Xiang, 2014). The result of the finite analysis occurring in multiple directions allows the Layered Shell model to capture out of plane deformation as well as better capture the effects of localized concrete cracking. The Fiber Beam-Column and the lumped plasticity spring models are unable to capture the localized cracking in the vertical direction with the same precision that the Layered Shell model can. The concrete material used is based on damage mechanics and the smeared crack model (Lu, 2015). The benefit to using a smeared crack model is that the accuracy of the results is not dependent on the size of the layers. In fact, the opposite is true, which is that if the layered sections are too small then the accuracy may then be affected. In an email to Dr. Lu inquiring about this point and how it applied to the models built for the comparison in this thesis, he replied that, "the original mesh size of 1' x 1' for a 20' long wall was too small and might be creating convergence issues". The smeared crack model is supposed to eliminate the need for smaller shell sizes to increase accuracy (Lu, 2015).

Mckenna (2014) suggests that the layered shell model may be best choice for detailed nonlinear wall modeling available in *OpenSees*. The shell model has increased ability to capture out of plane bending, the ability to take up real space in a model, geometrical accuracy in nodal loading, the ability to include the effects of horizontal rebar, and the ability to include the effects of both bending and shear without having to use additional shear springs. Though detailed information outside of Dr. Lu and his team is limited, Mckenna (2014) has produced a comparison of the layered shell model to professional nonlinear analysis software with

encouraging results (OpenSees Wiki, 2003). All modeling comparisons, to experimental testing data, or to other modeling software show excellent results. An example of one Dr. Lu's comparisons is presented in Figure 6.

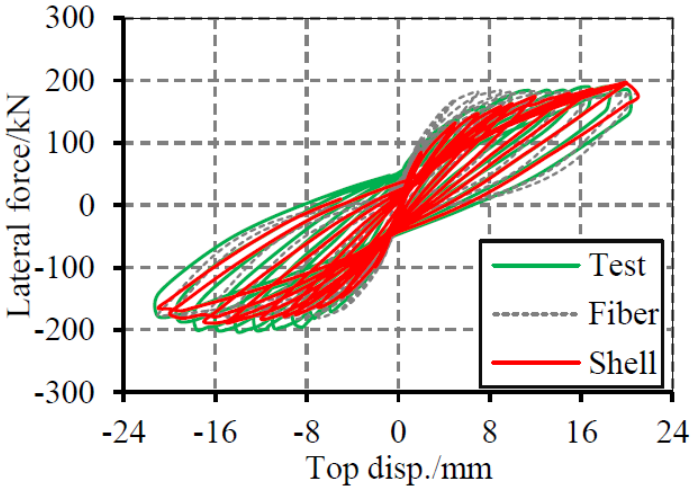

Figure 6: Example of Fiber vs. Shell vs. Test Results (Lu, 2015)

One major limitation in using this model, for the research conducted in this thesis, is that this model runs very slowly. This slow run time is not necessarily a problem if a super computer can be utilized. Unfortunately, the source code has not been made public property and therefore cannot be compiled on JANUS, CU's supercomputer. Another limitation to using this model, besides the long run time, is there is a lack of "proof" available for the layered shell model. This is the newest shear wall model available to *OpenSees* and official documentation by the creators has not yet been made public. The references to the designer's papers presented in this section have been made available by special permission from Dr. Lu, and additional modeling comparisons from external sources will not be available until researchers have had a greater opportunity to implement the layered shells into their building models.

3. Model Comparison: Layered Shell vs. Fiber Beam-Column

One of the motivations for the studies described in Chapters 4-6 is to develop a simple methodology that accurately assesses the true strength of a wall-frame structure, considering their interactions. In later chapters, nonlinear computer simulation is used as a tool to represent simplified hand calculations of cantilever wall and pure frame strengths analyzed separately and also to represent the wall-frame system strength. This chapter compares two *OpenSees* models, the Layered Shell model to the Fiber Beam-Column model, and the comparison helps determine an appropriate selection of which tool to use for conducting the analyses presented in the later chapters.

3.1. Geometric Details of Example Wall

The wall is 10” thick, 20’ long, and 84’ tall with 6 stories/horizontal loading positions. The rebar layout consists of 2 vertical #6 rebar placed with a 2” cover at the edges and at 1’ on center along the length of the wall. Figure 7 illustrates the rebar layout, shown in plan view. Reinforcement within the wall is designed to mimic the reinforcement of a typical pre 1980 building. Figure 8 shows a real example of a lateral force resisting wall built in 1980. The walls used for comparison are assumed to be non-shear critical and do not consider the contribution of confined concrete, thus making other details of the transverse reinforcement not necessary for the construct of the models.

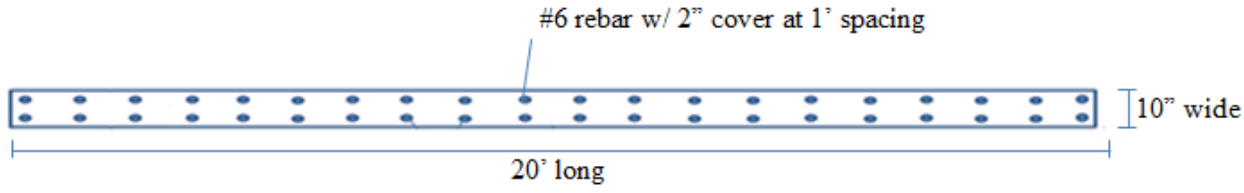

Figure 7: Plan View of Wall Showing Geometry and Reinforcement

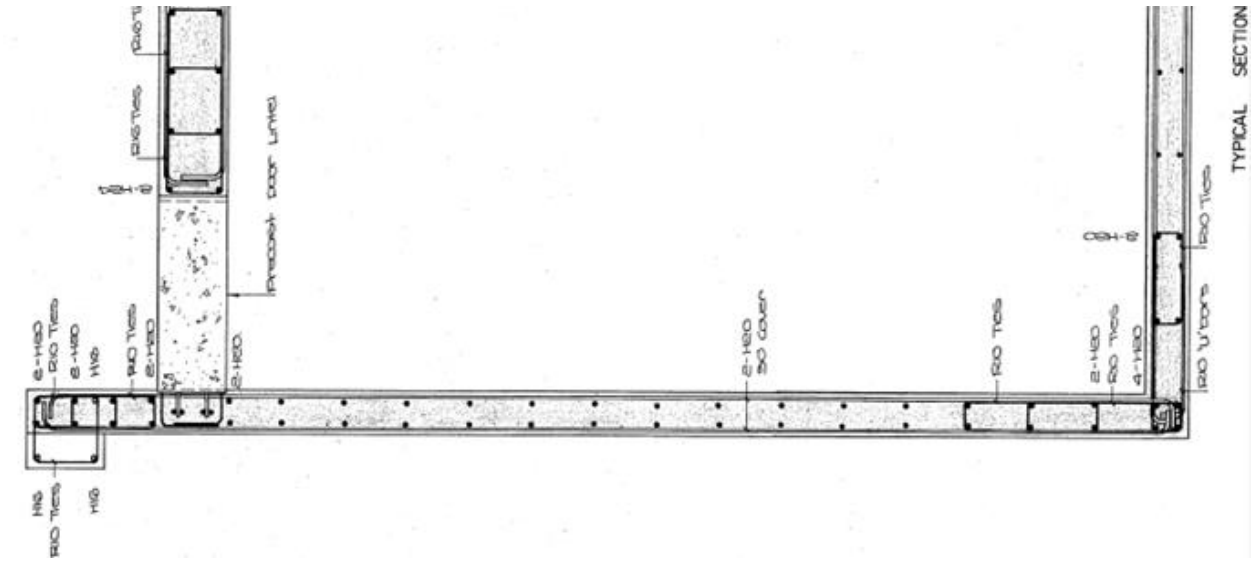

Figure 8: Building Plans for Lateral Force Resisting Wall Built in 1980

Figure 9 shows the geometry and the horizontal loading pattern assumed for both models. Both models are similar geometrically; however, they are not the same. This is because a Nonlinear Beam-Column element model has the capability to position the end reinforcement at the appropriate location within in the cover distance of the concrete within the section definition, whereas the Layered Shell Fiber model does not. Every effort has been made to account for the slight difference of the geometrical positioning of rebar at the ends of the shear wall for the subtle differences in the way that each model must be defined. The truss elements in the Layered Shell model, as illustrated in Figure 5, must be placed at the very end of the wall, which would suggest that the end section be reduced in length and the cover was neglected. The diagrams in Figure 3 and Figure 5 reflect these subtle differences. Neglecting the concrete cover for the Layered Shell model might be a good assumption if corrosion, cracking, or other reasons that would deteriorate concrete integrity were considered, but the global geometry of concrete for both models is kept identical in this comparison.

Only the mass due to the self-weight of the wall is considered for weight and eigenvalue analysis comparison. No vertical loading due to structural weight is considered for these comparison pushover analyses. The horizontal force applied to the wall uses an inverse triangular loading assumption.

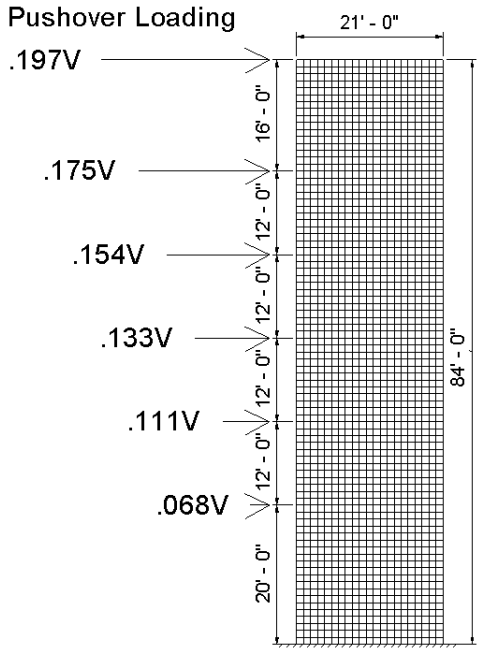

Figure 9: Geometry and Loading Details for Shear Wall Comparison

3.2. Material Property Details

Reinforcing material definitions in both models are identical and utilize the Steel02 *OpenSees* predefined material values to simulate rebar behavior. Concrete material definitions are a little more complicated. The Fiber Beam-Column Model uses a hysteretic pinching concrete material referred to as Concrete02 (Yassin, 1994) and the Layered Shell model uses a 2-dimensional concrete material referred to as Plane Stress User Material (Lu, 2015). The values describing the material behavioral curves are listed in Table 1. The Layered Shell model must use the Plain Stress User Material, while the Fiber Beam-Column model, though the material

model can be adjusted, is unable to use the Plain Stress User Material. This is because the Plain Stress User Material defines the concrete properties differently than Concrete02. For example Table 1 shows that Concrete02 defines compressive strength as a negative value and that the Plain Stress User Material defines the compressive strength as a positive value. Inconsistencies in property definitions make the Plain Stress User Material incompatible as a usable material for Fiber Beam-Column sections. Therefore, it is not possible to exactly match the concrete behaviors as demonstrated by the material curves in Figure 10. The biggest difference between the behaviors of the two materials is that the Concrete02 compression line begins to curve at very high stress and the Plain Stress User Material does not. This difference is illustrated by the red arrows in Figure 10. Another difference between the two behaviors is that the Plain Stress User Material incorporates a shear retention factor that Concrete02 does not. The shear retention factor is set to 1, which signifies that there is no shear retention being considered and thus eliminates this difference in the comparison.

Plain Stress User Material (Layered Shell)			Concrete02 (Fiber)		
Symbol	Description	Value	Symbol	Description	Value
f_c	Compressive Strength	4 ksi	f_{pc}	Compressive Strength	(-) 4 ksi
f_t	Tensile Strength	.56 ksi	f_t	Tensile Strength	.56 ksi
f_{cu}	Crushing Strength	(-) .8 ksi	fpcu	Crushing Strength	(-) .8 ksi
epsc0	Strain at Max Strength	(-) .003	espc0	Strain at Max Strength	(-) .003
epscu	Strain at Crushing Strength	(-) .01	espu	Strain at Crushing Strength	(-) .01
epstu	Ultimate Tensile Strain	.00028 ksi	lambda	Ratio: f_{pc}/epsc0	0.1
stc	Shear Retention Factor	1	Ets	Tension Softening Stiffness	2000

Table 1: Comparison of Concrete Material Definitions

Figure 10 shows the material behavioral curves for the concrete material properties specified in Table 1. The curves show how the concrete properties, despite the fact that both models are programmed with the same values as demonstrated in Table 1, have slight differences in behavior. This is because of the lambda*E_0 and the E_0 slope definitions that are defined by the Concrete02 and not by the Plane Stress User Material, meaning that the loading and reloading branches in the compression region are different for each material as shown by the red arrows and the dotted black lines in Figure 10. It is important to note this difference in the material behaviors because, though subtle, is the major reason that these models do not agree in the nonlinear range. The effect that this difference has on the pushover analysis is that the Layered Shell model demonstrates indefinite strain hardening while the Nonlinear Beam-Column model demonstrates perfectly plastic behavior.

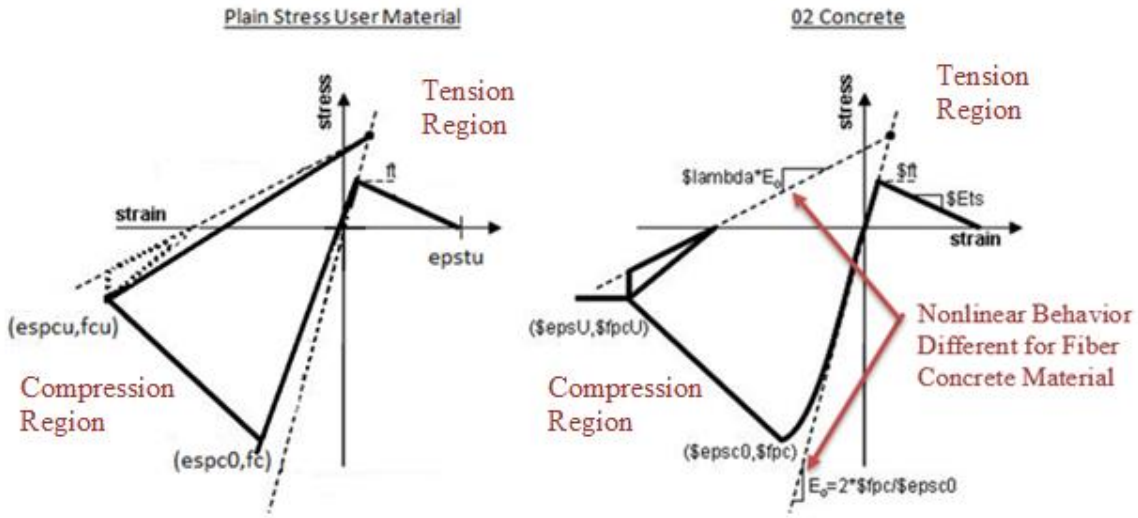

Figure 10: Concrete Material Behavior Comparison

3.3. Pushover Comparison

Figure 11 shows the results of four pushovers. It is a comparison of two versions of each of the Fiber Beam-Column and the Layered Shell models, using the geometries described in

Section 3.1. One version of each model uses concrete material properties exactly as described in Table 1. The other version eliminates tension, setting f_t to 0, in both models. The layered shell model inherently calculates shear response, but in this scenario the wall is not shear critical, and the fiber element model cannot capture shear deformations.

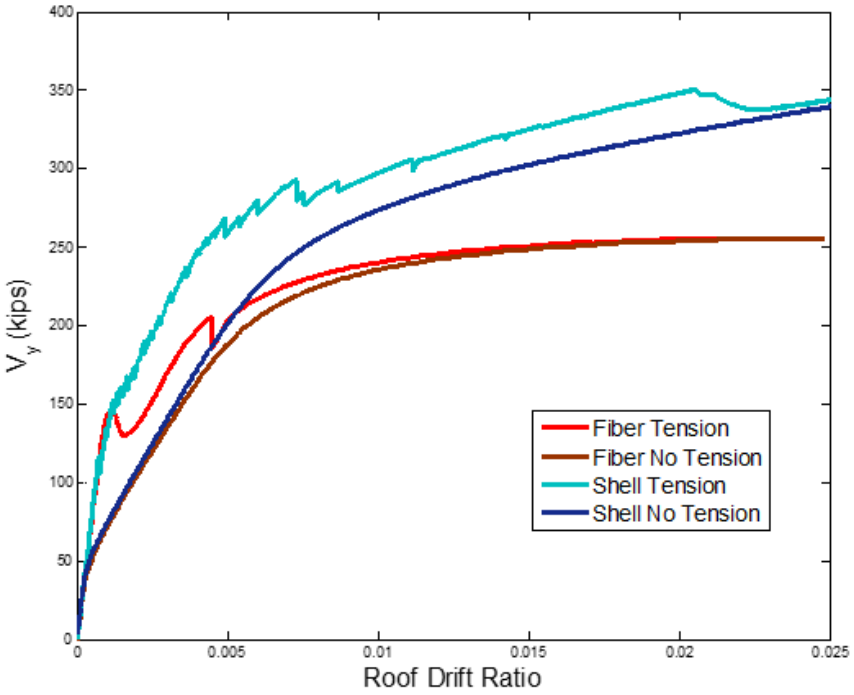

Figure 11: Pushovers of Layered Shell and Fiber Models

It is important to understand why these responses are different. Figure 12 is the same pushover comparison shown in Figure 11, but with annotations and alphabetical labels that identify specific sections where changes occur. Label A represents the elastic region. Label **B** represents the region where tensile strength delays cracking in the concrete for the models with concrete tension defined and the lines begin to split. Label **C** represents where the fiber and layered shell models begin to calculate concrete tensile cracking differently. Label **D** represents

the difference in ultimate strength of the models resulting from the difference in the nonlinear aspects of the material definitions as discussed in Section 3.2.

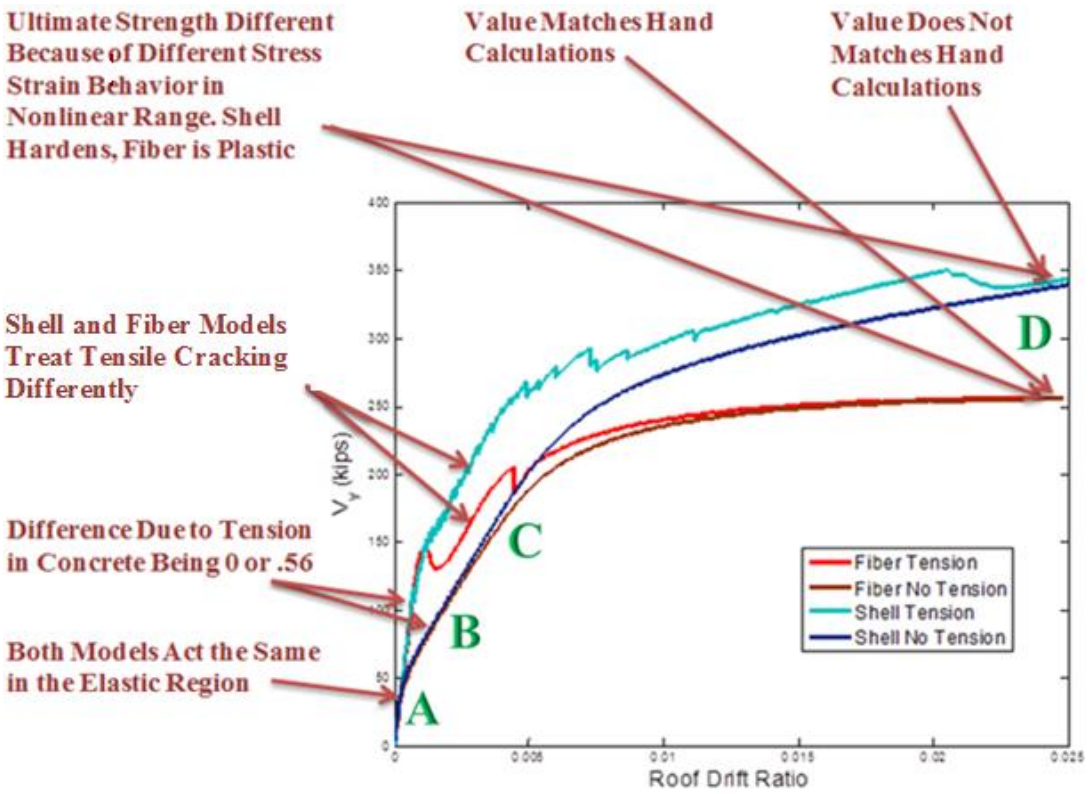

Figure 12: Annotated Pushover Comparison

3.4. Modeling Comparison Discussion

Section **A** in Figure 12 is the elastic region and all 4 models behave identically. This means that global geometry and elastic material definitions are identical.

Section **B** is more interesting because there is a split in the response curves. The split in the curves is due to the tensile property of the concrete (f_t), but the effects of the considering tensile affects are the same for the Fiber model and the Layered shell model. It is encouraging,

and elevates modeling confidence, that both models agree in this section with or without tension being considered in the concrete material.

Section **C** is where the difference in the behaviors becomes more complicated and we see differences between the Layered Shell and Fiber Models. Notice that there are two abrupt "swoops" in the Nonlinear Beam-Column models as demonstrated in Figure 13. These "swoops" result from a simplification due to the inability to calculate finite concrete cracking at individual locations along the height of the wall. The tension builds up then fails abruptly as shown by the swoops. The Layered Shell model is able to capture this effect individually at every node along the height because of the geometrical construct of the model and the finite analysis computation along the height of the wall (Xiang, 2014). This is the reason that the Nonlinear Beam-Column model has swoops and the Layered Shell model has jagged edges. The difference in the way each model calculates this is not necessarily significant for the later research studies, but is important for understanding why these models do not perfectly agree.

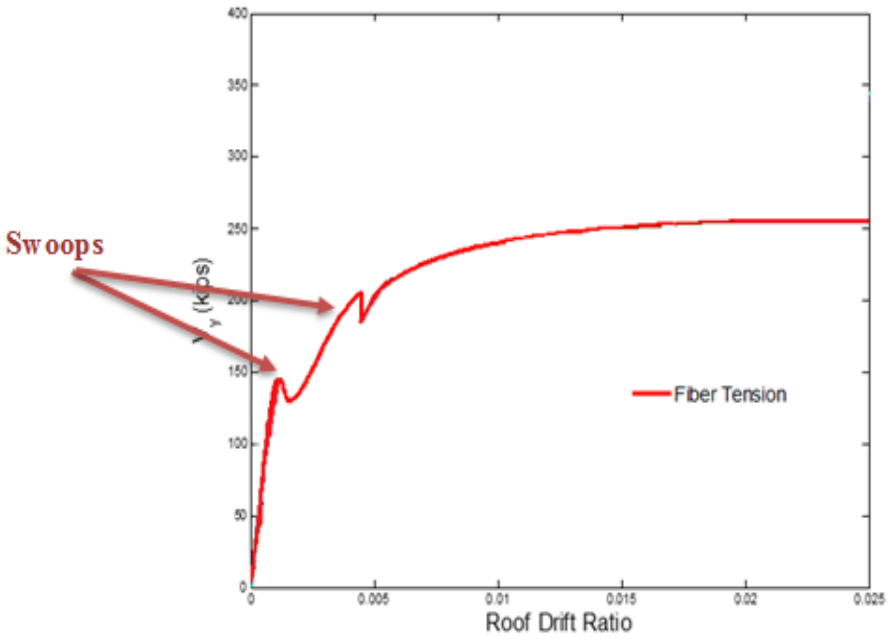

Figure 13: Example of "Swoops" in Nonlinear Beam-Column Element Model

Section **D** is where both models vary substantially. The Nonlinear Beam-Column model exhibits something close to perfectly plastic behavior, while the Layered Shell model exhibits strain hardening. Taking a step back and thinking about this conceptually, then the strain hardening model seems to make more sense. Whereas a column would reach strength and then not be able to resist any more load, whereas a wall may continue to increase in strength because of all the material compacting and not allowing the wall to bend, and the material in the middle of the wall which has not failed. Even after local crushing and yielding there will still be an abundance of steel and concrete providing bending resistance. The Fiber Beam-Section is designed for columns and it does not take into account some of the effects that will be different in a long wall. The material definition of Concrete02 defines the pushover behavior and is generally used for a beam or a column. The material will act differently when the out of plane effects and larger deformation begin to occur. One of Dr. Lu's studies, shown in Figure 6, illustrates that the Fiber Beam-Column model does not work as well for long walls.

3.5. Stress Strain Comparison along Base of Walls

Figure 14 compares the stress-strain values of the steel reinforcement for the two models containing tension in the concrete along the base of the shear wall. Each marker represents a location of a different vertical steel reinforcement along the base of the wall. There are fewer recorder locations for steel behavior in the Layered Shell model because of the 2' wide shell sections. Recorders are easier to use and are positioned at 1' spacing along the bottom of the wall for the Fiber Beam-Column models. The quantity of steel is identical.

To compare the models, all stress values are extracted from pushover analysis when the rebar at the tension end of the wall (left) first reaches 60ksi yielding. The noticeable difference in the models is that the Fiber model has more steel nearing yielding for a longer distance at the left end of the wall. This is because the section definition of rebar in the Fiber model treats the rebar as a strip acting along the entire length of the wall, while the Shell model treats each reinforcing bar as an individual truss with concrete in between. Figure 3 shows the location of the steel strip in the section used in the Fiber model and Figure 5 shows the truss layout in the Shell model. The steel behavior of the strip is different than that of the truss behavior because the steel is acting like a plate under bending. When the small end point of the plate is yielding, then a certain length of the plate which is close to the end is near yielding as illustrated by the green line in the upper left quadrant of the stress plot of Figure 14. The Layered Shell model is more sophisticated and at each node accounts for intermediate displacements, strains, and stresses (Xiang, 2014). Specifically, it is able to measure displacements in three directions at the node between each shell.

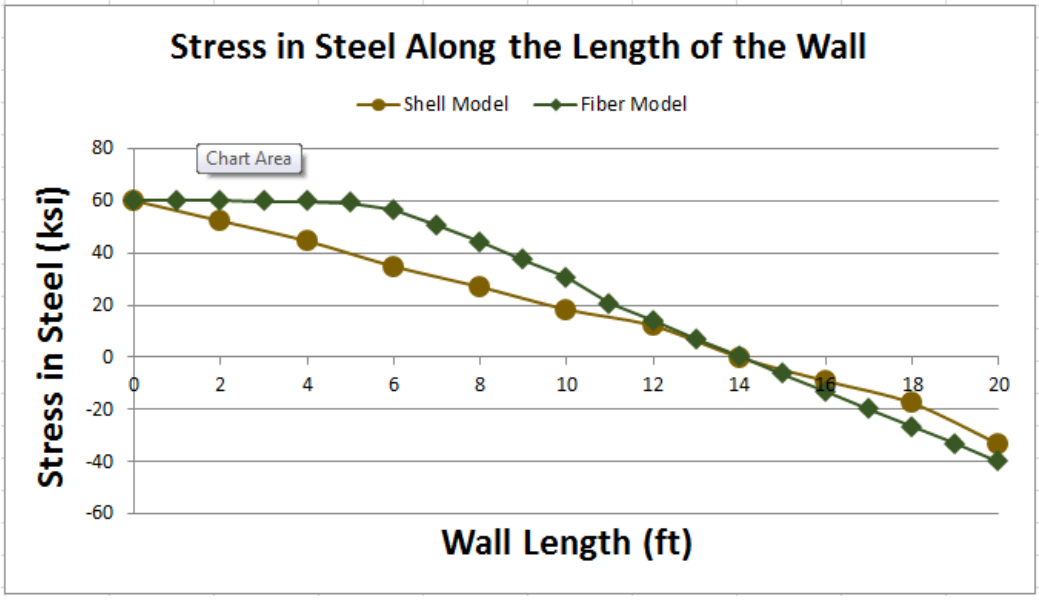

Figure 14: Comparison of Stress and Strain at Base of Shear Wall

One of the concerns that Orakcal & Wallace (2004) had about lumped plasticity models is that they were unable to account for the appropriate centroidal rocking axis of the shear wall. These results show that the Fiber Beam-Column model and the Layered Shell model have the same neutral (centroidal axis), as shown by the fact that the orange and blue markers line up exactly on top of each other at the 0 point of the x-axis with a symmetrical balance of rebar on either side of the y-axis.

3.6. Conclusions to the Model Comparison Study

The modeling comparison concludes that the Layered Shell model, though perhaps more accurate (Lu, 2015), is too time intensive and complex to build. The complexity in building/writing the script that defines the wall leaves excessive chance for human error to occur. The remaining analyses conducted in thesis require a multitude of wall dimension iterations. The author found that small errors were easy to make, happened often, and were hard to identify. It is easy to make little mistakes due to the multitude of code necessary to describe the wall, and as such, this is one reason that the Layered Shell model is not the optimal choice for the analyses that need to be conducted for the studies contained in the rest of this thesis.

In addition, we recall that the true motivation of this aspect of the ATC 78 project is to analyze the true strength of a building. Cyclic loading comparisons by Mckenna (2014) would suggest that the Layered Shell model is better at estimating the true strength of the wall than the Fiber model. However, the end result to this thesis is the development of parameter that quantifies the difference between simplified hand calculations and combined system strength. Simplified hand calculations are mimicked by pushover analysis of a cantilever wall. Likewise, the total system strength is mimicked by pushover analysis of a wall-frame building. The

difference between the cantilever and system strengths are expected to be the same despite the modeling approach that is used.

The final deciding factor against using the Layered Shell model is analysis run time. A pushover analysis on a Layered Shell model takes nearly a day to run, whereas the Nonlinear Beam-Column model can be run in less than an hour, times that both are extended when the wall is coupled to the frame. Due to the quantity of pushovers that that need to be evaluated, the Fiber Beam-Column model proves to be more efficient and suitable and will be used for the remaining studies contained in this thesis.

4. Lateral Strength of Wall-Frame Systems

This study is motivated by the needs of the existing ATC 78 methodology, which performs collapse risk analysis of RC frame structures. The goal is to modify the methodology, using simplified hand calculations that are quick and computationally efficient, to determine the collapse risk of RC wall-frame structures that were built before modern building codes. The methodology for pure frames is complete (ATC 78, 2014) and the next step is to include frame structures that also have lateral force resisting walls. Since many concrete structures have at least some walls, the ability to consider buildings with walls is important.

The first step in the new method is to determine the effective period of the wall-frame structure, which is a function of mass and secant stiffness. As envisioned in the ATC 78 method, the secant stiffness is a function of yield strength and yield drift obtained from a bilinear analysis of pushover results. The reason for using a strength-based period calculation is to avoid the need to build a nonlinear model for analysis and to capture stiffness in the nonlinear range. The challenge of determining secant stiffness is illustrated in Figure 15. First, this study will investigate yield strength of a wall-frame system, then effective period calculation and bilinear approximation details will be provided in Section 5.1 and Section 5.2.

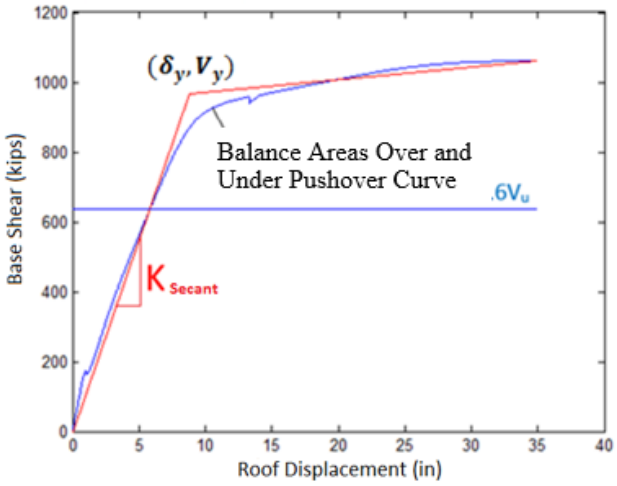

Figure 15: Example of Bilinear Approximation of Pushover Curve

The ATC 78 methodology requires a simplified hand calculation to determine nonlinear yield strength rather than a pushover analysis. The reason that this is not easy is that the force interaction between the wall and the frame is complicated. It is important to apply the appropriate force distribution applied to the wall from the frame in order to determine the true strength of a wall-frame system using hand calculations. The ATC 78 committee is in agreement that the methodology should calculate the shear strength of the wall due to flexure using an inverse triangular loading assumption and that the wall acts as a cantilever beam. Specifics pertaining to simplified wall calculations are provided in Section 4.2. This study outlines the difficulties in capturing the true strength of the wall-frame system and searches for a linear relation between the simplified calculation and the pushover strength, which can be used to develop an engineering parameter that can be used in the hand calculations. The engineering parameter is developed in Chapter 5.

Accurate yield strength and drift values are crucial for calculating the effective period of a structure which is necessary to accurately approximate the demand on the structure through the ATC 78 simplified calculation procedure. The effective period of a structure considers strength and ductility of a structure after certain nonlinearities begin to occur, such as concrete cracking and rebar yielding. Therefore, the first step towards solving this problem is close investigation into the different behaviors between a wall acting as a cantilever and a wall acting within a wall-frame system, along with close analysis of the available options for computing strength.

4.1. Overview of Study

Nine frame structures are developed in a matrix of geometries that vary among 3, 5, and 7 bays, and 3, 6, and 9 stories. Some of the important aspects of the frames considered are that the ratio of column to beam strengths (M_c/M_b) ratio is 1 at all joints, and that the ratio of shear to flexural strength in columns (V_p/V_n) is 0.6. This signifies that the flexural failure is expected to occur in the columns and that it is not a shear critical structure. A lateral force resisting wall is attached to the frames. The wall composition, width and height are all consistent throughout this study with rebar layout of 2 #6 60ksi vertical rebar at 1' on center, a width of 10" and a length of 20'. Wall height is always equivalent to the total frame height to which it is attached.

All of the wall-frame models are built in *OpenSees.* Figure 16 is a diagram of a typical beam-column moment resisting frame joint, which utilizes elastic beam column elements with lumped plasticity flexural springs. These frame models are based on previous work conducted by members of the ATC 78 committee (Galanis & Moehle, 2014). The RC walls are constructed from nonlinear displacement beam column element fiber models, in accordance with the conclusion of the wall comparison described in Chapter 3 of this thesis. The nonlinear modeling results are then compared to multiple variations of simplified hand calculations in search of the most efficient solution which can be implemented into the ATC 78 methodology.

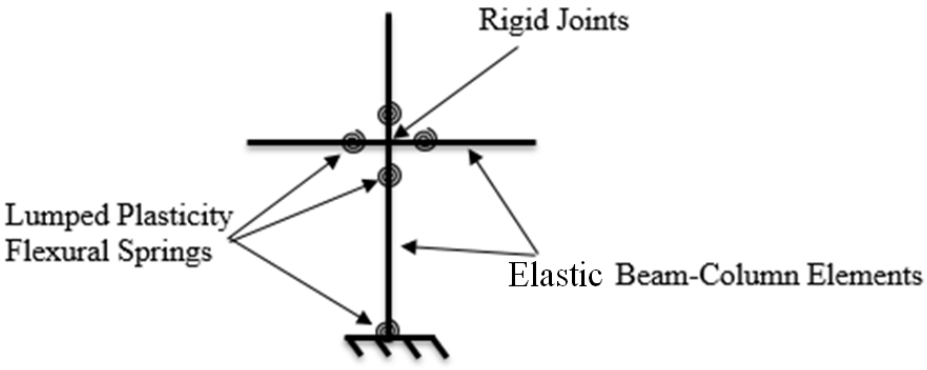

Figure 16: Modeling Details

4.2. Wall Strength Hand Calculations

The flexural capacity of the shear wall is estimated by calculating the moment around the neutral axis of the wall, similar to the way that the strength of a beam would be calculated. Flexural capacity moment calculation procedures are illustrated in Figure 17 and described with Equation 1. Expected material strengths from (ASCE_41, 2013) are used in this calculation. It is anticipated that this is the method that will be adopted by the ATC committee. If expected material strengths are used in this calculation, as the ATC method uses, then the results are very close to the pushover strengths from pushover results as presented later in Figure 25.

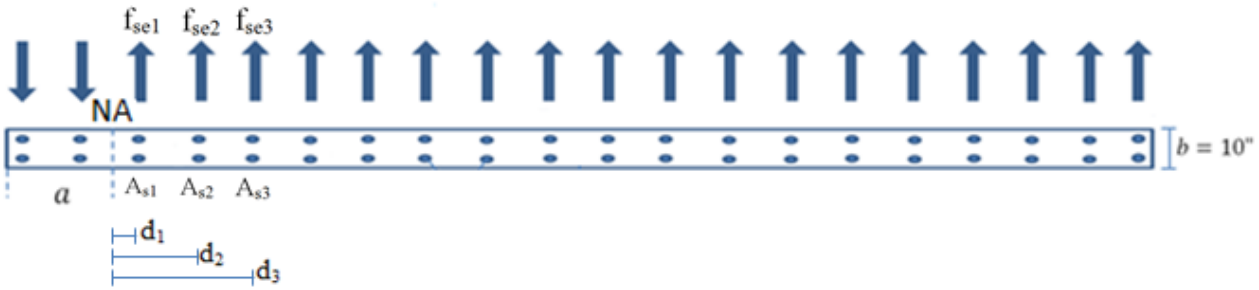

Figure 17: Illustration of Shear Wall Capacity Moment Calculations.

Equation 1: Compression Block Length of Shear Wall

$$a = \frac{A_s f_{se}}{f'_{ce} b}$$

Equation 2: Moment Capacity of Shear Wall at Base

$$M_{c,wall} = \Sigma(A_s f_{se} d)$$

In these equations, f'_{ce} is the expected strength of the concrete at $1.5*f'_c$, f_{se} is the expected strength of the steel at $1.25*f_y$, A_s is the area of steel, d is the moment arm distance to center of force, and b is the thickness of the shear wall.

Demand on the wall is calculated using the inverse loading triangle as illustrated in Figure 18. The loading points illustrated are then used to calculate the moment at the base of the wall if it is treated as a cantilever beam. This calculation will yield $M_{D,wall}$ and be in terms of V. Demand is then equated to capacity, based on the calculations above. This equality can then be solved for $V_{u,wall}$. This is the wall capacity due to flexure. The accuracy of hand calculations using this method compared to pushover results can be seen in Figure 25.

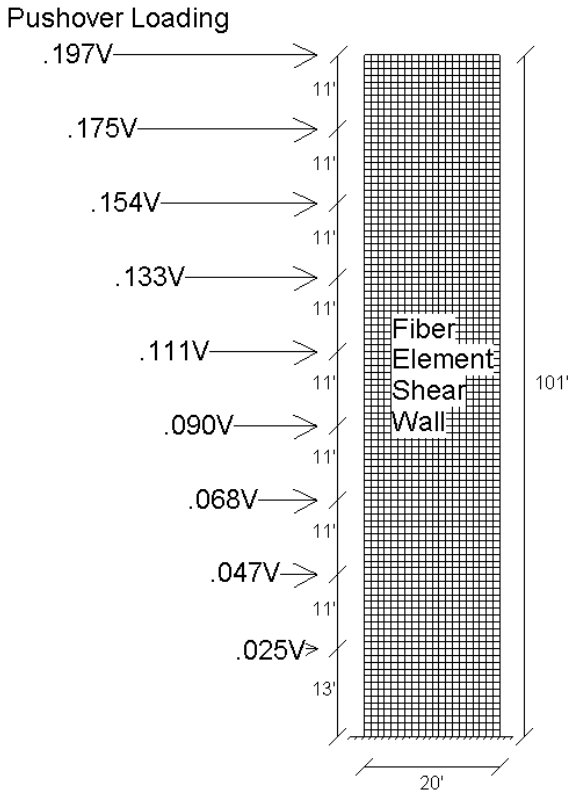

Figure 18: Triangular Loading Distribution for Flexural Capacity Calculations of Wall

Note that the wall-frame strength analyses conducted in this chapter are an estimation of ultimate strength of the building as notated using the "u" subscript, i.e. the peak point of the pushover. The next chapter is conducted using a bilinear approximation of pushover results that determines a nonlinear yielding strength and will be notated using the "y" subscript. The wall is assumed to be flexure, rather than shear controlled, so the shear capacity is not computed.

4.3. Frame Hand Calculations

Frame strength is calculated using the moment capacities of the column springs in the first story and assuming an inflection point 6/10 of the way up from the base. This strength is determined to be the shear capacity due to flexure in the structure, computed according to Equation 3. Frame models have identical flexural spring calibrations to models created by Galanis & Moehle (2014). Recreating frame strengths from a specific column composition is not crucial for this study since the column methodology of the ATC 78 project is complete. The models have been shown to produce the appropriate strength (Galanis & Moehle, 2014).

Equation 3: Ultimate Shear Capacity Due to Flexure

$$V_u = \Sigma \frac{M_{spring}}{.6L_1}$$

In this equation, V_u is the ultimate shear capacity of the structure summed up over all of the columns, L_1 is the height of the first story columns, and M_{spring} is the moment capacity of the spring at the base of each column in the structure.

4.4. OpenSees Models of Wall-Frame System

Figure 19 reflects the typical composition for all nine of the *OpenSees* models, and is specifically the tallest and widest building analyzed (9 stories, 7 bays). Every model in the nine building matrix is analyzed as the combined system to help understand the wall-frame interaction. In addition, each model is desegregated into two models, consisting of a pure frame and a cantilever wall, for comparison. The wall-only and frame-only models represent simplified hand calculations and can then be compared to the actual strength of the combined system. It is assumed for each structure the building is square, and that the frame and shear wall shown provide the load path for the lateral loading associated with half of the mass of half the building in the direction of consideration. P-Δ columns were considered, and then removed because of insignificant change in strength and drift behavior for a pushover analysis.

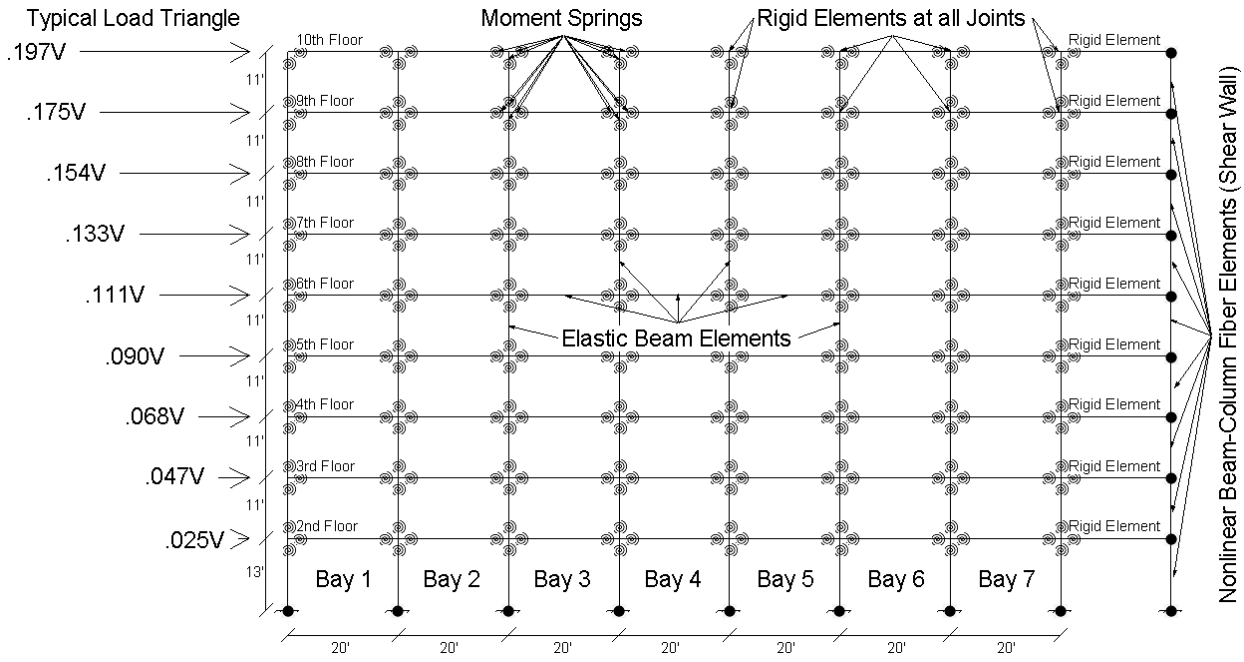

Figure 19: Typical Composition for buildings modeled in OpenSees

4.5. Pushover Results

Examples of typical pushover results can be seen in Figure 20 and Figure 21. Figure 20 shows results of a pure frame and a cantilever wall analyzed independently. Figure 21 shows the pushover results of the combined system. The wall and frame reactions are separated to help identify changes in drift and strength that result from the interaction between the two systems.

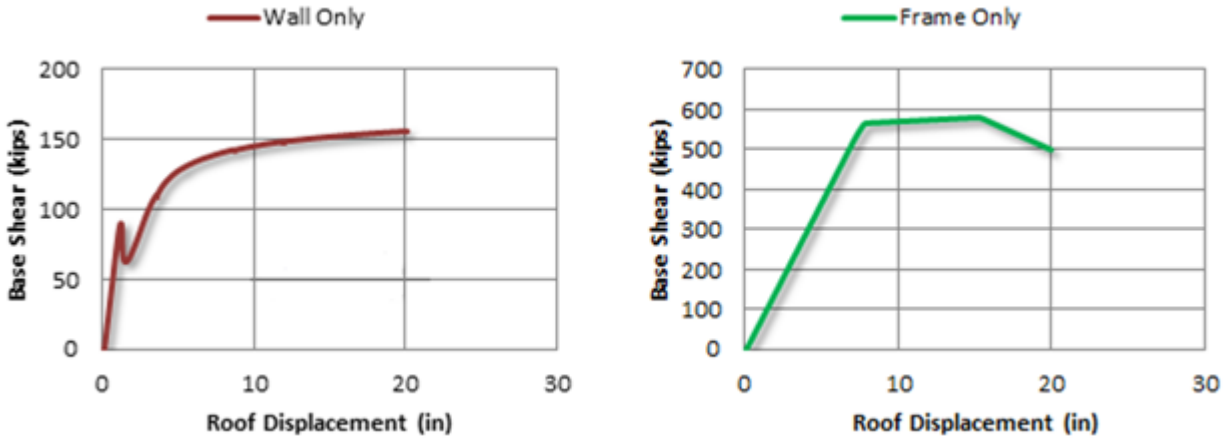

Figure 20: Pushover Plots of Frame and Wall Alone (De-Coupled from System)

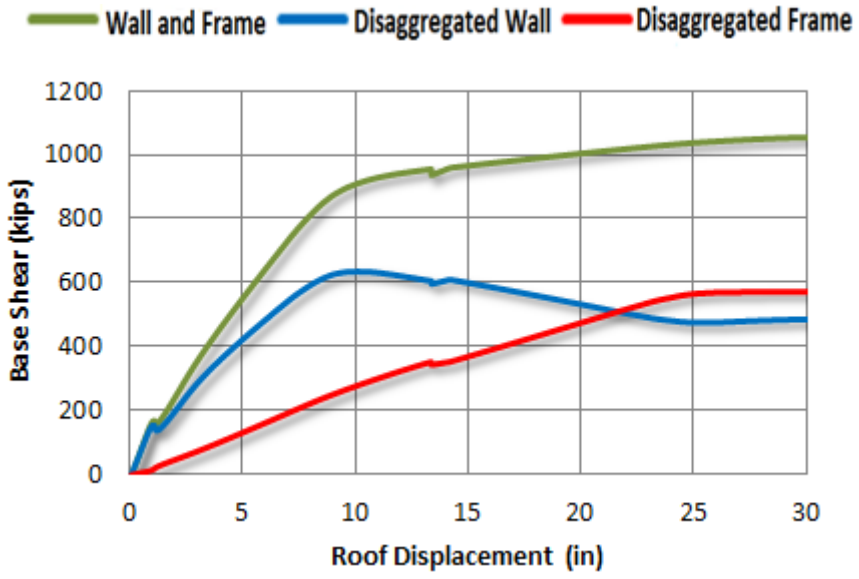

Figure 21: Pushovers of Wall and Frame Disaggregated from the Wall-Frame System

Figure 22 provides a comparison of all of the pushover curves in Figure 20 and Figure 21. The bright red and green lines show the frame acting with and without the wall. In both cases the frame exhibits the same strength, but the equivalent strength of the frame in the combined system is reached at three times the roof drift of the frame without the wall. This is a result of the change in failure mechanism. The frame acting alone exhibits weak or soft story behavior in the first story, but when the wall is coupled into the system the mechanism changes. The wall allows displacement to be divided over the entire height of the structure as opposed to only the 1st story.

The wall response also differs when coupled with the system. However, it is not a change in drift like the frame, but instead a change total capacity as shown by the dark blue and dark red lines in Figure 22. Specifically, when the wall is analyzed alone, it acts like a cantilever beam under triangular loading. Then once the wall is coupled with the frame, the distribution of forces between the wall and frame change the loading pattern dramatically. The pushover prediction of strength is higher in the wall disaggregated from the total system as compared to the strength when the wall is analyzed alone.

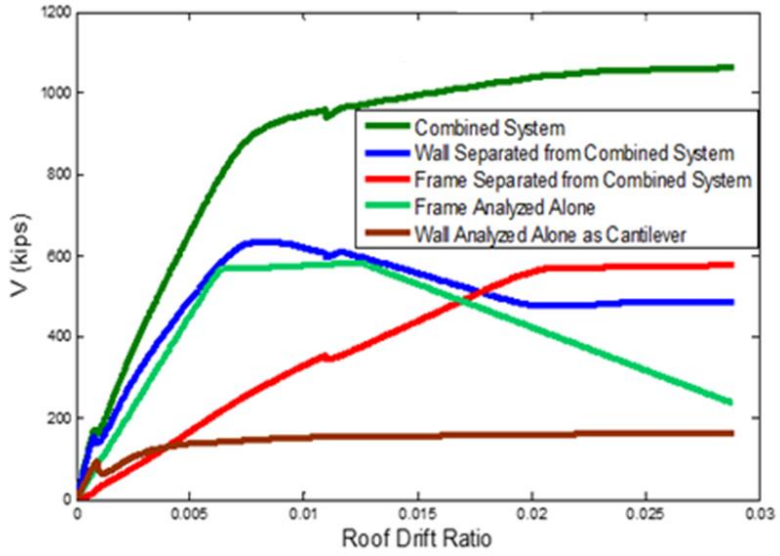

Figure 22: Typical Pushover Result Comparison

4.6. Displacement Profiles

The displacement profile will help to determine the curvature of the structure, interstory drift relations, and if there is a soft story mechanism. The displacement profile plot is obtained by normalizing the horizontal displacements at each floor at the point by the horizontal displacement at the first floor. This calculation is carried out at the point in the pushover when the system has reached ultimate strength. Figure 23 shows that the displacement profile of the system acting together has the same shape as the shear wall acting alone. The pure frame structure shows soft story behavior, indicated by the concentration of deformation in the first story. This behavior is eliminated when the wall is added to the system. In fact, the 1st story has the smallest drift in the structure when the wall is added. The plot helps to illustrate the reason that the disaggregated frame has much more drift when it reaches its ultimate capacity as opposed to a pure frame system. Both the pure frame system and the wall-frame system have the same drift ratios, however the drift ratio of the pure frame is compared to the story height and the drift ratio of the wall-frame is compared to the entire structure's height.

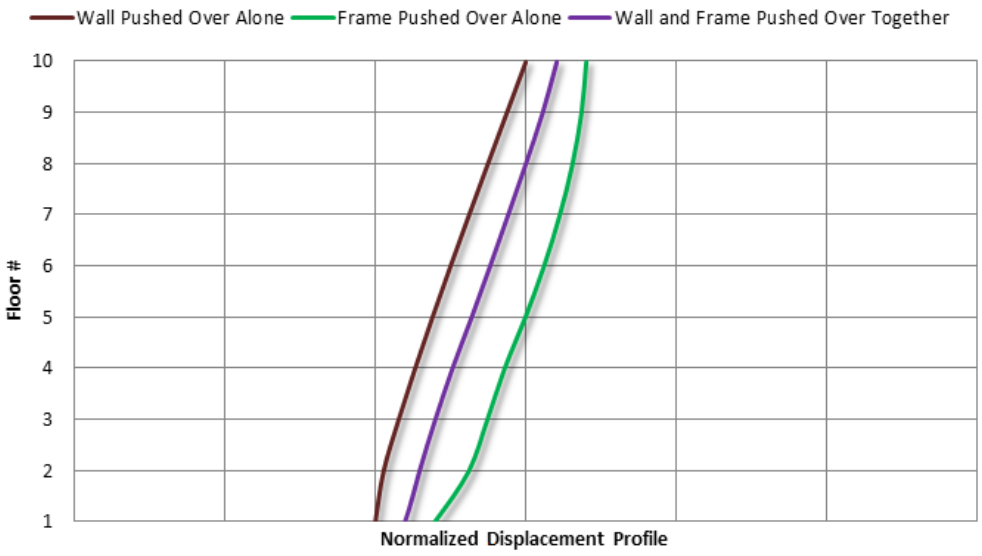

Figure 23: Displacement Profiles

4.7. Strength Trends

Results for all of the structures analyzed are similar to the pushover results above, i.e. the cantilever wall and pure frame ultimate strengths do not equal the ultimate strength of the wall-frame system. In each case the strength of the combined system is computed from the peak strength observed in the pushover analysis. Figure 24 shows the trend. The black line represents the case where the hand calculations are equivalent to the pushover results. If the frame and wall structures are analyzed independently in pushover analysis, the results fall on this line and are represented by squares and triangles. For the combined systems, the distance between the circle markers and the line show the strength underestimation that occurs if the strengths of the wall and frame are simply added (i.e. hand calculations) rather than treating the response as a system (i.e. pushover calculations).

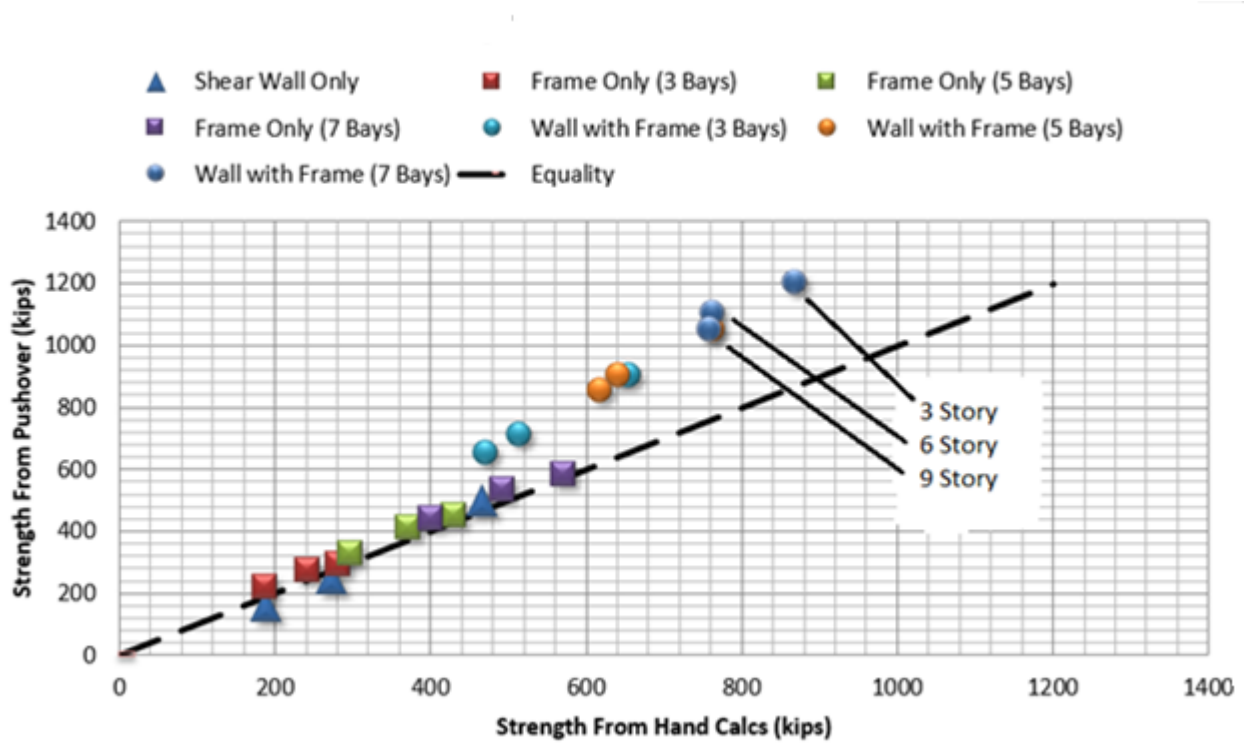

Figure 24: Compare Hand Strength Calculations to Pushover Strength Results

4.8. Shear Wall Capacities

Figure 25 shows the numerical difference in wall strength between the simplified hand calculations calculated in accordance with Section 4.2 and the ultimate strength values from the pushover results. The blue and green triangles show that the ATC 78 hand calculation method provides a close approximation to the strength of the wall when it is analyzed alone as a cantilever beam. The red, purple, and blue squares on the right side of the plot, show the strength of the wall when the strength values of the wall only are disaggregated from the pushover curve of the entire system. As we saw before, the wall is stronger when part of the combined system because of the change in the load distribution on the wall. In Figure 25 the difference between the strength of a pure wall (cantilever wall) and the strength of the disaggregated wall increases not only as the height of the structure increases, but also as the number of bays in the structure increases.

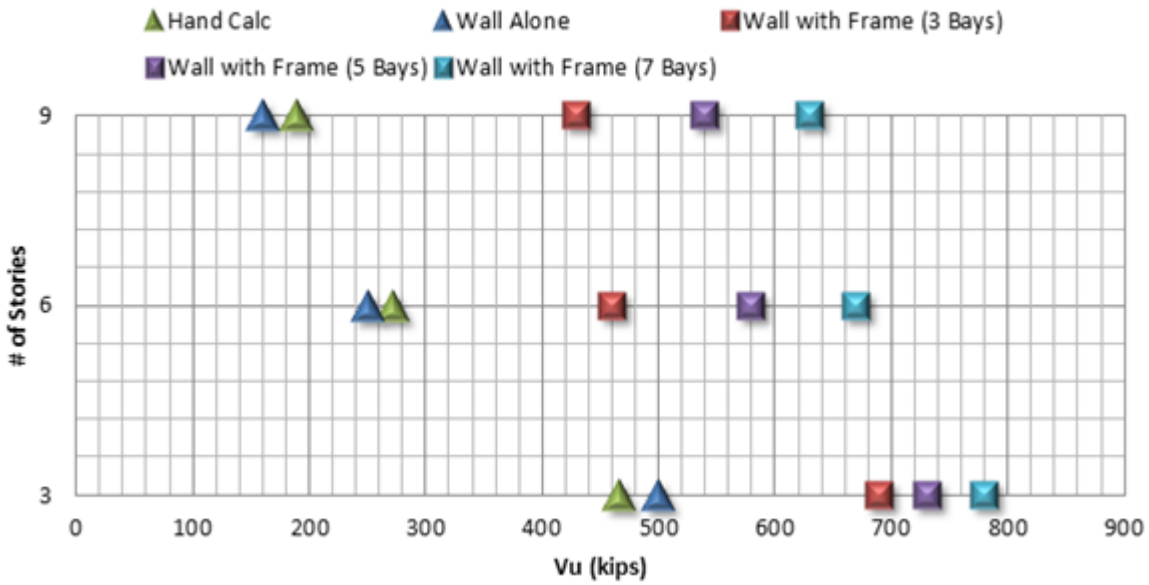

Figure 25: Shear Wall Capacities

Figure 26 shows the difference between the triangle and the square markers in Figure 25, presented as a percentage of overall strength increase described by Equation 4.

Equation 4: Percentage Strength Increase in Shear Walls

$$\frac{V_{u,Disaggregated\ Wall} - V_{u,Cantilever\ Wall}}{V_{u,Disaggregated\ Wall}} * 100\%$$

Figure 26 is designed to help better explain the two main trends described in the last section. The first trend is strength increase between a cantilever wall and a disaggregated wall as the height of the building increases. There is less difference for the 3 story structure and greater difference as the structures increase in height. The second trend is the strength increase in the wall as the number of bays increase.

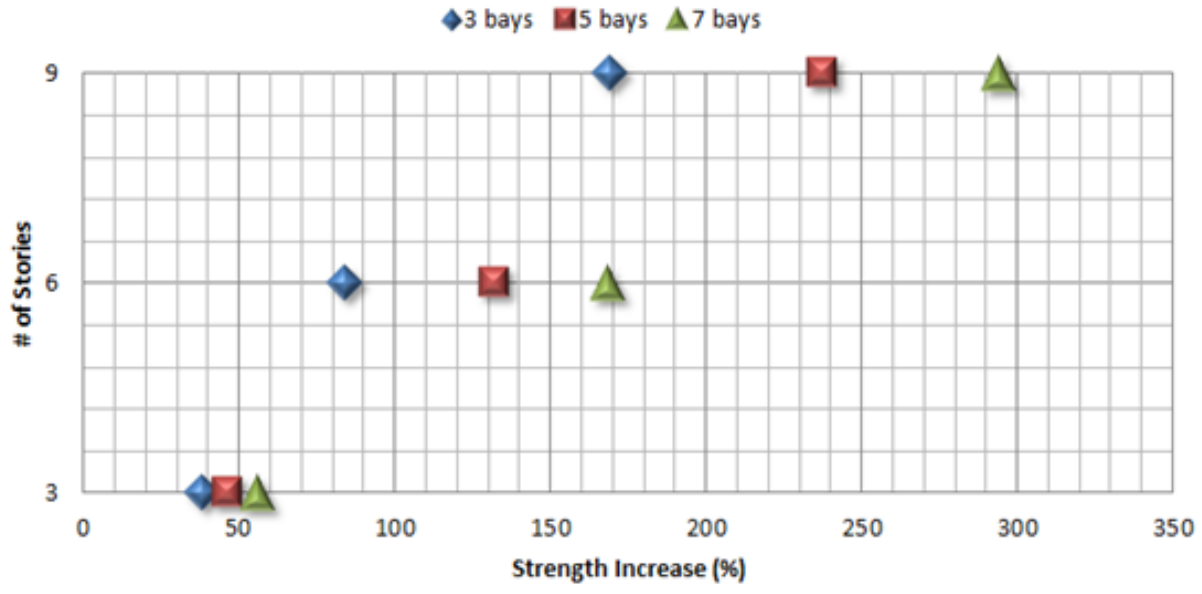

Figure 26: Strength Increase in Shear Walls

4.9. Interaction Forces between the Frame and the Shear Wall

In order to develop a simple method to determine the strength of a wall acting within a wall-frame system it is necessary to understand the interaction force between the the frame and the wall in each building. Figure 27 shows the interaction force between the frame and the wall at the end of the elastic portion of the pushover. The magnitudes of the forces are normalized at the second floor and the positive or negative value of the magnitude indicates the direction in which the force is acting on the wall. As shown in Figure 27, the forces acting on the wall no longer act as an inverse triangle when the forces in the rigid members connecting the wall to the frame are analyzed. The six and nine story structures have a load reversal acting at the roof level, while the three story structure does not. Others, such as MacLeod (1972), have previously observed these effects which come from the displacement incompatibility of the frame and wall, but it is important for us to explore how it influences our strength calculation.

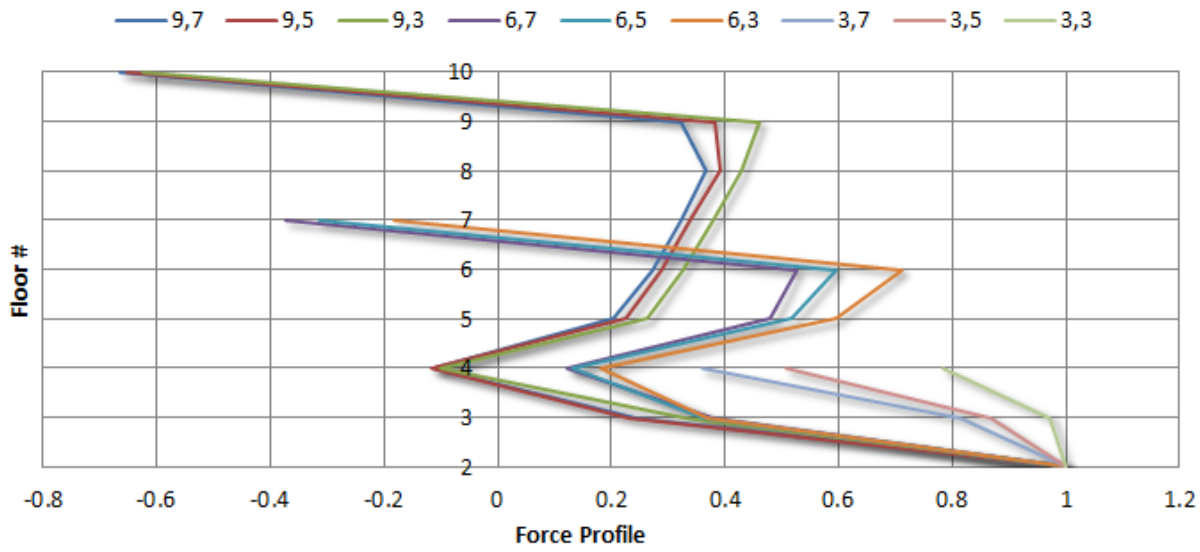

Figure 27: Force Profile at Elastic Portion of Shear Wall for all 9 Structures

Figure 28 shows more force profiles compared at different locations of the pushover as indicated by the color coded stars in Figure 29. This plot illustrates the difficulty in accurately estimating force interaction between the wall and frame at any point during the pushover as the wall and frame begin to yield. Nonlinearities such as concrete cracking, crushing, and rebar yielding all cause changes to this interaction, adding to the difficulty of making a good estimation of the direction and the magnitude that the forces are going to act. The nature of these force interactions strongly influence our wall strength calculations.

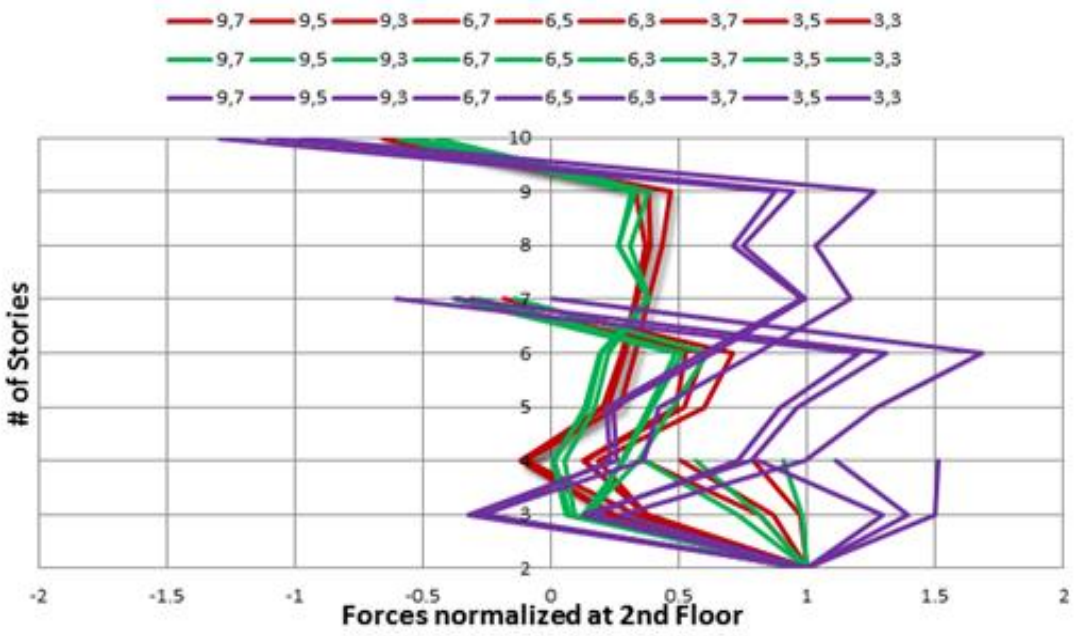

Figure 28: Force Profile Comparison at Different Locations on Pushover Curve

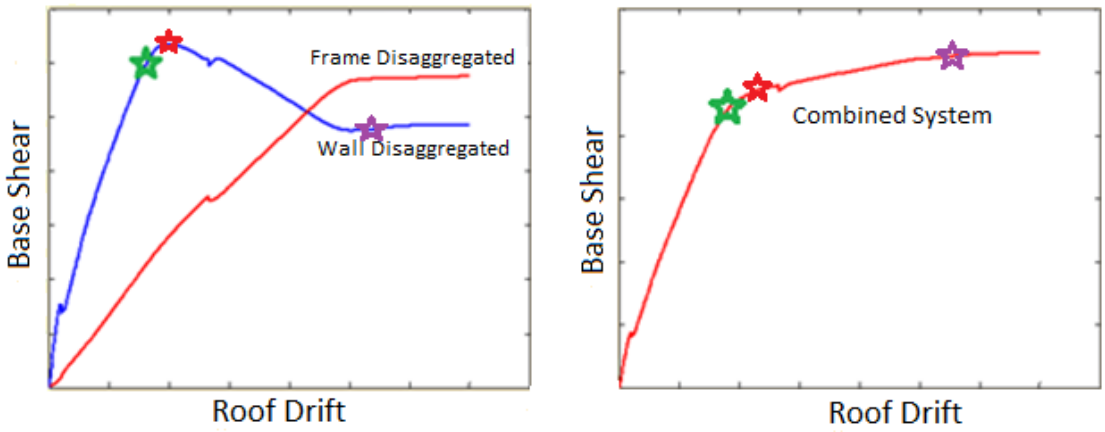

Figure 29: Mapping of Locations of Force Profiles

4.10. Implications of Interaction Forces for Strength Calculations

It is clear that it will be difficult to predict the accurate force profile acting on the disaggregated wall, but if the force profile could be predicted this section shows that it is still difficult to compute the correct strength of the wall. The first challenge is determining the force interaction, whether is when the structure is behaving elastically or after the structure has begun to show plastic behavior. The second challenge is calculating the correct strength.

Figure 30 shows the wall strengths when the force profiles above are used to calculate the strength in the shear wall, rather than the inverse triangular loading profile used in the previous analysis. Each calculation is compared to the pushover wall strengths at the same point in the analysis at which the force profiles were obtained, and the error is represented by the deviation from the black dotted line. The color coding matches the force profiles in Figure 28. The results show that simply altering the force profiles in the hand calculations does not accurately capture the strength in the wall as well as might be expected. The reason is that calculations are extremely sensitive to the location, direction, and magnitude of the force profile being used because very small changes to the force profile change the resultant force substantially.

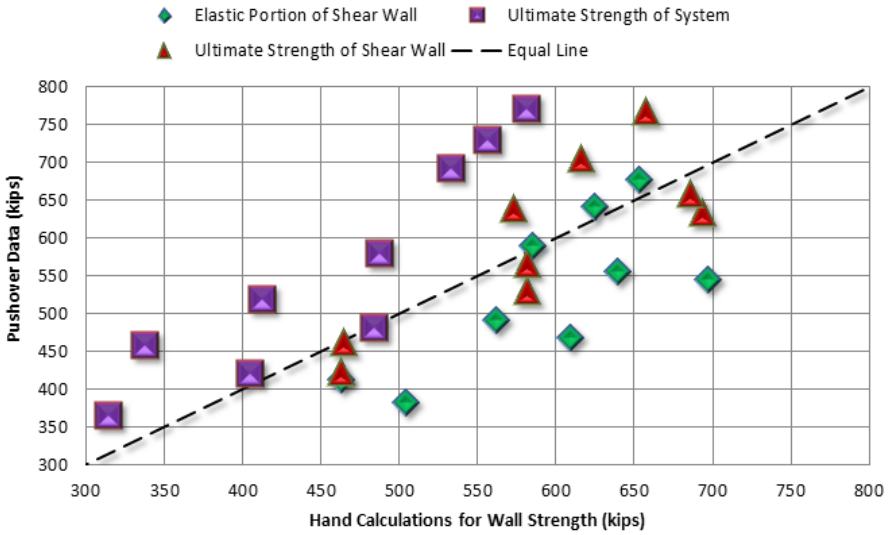

Figure 30: Wall Strength Using Force Profiles: Hand Calculations vs. Pushover Strengths

4.11. Mode Shapes and Wall-Frame Interaction

In an effort to understand if the force profiles are related to the different mode shapes of the structure, Figure 31 was developed. This plot shows the first three mode shapes for the nine story structures extracted from *OpenSees*. Visually, mode shapes appear to have a relation to the force profile. The third mode shows behavior that is most similar to the force distribution observed at the top of the structure. The second mode looks similar to the force distribution observed in pushover at the middle of the structure. Also, the first mode has similar trends to that of the lower part of the structure despite the 2nd floor.

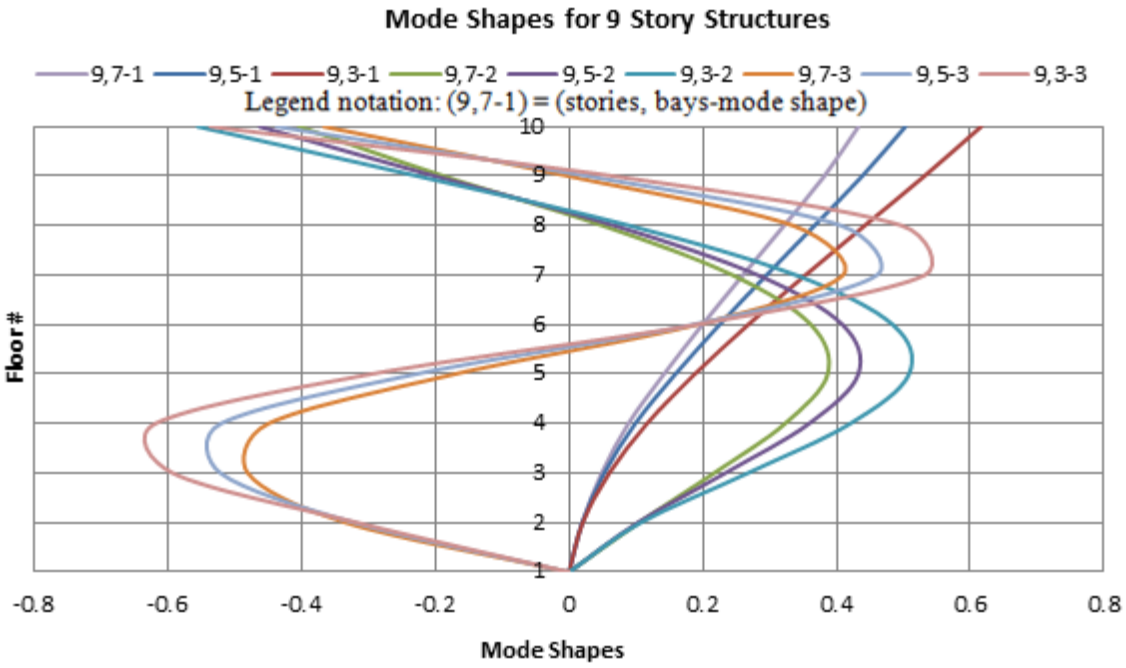

Figure 31: Mode Shapes for Nine Story Structures

Figure 32 compares the shape created by the first three modes multiplied by their participation factors, compared to the force profiles of the nine story structures, to see how the interaction forces relate to the mode shapes. Participation factors are used so that the significance of each mode is considered. The general shapes of the weighted mode shapes compared to the

force profiles are similar, but not similar enough to use for strength calculations. If the shapes were better correlated, then it might have been possible to use eigenvalue analysis to predict the interaction forces without doing a full pushover analysis.

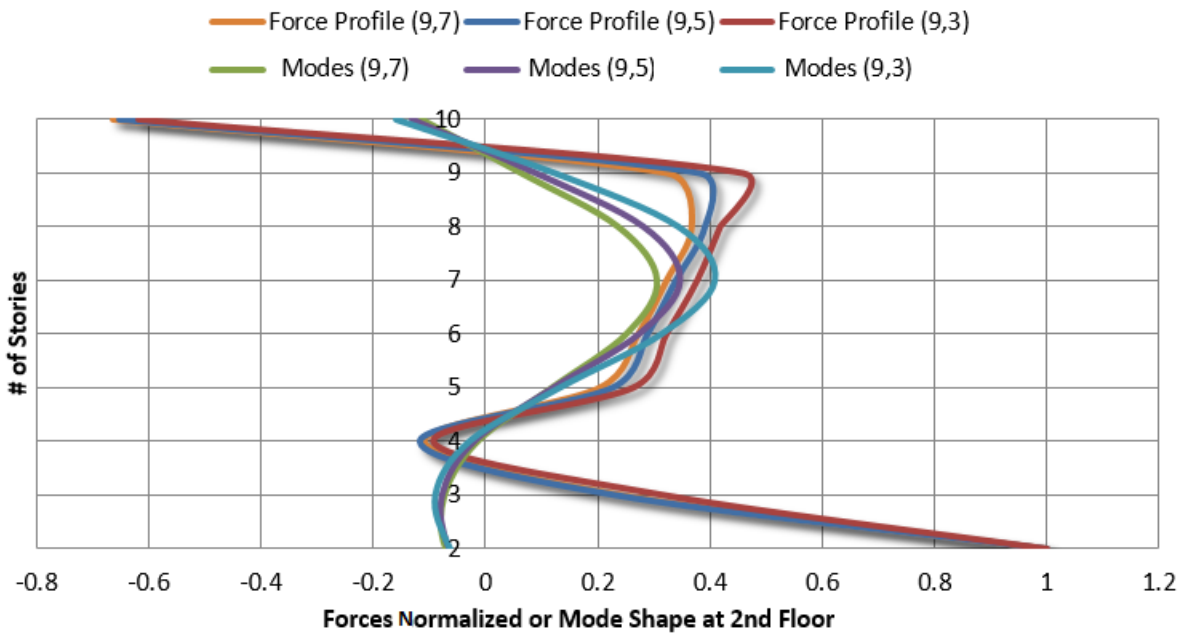

Figure 32: Compare Force Profile to Sum of First Three Modes x Participation Factors

4.12. Roof Load Reversal Sensitivity Studies

Three sensitivity studies are conducted in an effort to find a way of simply adding a reversed load to the top of the wall, which can then be used to calculate the correct strength of the wall. Only one sensitivity study is included in this thesis since all of the results are similar. Adding a reversed load to the top of the wall effectively changes the location of the resultant force which is used to calculate the strength of the cantilever. The goal of these studies is to look into the possibility of being able to make a generalized rule to adjust the height of that resultant force.

In Sensitivity Analysis 1, the magnitude of the reverse load applied to the top of the wall calculated from -.1*.197V to -.8*.197V. Figure 33 is the visual description of the changes made to the force profile. For each load distribution used in the sensitivity analysis, similar to the loading distribution diagram in Figure 33, the hand calculations for wall strengths are computed based on this load diagram. Then the results of the hand calculations are compared to the pushover analysis results of the disaggregated wall. These results are shown in Figure 34.

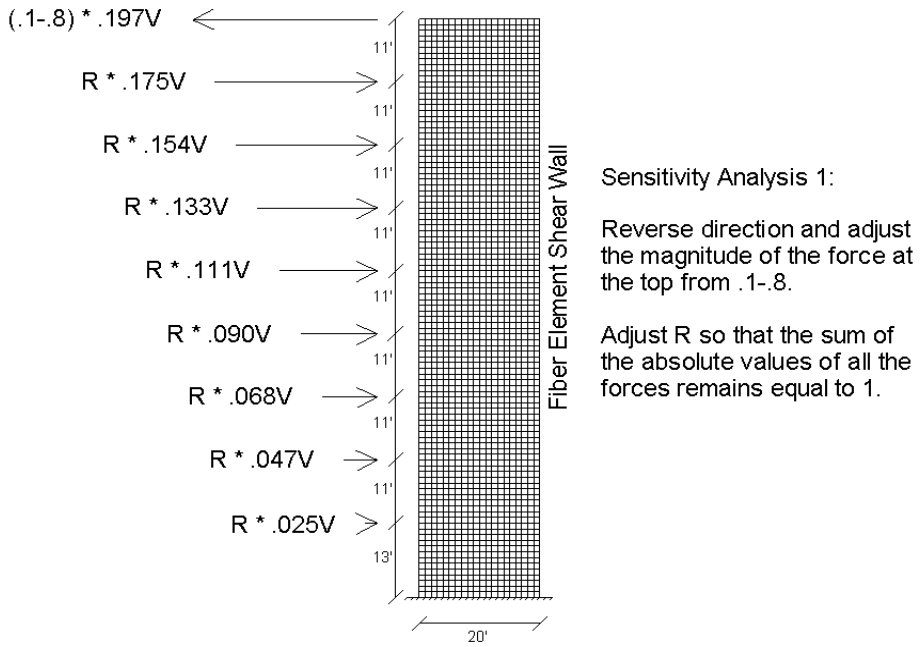

Figure 33: Visual Description of Sensitivity Analysis 1

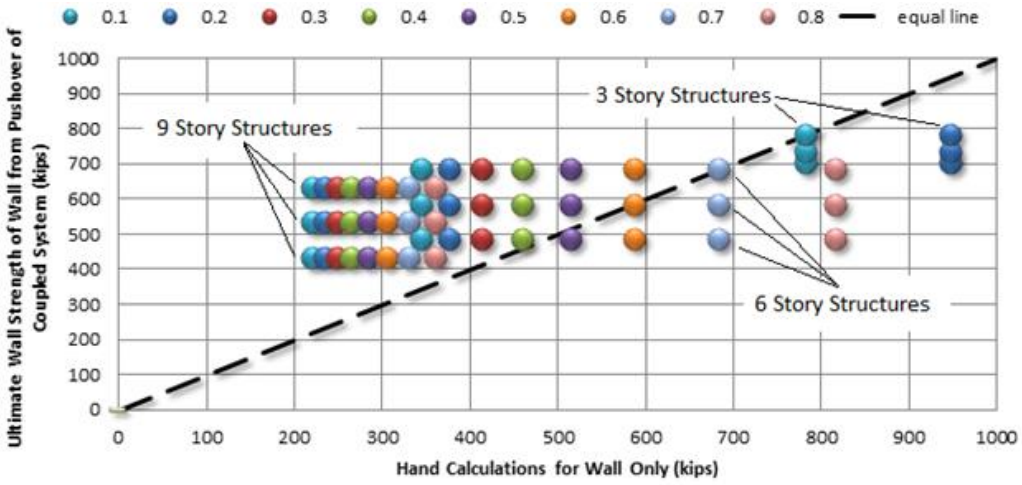

Figure 34: Strength Calculation Results of Sensitivity Study 1

The other sensitivity studies are similar to the one shown except that different variations of the interaction load are used. Results for Sensitivity Analysis 1, presented in Figure 34, are similar to the results of the other sensitivity studies and show that this is not an accurate way for calculating strength. The consideration of an interaction force at the top of the six and nine story structures makes sense because of the results of the force profile analysis. However, these sensitivity studies have not revealed a simple rule for adding the force that accurately captures strength of the disaggregated wall for those six cases. The strength differences that vary between the cantilever wall calculations and the disaggregated wall strength from pushover, which vary in accordance with the change in height and change in the number of bays in the frame, are not being estimated accurately by simply adding a load to the top of the wall. In addition, the force profiles show that there is not a load reversal for three story structures and it is unknown what the force profiles of structures taller than nine stories look like, so this method has many limitations.

4.13. MacLeod Method for Calculating Interaction Force at Top of Wall

Up until now this chapter has used force profiles, mode shapes, and load reversal at the top of the structure in effort to find an easy method to calculate the strength of the RC wall. Unfortunately, none of these methods work. Next, a method for calculating wall strength will be conducted in accordance with a method developed by MacLeod (1972). This method is designed to be an approximate method of distributing lateral load between walls and frames (MacLeod, 1972). The equation and diagram in Figure 35 helps to explain the details of the MacLeod (1972) approach. The approximate distribution of load is derived using the Component Stiffness Method, which MacLeod describes as controversial. The method approximates a relation

between an appropriate interaction force, which can be used with different loading assumptions for structural analysis, and a ratio of a single value of stiffness for the wall and a single value of stiffness for the frame. MacLeod designed this method to use for preliminary member sizing which could avoid the use of computer programs and laborious calculations (MacLeod, 1972). MacLeod highlights the point that this is only an approximation to be used for preliminary design and that for a more accurate structural analysis of the interaction between a wall and a frame that a computer program should be used.

The equation is derived by considering equal displacement at the top of the wall and the frame. The displacement of the frame is then treated as a *P* interaction force over spring of stiffness K_f, where K_f is a simplified single value of stiffness used to define the entire frame as a spring acting at that one point. The displacement of the wall is defined as the displacement of a cantilever beam with a point load at the end subtracted from the displacement of a cantilever beam with a triangular loading assumption. Simplifying and solving for P/W yields the equation in Figure 35. The *W* in the equation displayed in Figure 35 represents an inverse triangular loading pattern, *P* is the interaction force between wall and frame, and K_w and K_f are the stiffness's of the wall and frame respectively.

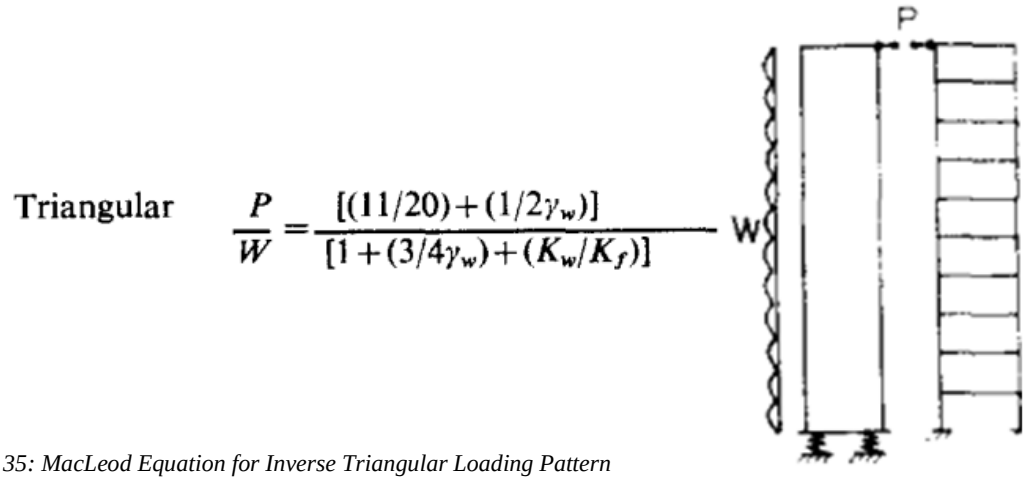

Figure 35: MacLeod Equation for Inverse Triangular Loading Pattern

The terms containing γ_w reflect the rotation at the base of the wall (MacLeod, 1972). Since the *OpenSees* models utilize fixed bases and do not consider foundation rocking, the rotation at the base of the shear wall is neglected. The equation is then reduced to Equation 5.

Equation 5: Simplified MacLeod Equation

$$\frac{P}{W} = \frac{11/20}{1 + K_w/K_f}$$

The stiffness of the wall is calculated by treating the wall as an un-cracked cantilever beam using the relation in Equation 6, where I_w is the moment of inertia of the wall, E is Young's modulus, and H is the total wall height. This equation roots from an application of Hooke's law which states the strain of an elastic body is proportional to the stress. Strain is a measure of deflection which allows the stiffness of the elastic member to be determined.

Equation 6: Stiffness of Cantilever Wall

$$K_w = \frac{3EI_w}{H^3}$$

Frame stiffness is calculated according to Equation 7 and considers the elastic behavior of the building through F_s and F_g.

Equation 7: Stiffness of Frame

$$K_f = \frac{P}{\Delta_B}$$

Equation 8: Inverse of Frame Stiffness

$$\frac{\Delta_B}{P} = \frac{h^2 H}{12EI_c} * (F_s + F_g 2\lambda)$$

where h is the average story height, H is the total building height, E is Young's modulus, I_c is the moment of inertia of the columns, λ is a geometric ratio of beams to columns, and F_s and F_g come from the chart in Figure 36. F_s and F_g are found using the s and g ratios shown in Figure

36. These are parameters developed by MacLeod which vary to account for different loading assumptions (uniform, triangular, and point) and consider the geometric relation between beam and column sizes at the base and roof of the structure. Note that the chart provided by MacLeod (1971) is limited to elastic structures. If concrete cracking is considered at the base of the structure and not at the top then *s* and *g* will be greater than 1 which will make F_s and F_g very small. Values for that situation are not available on this chart.

$$s = \text{Ratio}\ \frac{I_c \text{ at top of structure}}{I_c \text{ at bottom of structure}}$$

$$g = \text{Ratio}\ \frac{I_b \text{ at top of structure}}{I_b \text{ at bottom of structure}}$$

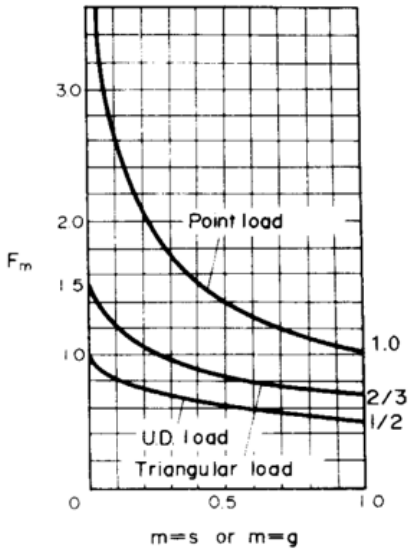

Figure 36: F_s and F_g Values for Frame Stiffness Equation

Results for the same nine-story seven-bay structure that is an example used throughout this study has a wall stiffness of 70kip/in. Considering the case where the example structure is still in the elastic region, then the example problem will yield a value of $F_s = .77\ and\ F_g = .70$, as determined from Figure 36. Now λ is calculated to be 0.180, and all of the variables can be used to calculate the frame stiffness of 54.0 kip/in. Insert all of the variables back into the

MacLeod equation permits calculation the reverse loading at the top of the wall, which is illustrated in Figure 37.

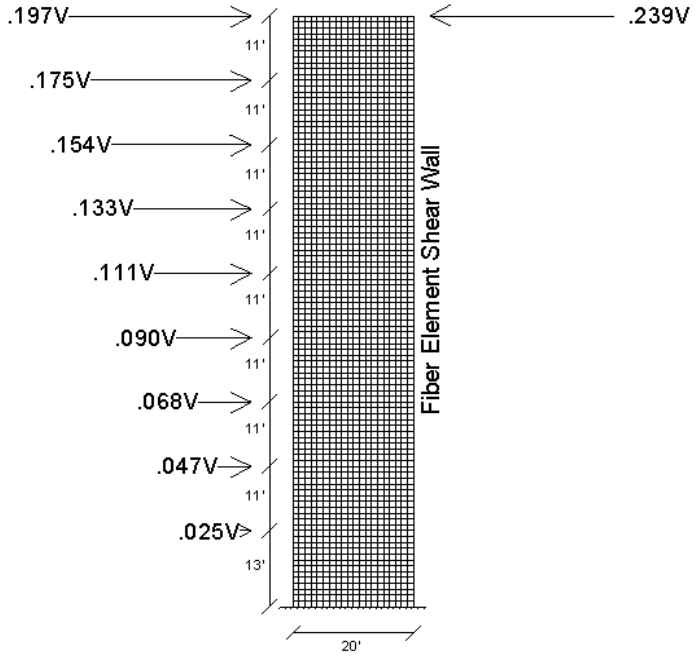

Figure 37: MacLeod Loading for Example Problem

4.14. Comparison of MacLeod Strength to Pushover Strength

Figure 38 compares the MacLeod strengths to the pushover strengths at point 1 of the pushover, as indicated by the green stars in Figure 39. Point 1 aligns with the ultimate strength of the disaggregated wall. MacLeod's equation is calibrated for elastic strength that exists somewhere before point 1, but this point was selected for plotting since is not clear exactly where the elastic range of the wall ends. Figure 38 shows a comparison of strengths calculated using the MacLeod interaction load compared to the strengths from pushover results at point 1. The arrangements of the points begin to take the shape of the black line, indicating that the equation is beginning to capture the trends with respect to height and number of bays.

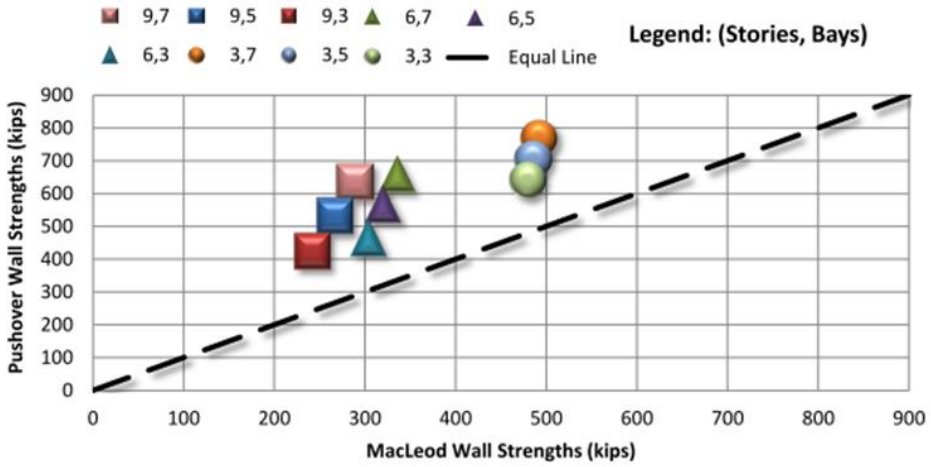

Figure 38: MacLeod Method Compared to Strength of Wall at Point 1

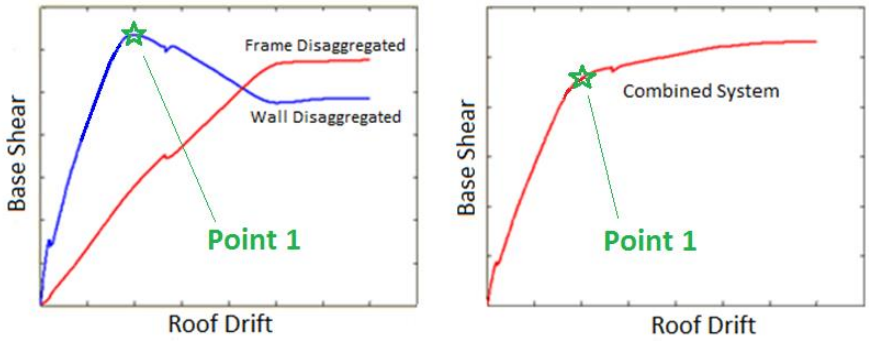

Figure 39: Pushover Points used for MacLeod Method Strength Comparison

Figure 40 compares the MacLeod method at point 2 of the pushover, the location of which is indicated by the green stars in Figure 41. The trends are better in Figure 40 than in Figure 38, but the MacLeod-based method still produces strengths lower than those from pushover. This shows that the MacLeod equation has some conservativeness built in to the calculations.

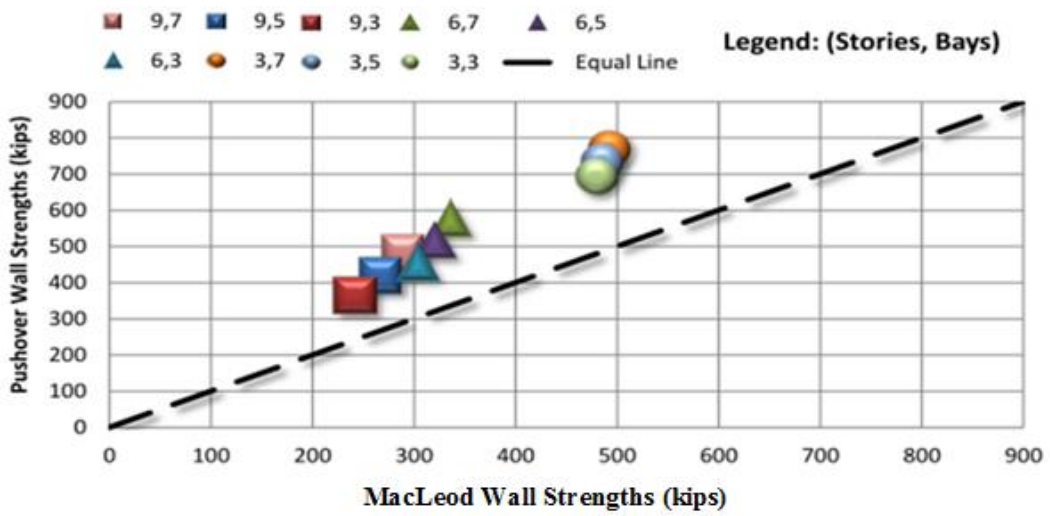

Figure 40: MacLeod Method Compared to Pushover at Point 2

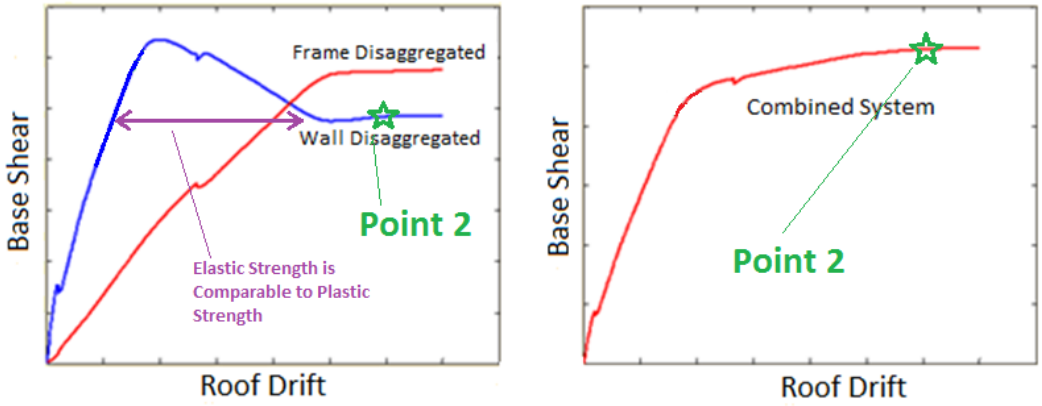

Figure 41: Location of Point 2 for MacLeod Comparison

4.15. MacLeod Sensitivity Studies

The next few sections study how the strength results of the MacLeod method vary as some of the equation variables are adjusted. All MacLeod comparisons are made to points 1 and 2, as shown in Figure 39 and Figure 41 respectively. The first adjustment made to the equation is the coefficient that accounts for the loading assumption (uniform, triangular, or point). The second adjustment made to the MacLeod equation is to change the F_s and F_g values, by assuming

cracked sections at the 1st story of the structure. This assumption is an attempt to understand how the equation could potentially be adapted to behave in the nonlinear range.

The first adjustment made to the MacLeod equation is to adjust the 11/20 coefficient. This adjustment is made by back solving what the coefficient would need to be for the strength of the largest building (9 stories, 7 bays) to exactly match the pushover results. The coefficient change is the difference between Equation 5 and Equation 9. Figure 42 shows a comparison of all of the structures calculated using the new coefficient, and compared to the pushover results at point 1. The three-story structures are less sensitive to coefficient changes than the nine-story structures since they have a greater wall to frame stiffness ratio and, as such, the coefficient is being multiplied by a smaller number. So the conclusion is that strength calculations for wall-frame systems that are dominated by the strength of the frame are more sensitive to the details of the MacLeod approach. The results for changing coefficient are similar at point 2 so the plot is omitted in this thesis.

Equation 9: MacLeod Equation with Coefficient Adjusted for Point 1

$$\frac{P}{W} = \frac{1.12}{1 + K_w/K_f}$$

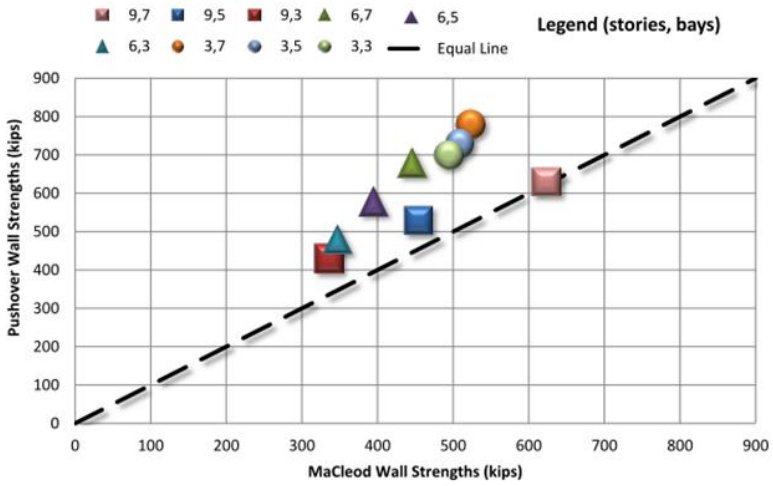

Figure 42: Change MacLeod Equation and Compare to Strength at Point 1

In the next sensitivity study, we adjust the values of F_s to adjust the MacLeod method to represent the nonlinear response of the frame. As the value of F_s becomes increasingly smaller it is representative of the columns cracking and having a smaller moment of inertia at the first story compared to the roof. The results in Figure 43 and Figure 44 are compared to points 1 and 2 respectively. As F_s becomes smaller, the equation is correctly accounting for the strength and stiffness differences between the frame and wall that vary with height and bay width of the frame. There is minimal additional change when the value of $F_s < .01$.

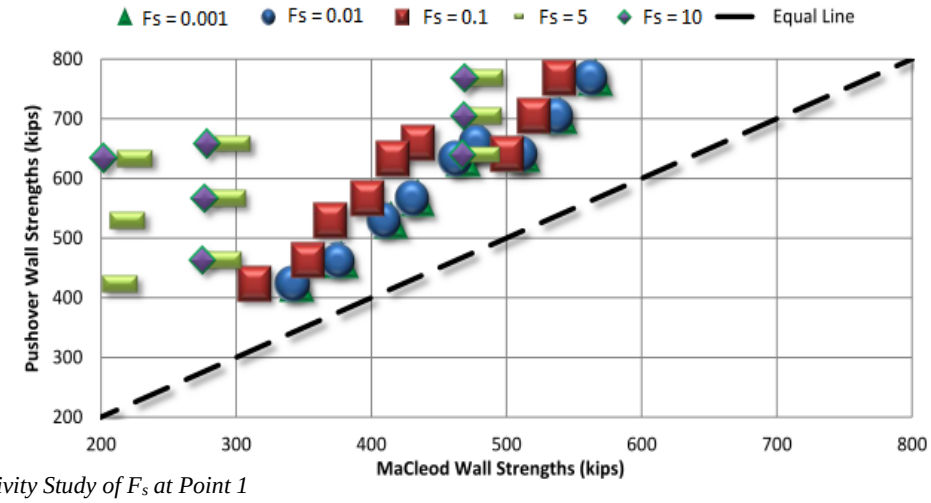

Figure 43: Sensitivity Study of F_s at Point 1

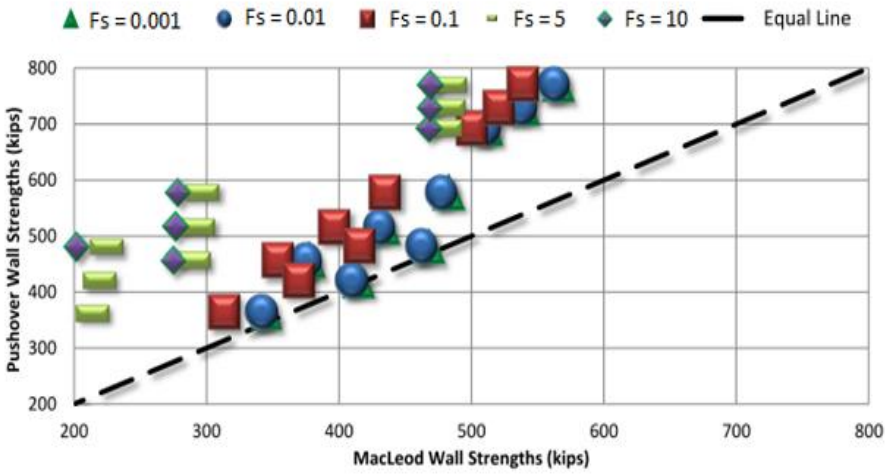

Figure 44: MacLeod Sensitivity Study of F_s at Point 2

The next sensitivity study adjusts the value of F_g. As the value of F_g grows increasingly smaller it is representative of beams cracking at the first story and remaining intact at the roof level. This is another factor that can be adjusted to account for nonlinearities, since damage is likely to start at the base fo the building. Figure 45 and Figure 46 show that the MacLeod equation is not as sensitive to changes in F_g as it was to F_s. Additionally, there is little to no change for the value of F_g being lower than 0.1.

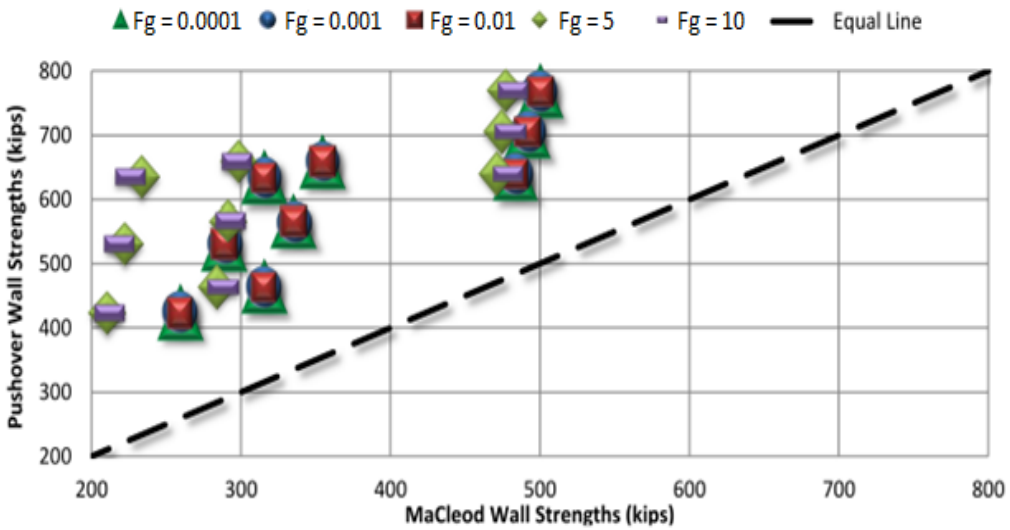

Figure 45: MacLeod Sensitivity Study of F_g at Point 1

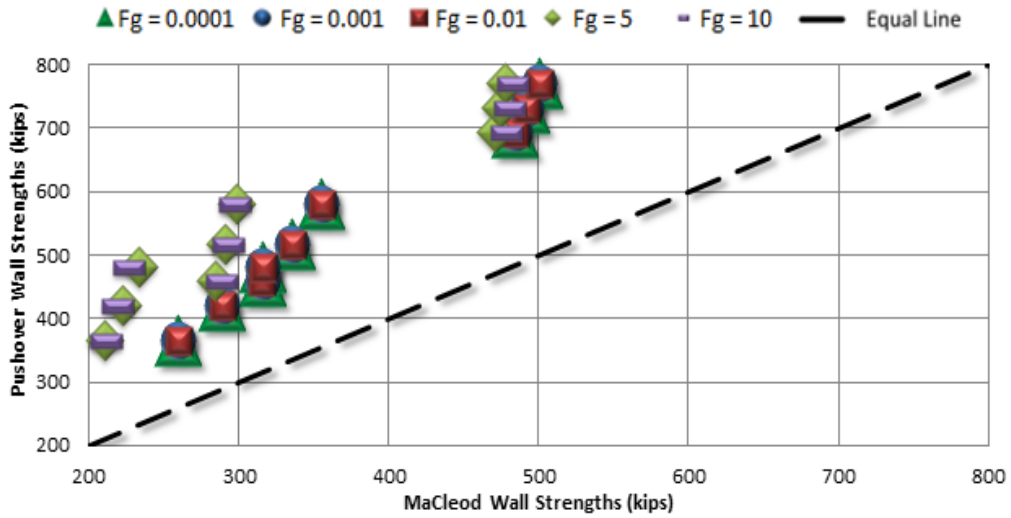

Figure 46: MacLeod Sensitivity Study of F_g at Point 2

To optimize the MacLeod equation to be nearly exact for the largest structure, the values of F_g and F_s are changed to 0.1 and 0.15. Figure 47 and shows the results of these changes. The results are not perfect, but the MacLeod method does begin to capture the two trends that affect the wall strength calculations, change in height and change in the number of bays in the frame. Due to the complexity of this method and the fact that the equations use a stiffness relation and not a strength relation it is unlikely that this method will ever be adopted by the ATC committee. ATC 78 is a strength based procedure.

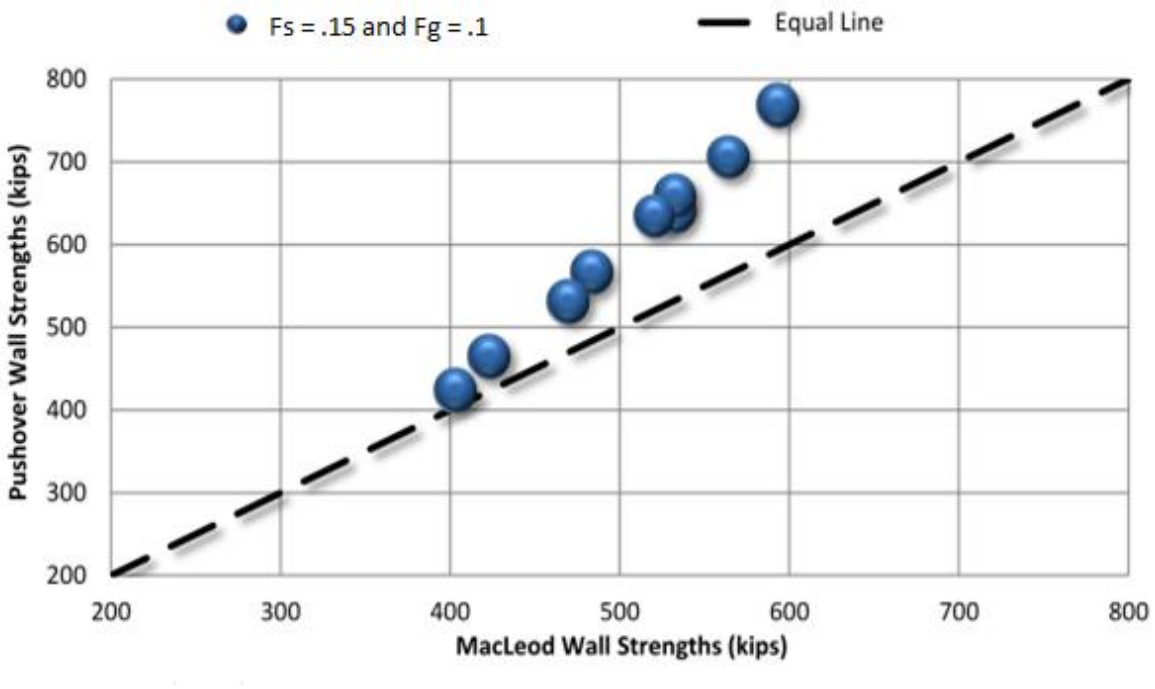

Figure 47: Sensitivity Study Conclusion at Point 1

5. Effective Period of Wall-Frame Systems

The ATC 78 methodology for calculating building period uses secant stiffness obtained from a bilinear approximation of a pushover curve that is outlined in (FEMA_356, 2000) and (ASCE_41, 2013), which is described in detail in section 5.1. To calculate effective period ATC 78 uses an assumed yielding drift ratio of 0.75% times the total height of the structure. Then, the appropriate yield strength must be estimated, which is the reason for the discussion of building strength in Chapter 4.

This chapter compares the results of a variety of different methods for calculating effective periods of the nine example buildings analyzed in Chapter 4. The major question that must be answered is: Is the roof drift assumption of .75% x the height that is used for pure frame structures acceptable for structures that also have walls? Shear wall buildings are stiffer than frame buildings, but that does not necessarily mean that the average yielding drift is a different value than a pure frame system.

5.1. FEMA 356 Method for Calculating Effective Period

The effective period that the ATC 78 method roots from is the FEMA 356 recommendation of using Equation 10,

Equation 10: FEMA 356 Equation for Calculating Effective Period

$$T_e = 2\pi\sqrt{\frac{m}{K_e}}$$

For Equation 10, m is mass, and K_e is the effective stiffness. This equation represents the effective period for an equivalent single degree of freedom oscillator. To transform the equation

into a multi-degree of freedom system the yield drift is taken at 2/3 times the total height of the structure (ATC 78, 2014). Assuming a linear relation between building height and yielding displacement then taking 2/3 x δ_y can be used in the FEMA 356 equation. Please reference Equation 11 and Equation 12.

Equation 11: Effective Stiffness

$$K_e = \frac{V_y}{\delta}$$

For Equation 11, V_y is yield strength obtained from bilinear approximation of pushover results, and δ is lateral displacement adjusted to turn the SDOF oscillator equation into a MDOF system,

Equation 12: Adjustment Made to Yield Drift to Change SDOF Oscillator into MDOF System

$$\delta = \frac{2}{3}\delta_y$$

For Equation 12, δ_y is the yielding displacement obtained from bilinear approximation of pushover results.

Yielding displacement δ_y and yielding strength V_y are obtained from the FEMA 356 recommended bilinear approximation of the pushover plot shown in Figure 48. In this method, the secant stiffness can be determined by positioning one point of the vertical part of the bilinear line to intersect the pushover curve through 60% of the ultimate strength. The right point of the horizontal part of the bilinear line should be positioned at the ultimate strength of the system, and then the areas above and below the pushover curve are balanced to reveal the recommended δ_y and V_y. To compute the K_e required for Equation 10, only two-thirds of the δ_y should be used to account for a MDOF structure. Mass is determined by considering how much of the structure is laterally supported by the system. In this case the lateral force resisting system is for one-half of

the structure, and thus *m* in Equation 10 is the mass of half of the structure. Note that this is the same example pushover curve that is in Figure 21, with the addition of the bilinear approximation curve.

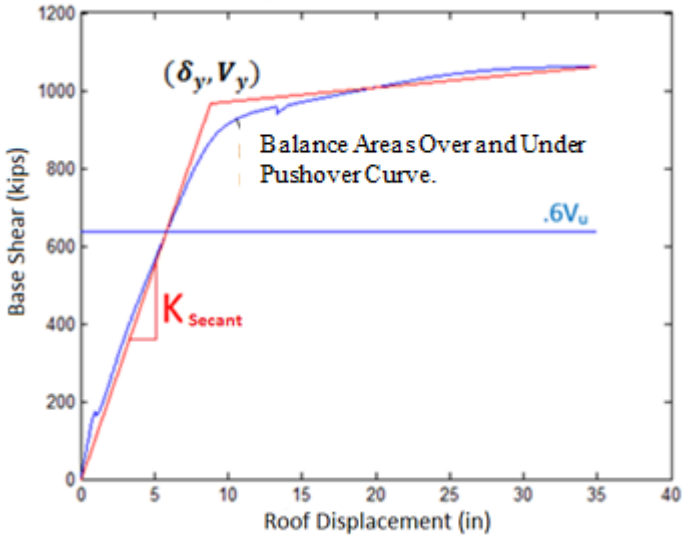

Figure 48: Obtaining Secant Stiffness from Bilinear Approximation of Pushover Curve

5.2. ATC 78 Method for Calculating Effective Period

The ATC 78 equation for calculating the effective period of a pure frame structure is shown in Equation 13. It is unknown at this time whether this equation is suitable for wall-frame systems.

Equation 13: ATC Equation for Calculating Effective Period

$$T_e = 0.078\sqrt{\frac{h_n W}{V_y}}$$

For Equation 13, h_n is the total height of the structure, W is the weight of the structure tributary to the frame and wall, and V_y is the yield strength derived from the pushover curves.

Equation 13 is derived from **Error! Reference source not found.** using a yielding drift ssumption of .75% x height equal at 2/3 the total height of the structure, both assumptions that are considered in the *0.078* coefficient and shown in the derivation presented in Equation 14.

Equation 14: Derivation of ATC 78 Effective Period from FEMA 356 Effective Period

$$T_e = 2\pi\sqrt{\frac{m}{K_e}} = 2\pi\sqrt{\frac{mg}{V_y g/\delta_y}} = 2\pi\sqrt{\frac{mg}{V_y g/(.0075\left(\frac{2}{3}\right)h_n)}} = \frac{2\pi\sqrt{\left(\frac{2}{3}\right).0075}}{\sqrt{32.2}}\sqrt{\frac{h_n W}{V_y}} = 0.078\sqrt{\frac{h_n W}{V_y}}$$

The comparison between ATC 78 (Equation 13) and FEMA 356 (Equation 10) will allow quantification of the error in the .0075 drift ratio assumption to be determined, thus helping to determine if this equation is suitable for wall-frame systems.

5.3. Periods from Instrumented Buildings

The final period comparison used investigates recommendations provided by Chopra (1998). Chopra developed these periods using building acceleration data recorded during the Northridge Earthquake (Chopra, 1998). Chopra (1998) then provides equations for elastic periods, as opposed to effective periods that are used in the FEMA and ATC equations, since the recorded data used was from buildings that never left the elastic range during the earthquake.

Chopra provides lower end and upper end equations, which are presented in Equation 15 and Equation 16. It should be noted that the low end Chopra equation presented in Equation 15, is the same equation that has been adopted by ASCE 7-10 (equation 12.8-9) for shear wall design purposes. ASCE 7-10 has adopted this equation because it is simple, conservative, and elastic.

Equation 15: Low End Chopra Period Calculation

$$T_L = .0019 \frac{1}{\sqrt{\overline{A}_e}} H$$

Equation 16: Upper End Chopra Period Calculation

$$T_U = .0026 \frac{1}{\sqrt{\overline{A}_e}} H$$

For both equations, *H* is the total height of the building above the foundation, and $\overline{A}_e$ is shear area of the wall expressed as a percentage of plan area (Chopra, 1998).

Figure 49 is from (Chopra, 1998), and shows how the T_U and T_L equations presented in Equation 15 and Equation 16, relate in comparison to the accelerometer data that was collected. The coefficients in the Chopra equations are developed from this experimental data and the results work well for that data. However, Chopra notes that the most useful data necessary to create these curves is hard to come by because the building needs to shake strong enough to reach the end of the elastic region, but not go into the inelastic region (Chopra, 1998). Most of the buildings that he used in creating these plots do not fall into that category, and therefore these equations may be on the low side, which is conservative for force-based design methods, but not necessarily conservative for drift prediction, which is the goal of ATC 78.

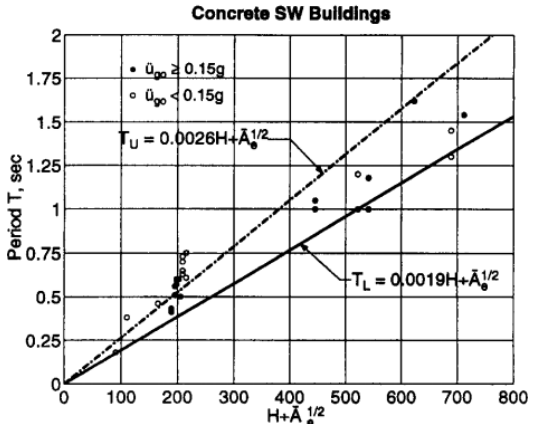

Figure 49: Upper and Lower End Period Approximations from Chopra Paper

Figure 50 shows elastic period values derived from an eigenvalue analysis for each of the nine buildings in the study compared to Chopra's two equations. The elastic periods are not calculated using the FEMA or ATC equations, only eigenvalue analysis for this plot, and are represented by the black dotted line. The elastic periods are then compared to the elastic periods calculated using Chopra's Equation 15 and Equation 16, which are represented by the red and blue lines. If the Chopra equations were unbiased then the black line would land in the middle of the red and blue lines. This is not the case because the Chopra equations are too low, as indicated by Chopra (1998).

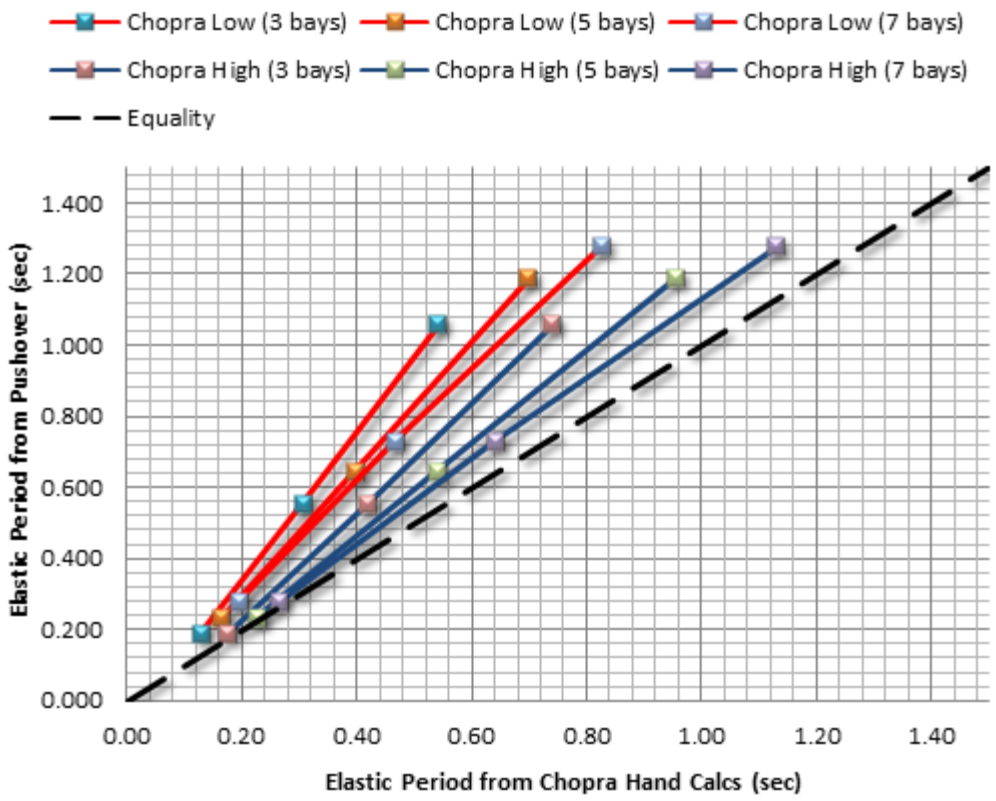

Figure 50: Elastic Period Comparison of Chopra vs. Pushover

5.4. Effective Period Comparison

Now, Figure 51 compares the difference between the ATC 78 effective period calculations and the Chopra low (same as ASCE 7-10) end elastic period calculations, compared to the FEMA 356 effective period calculations. The FEMA 356-based effective periods are longer than the eigenvalue periods compared in Figure 50. Trends are reasonable, but the results show that they become increasingly farther apart as the buildings gain height. These discrepancies are due to the yield drift ratio assumption of 0.0075 not being exactly correct for this case. The trend for this case is that as the building gets taller, the more error there is in using the ATC method to calculate the effective period. The Chopra values are included to demonstrate where the effective period calculations lie in respect to the elastic period calculations.

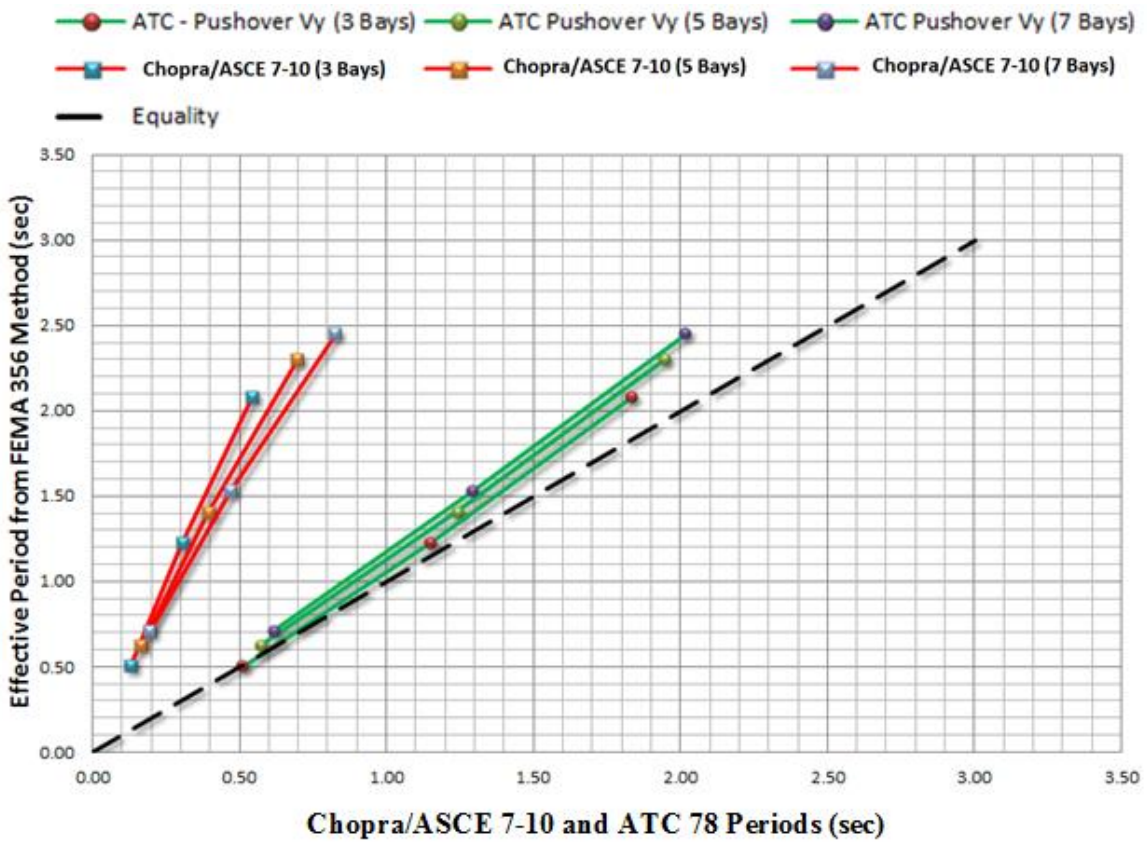

Figure 51: Compare Building Periods: FEMA vs. ATC and Chopra

6. Hand-Calculations for Building Strength

The Chapter 4 study was able to show that adding a generalized load reversal at the top of the top of the shear wall is not an accurate method to calculate the strength of a wall in a wall-frame system. Also, it showed that the MacLeod (1972) method would need to be adjusted to determine strengths outside of the elastic region, but that it does capture the correct trends in strength change due to both change in height and bay width of the structures analyzed. Then Chapter 5 showed that the .0075 drift ratio assumption used in the ATC 78 period approximation is close, but does introduce some error.

The goal of the ATC 78 methodology being developed is to build a quick and easy framework that determines the true strength of a structure, and thus being able to accurately determine the collapse risk of the structure. Therefore, instead of calculating the strength of the wall using load reversal or (MacLeod, 1972), a new engineering parameter is desired to calculate strength. The parameter utilizes a linear relation between the actual strength of the wall-frame system and simplified strength calculations of a cantilever wall and a pure frame.

6.1. The Beta Factor (New Engineering Parameter)

The end result to the search for a relation between the strengths from simplified hand calculations and the actual strength of a wall-frame system from the pushover results is shown in Figure 52. The figure relates ($V_{yw} + V_{yf}$) to $V_{y,}$ and shows that they appear to have linear relation. Here, V_{yw} is the strength obtained from using a simplified calculation for the shear wall, consistent with the method previously described in Chapter 4, V_{yf} is the previously developed ATC 78 methodology for frames only, and V_y is the actual strength from a bilinear

approximation of the pushover curve of the combined system. Bilinear approximations of all the nine buildings in Chapter 4 are included in the appendix.

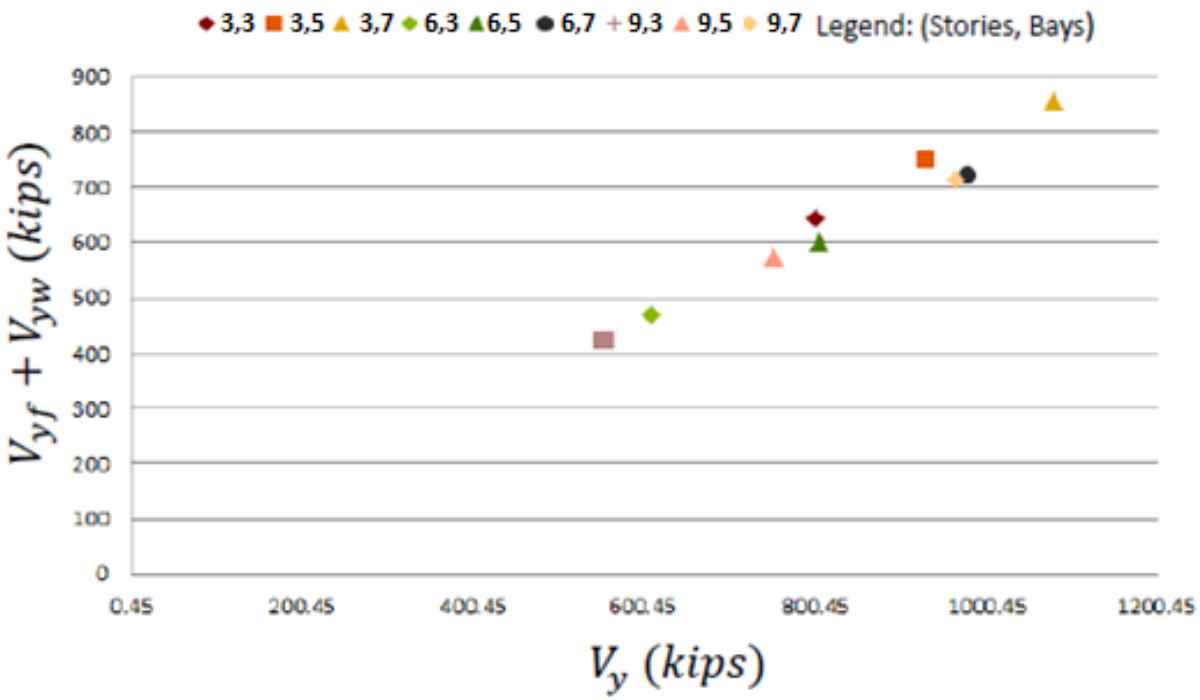

Figure 52: Linear Relation between Simplified Hand Calculations and Actual Strengths

The new engineering parameter that uses the linear relation identified in Figure 52 and is presented in Equation 17 will now be referred to as β:.

Equation 17: Beta Factor

$$\beta = \frac{V_y}{V_{yw} + V_{yf}}$$

The intended use of β is to create a multiplier that adjusts the value of the summation of the simplified hand calculations, and thus approximates the actual strength of wall-frame structures.

Figure 53 identifies β based on the results of the nine building study. The horizontal axis of Figure 53 is the ratio of the strength of the wall to the frame, from hand calculations. Note that the center of the plot is when wall strength and frame strength are equal. The left side of the plot is when the strength of the frame is greater than the strength of the wall and the far left edge represents a pure frame system. The right side of the plot is when the strength of the wall is greater than the strength of the frame and the far right side of the plot is a cantilever (pure) wall system. This plot shows that the nine buildings analyzed have system strengths that range from 24% to 36% greater than the summation of the simplified hand calculations.

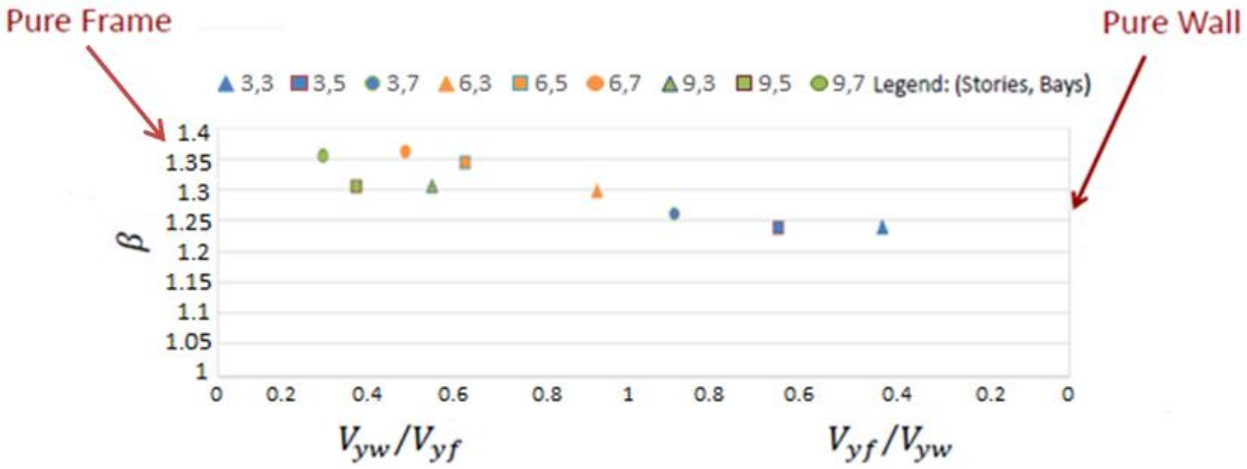

Figure 53: Preliminary β Strength Relation

6.2. New Analyses to Develop the Beta Parameter

Figure 53 contains a limited number of data points due to an insufficient array of building analyses. There are only three data points on the right side of the plot from the three story structures, and six data points on the left side of the plot from the taller structures. The foundation for the study in this chapter is to completely develop lines for the same three building heights used in the nine building study, but design structures that span the entire strength ratio

spectrum. Only the five bay structures are used for each of the three building heights and the length of the shear wall is adjusted to provide strength ratios that span the entire spectrum. In all, 37 structures with varying parameters are evaluated for strength and drift ratios of wall alone, frame alone, and the combined system. All strengths and drift ratios are based on a bilinear approximation, and the pushover results can be seen in the appendix.

Figure 54 shows β for all three heights of building analyzed for a broader range of relative wall and frame strengths. The results show that as soon as a wall is introduced to a pure frame system, there is a large strength benefit beyond the simplified strength calculation of a cantilever wall. This is because of the change of the force interaction between the frame and the wall. That strength difference peaks in walls of 10-20% of the frame strength, then the strength difference diminishes as the strength ratio increases to favor the wall (towards the right side of the plot).

Most of the focus for this study will be for structures that have wall to frame strengths ratios located more towards the left side of the plot. That is because this study is designed for wall-frame structures where both the wall and the frame resist lateral load. The far right side of the plot is representative of pure cantilever wall structures. The average β at the left side of the plot for all three lines is roughly 1.3, which will be used as one of the simplified β assumptions and later used for comparison.

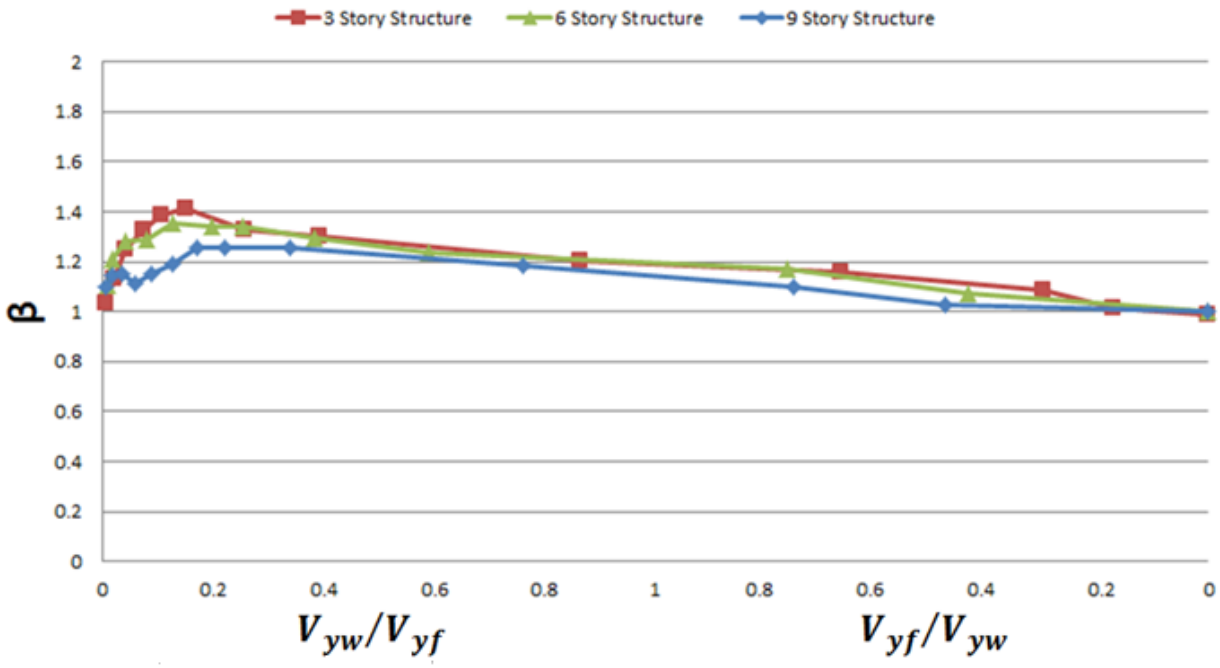

Figure 54: Fully Developed Beta Factor

6.3. Yield Drift of Flexure Wall-Frame Systems

The yield drift of a wall frame system is important since the current ATC 78 effective period calculation uses the assumption of a yielding displacement of 0.75% times the height of the structure. The yielding displacement values from bilinear approximation for all of the structures of the study in this chapter are shown in Figure 55. This plot shows that the 0.0075 yield drift ratio assumption may be appropriate for the three story structures that have 5-20% wall to frame strength ratios, but as the structure increases in height then the yielding drift assumption becomes less. This explains the difference between the FEMA 356 and the ATC 78 period approximations in Figure 51, and may lead to a reconfiguration of the .078 coefficient in the ATC 78 effective period Equation 13. The average yield drift for these structures in the

critical area (left side of the plot) is about .65% times the total height as opposed to .75% as is used for pure frame structures.

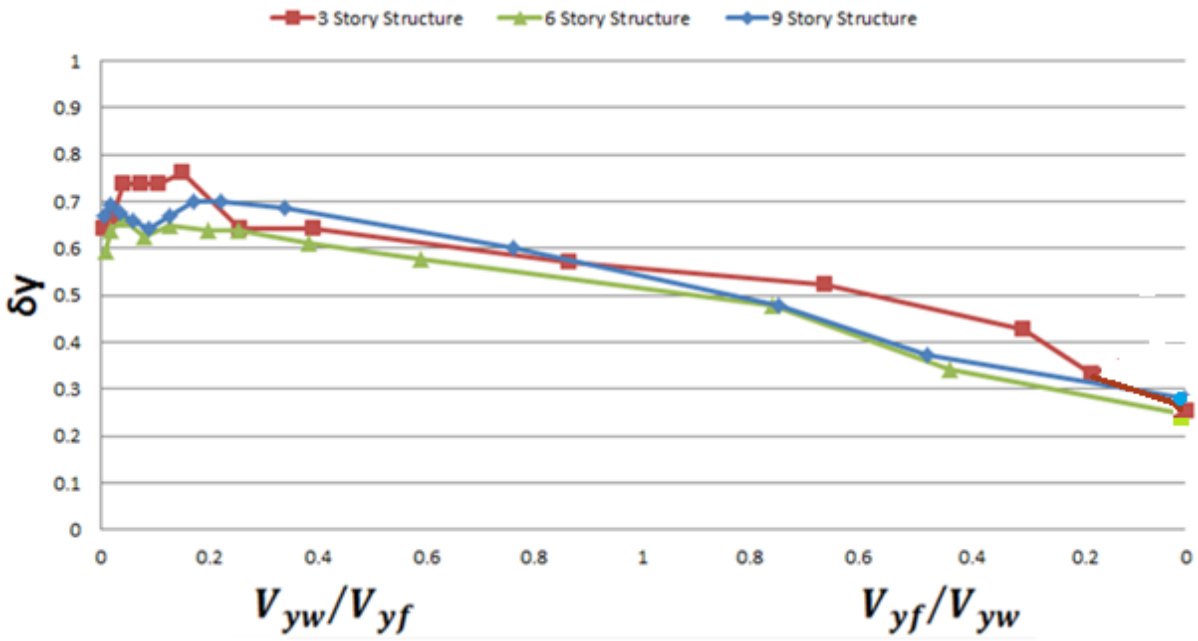

Figure 55: Yield Drift for Flexural Models

6.4. Effective Period Calculations

Figure 56, Figure 57 and Figure 58 compare effective periods calculated using both the FEMA 356 method described by Equation 10 and the ATC 78 method described by Equation 13. The β is then applied to the ATC method as described by Equation 18.

Equation 18: Using Beta with ATC Effective Period Calculation

$$T_e = 0.078\sqrt{\frac{h_n W}{V_y}}, \qquad Where \;\; V_y = (V_{yf} + V_{yw})\beta$$

Note that when β = exact, the equation uses the exact strength of the wall-frame system from bilinear approximation of pushover analysis, and is the same strength value used for K_e in the FEMA 356 equation. When β = 1.0 it represents the summation of simplified wall and frame

calculations without a strength increase, and when β = 1.3 it is a simplification of β which represents a 30% strength increase beyond the simplified hand calculations.

Differences between the red (ATC) and blue (FEMA) lines in Figure 56 reflect the error in the .75% roof drift ratio assumption used for the ATC 78 equation. To clarify, both the red and blue lines use the exact strength from pushover, so the assumption about yield drift is the only changing variable. The plots show that the differences between FEMA and ATC calculations are small towards the left side of the plots, but increase in error towards the right side of the plot where the wall is very strong and there is less drift in the models. The other values of β represented by the green and purple lines show the error in using a constant value of β with respect to the equations that use the exact strengths.

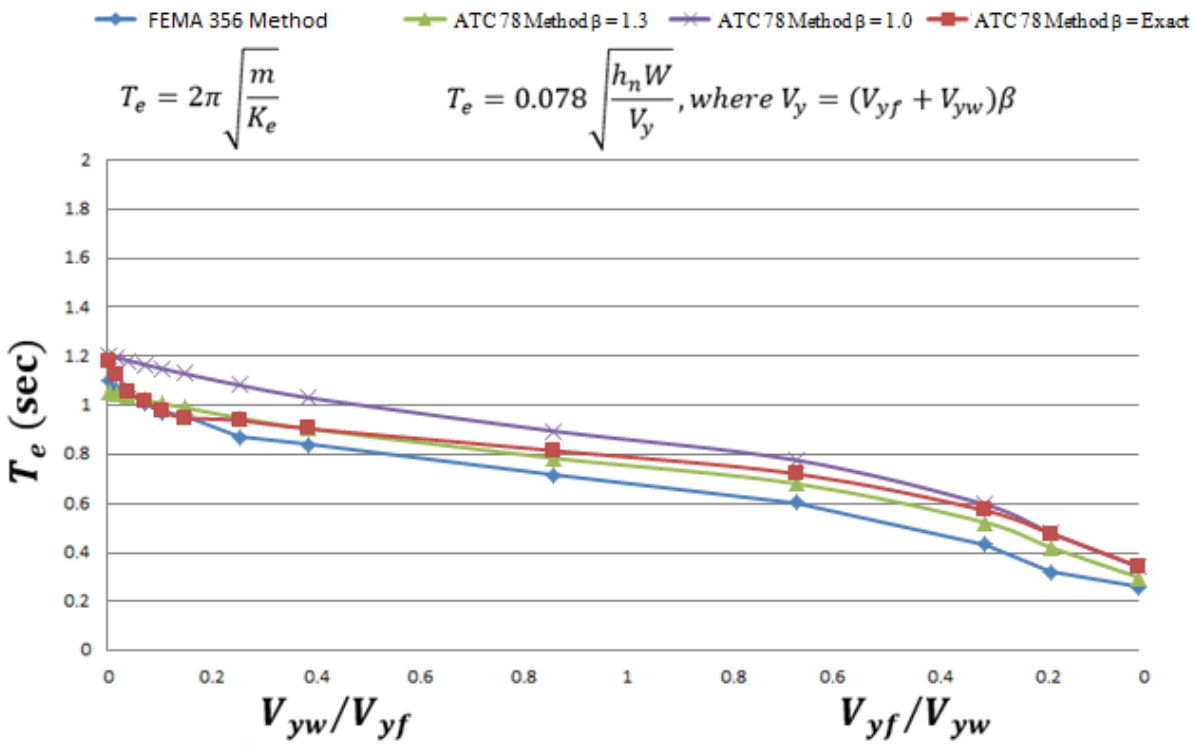

Figure 56: Period Comparison of 3 Story Structures

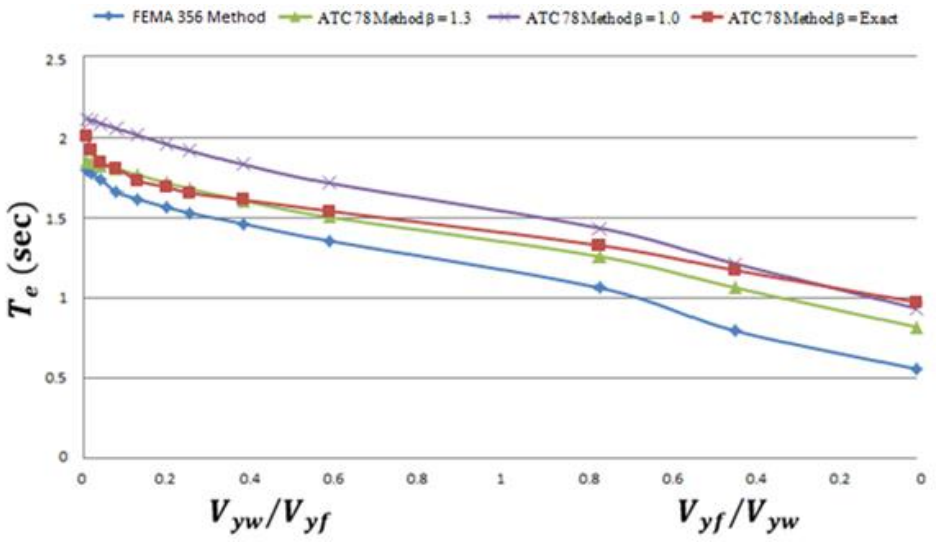

Figure 57: Period Comparison of 6 Story Structures

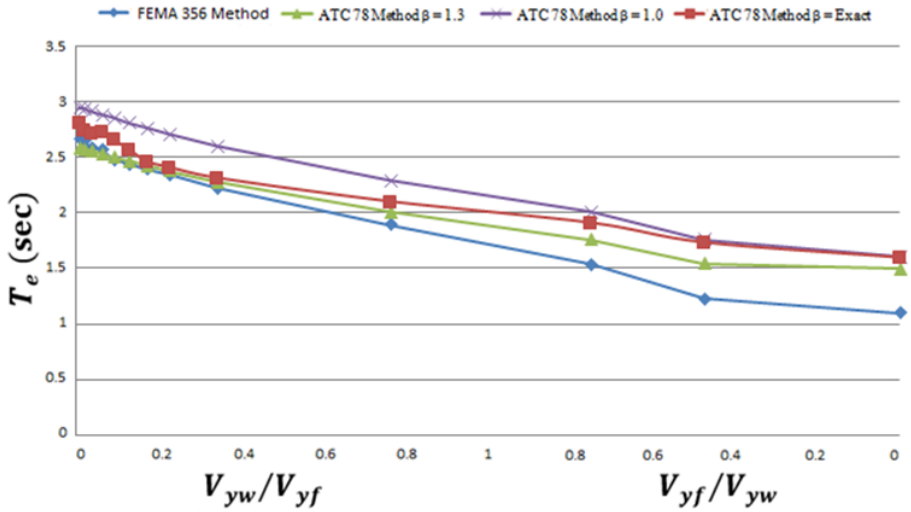

Figure 58: Period Comparison of 9 Story Structures

Based on the effective period comparison plots in Figure 56, Figure 57 and Figure 58 using a β assumption of 1.3 would be a reasonable value to use in the ATC methodology, as long as the coefficient of the effective period calculation of 0.078 was adjusted to account for less drift. This can be determined by the green line being close to the red line along the left half of the plot.

6.5. Error in Effective Period Calculations

Figure 59 shows the error in the period calculations in Figure 56 for the three story structures. The baseline comparison for this plot is the FEMA effective period calculation and the different ATC effective period calculations using different β values are compared to that FEMA 356 value. Only the left side of the plots above are considered up until the frame strength is equal to the wall strength. This is because at that point the wall is very long and the structure is very strong. The results show that using a β = exact or a β = 1.3 both have very small errors usually less than 8%. If the overstrength of the disaggregated wall over the cantilever wall calculations is not taken into account ($\beta = 1.0$) then the average error is around 20%.

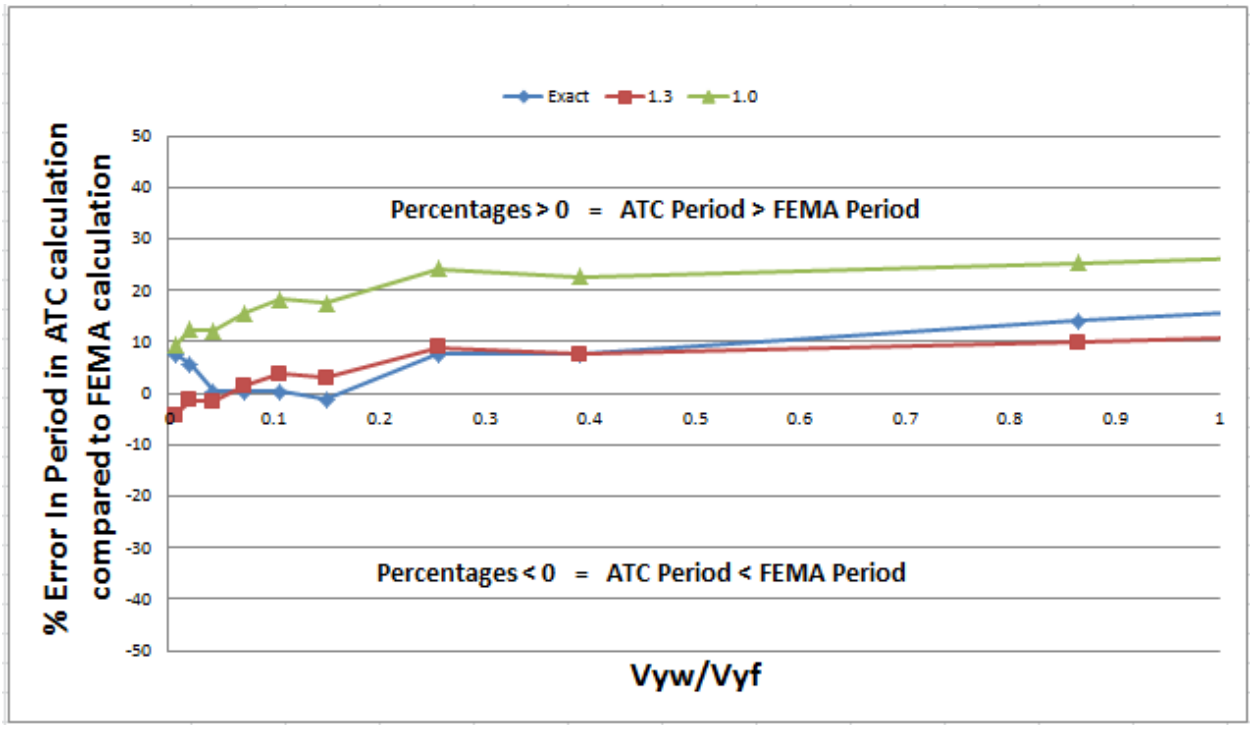

Figure 59: Error in Period of 3 Story Structure with .075% Roof Drift at Yielding

The coefficient of the ATC 78 effective period calculation can be recalibrated to consider a roof drift of .65% instead of .75%. That would change the value of the coefficient to .073 instead of .078. This is a reasonable approach since on average the wall-frame systems demonstrate less yielding drift than pure frame structures. Figure 60 shows that the average error in the period calculation will be reduced for this case, but that there is more error for situations where the wall is very short. Assuming a .65% roof drift compared to structural height is better because the maximum error is never greater than 9%, whether the period is being approximated too high or too low. The remaining plots show the same results for the six and the nine story structures.

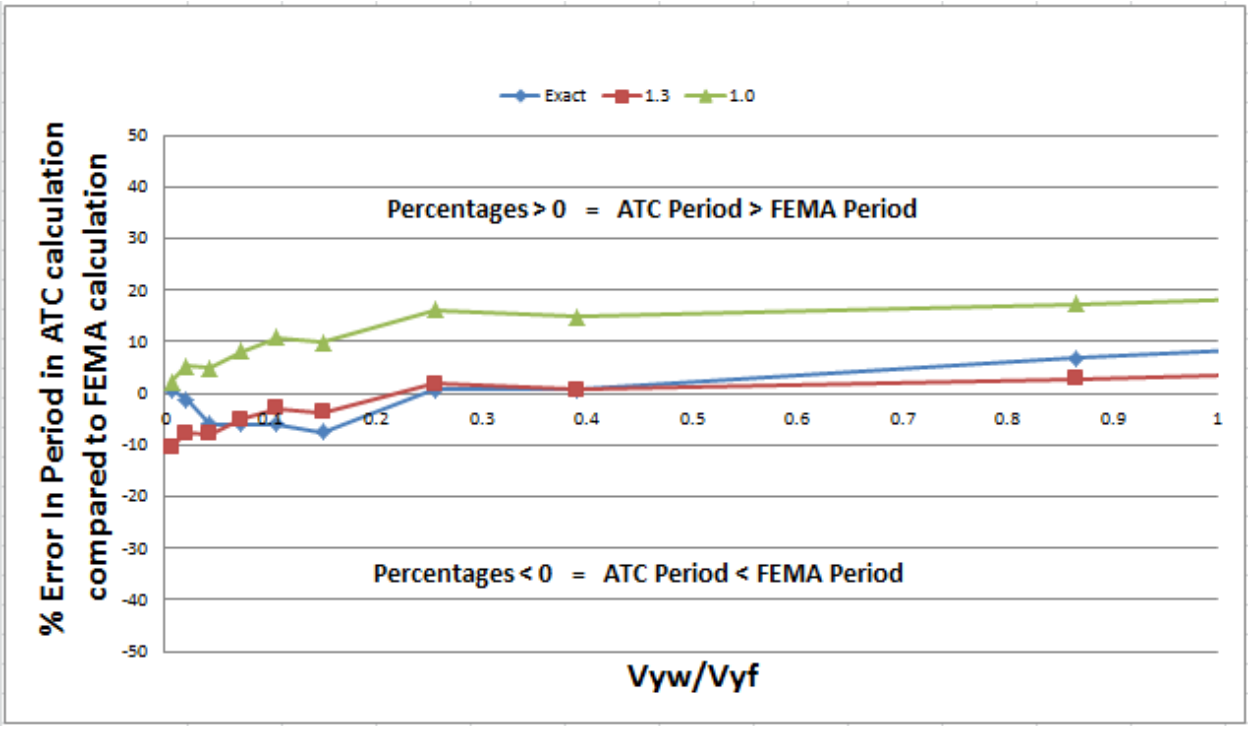

Figure 60: Error in Period of 3 Story Structure with .065% Roof Drift at Yielding

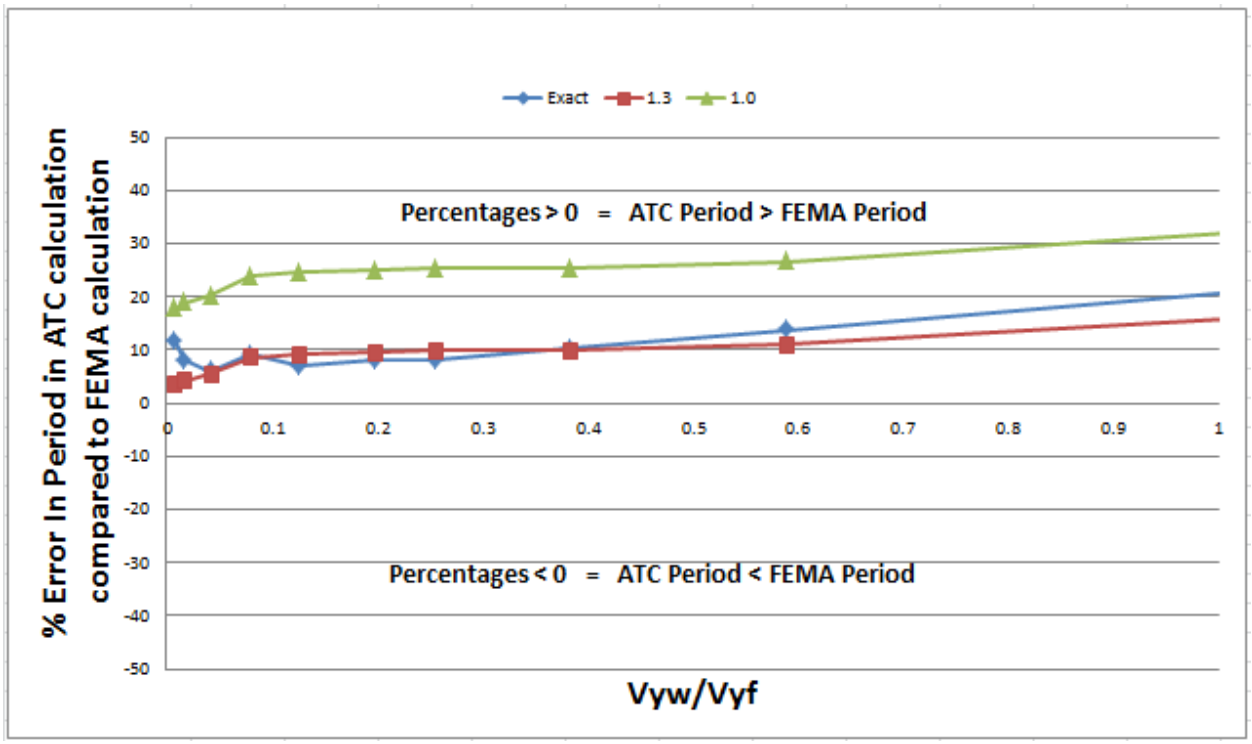

Figure 61: Error in Period of 6 Story Structure with .075% Roof Drift at Yielding

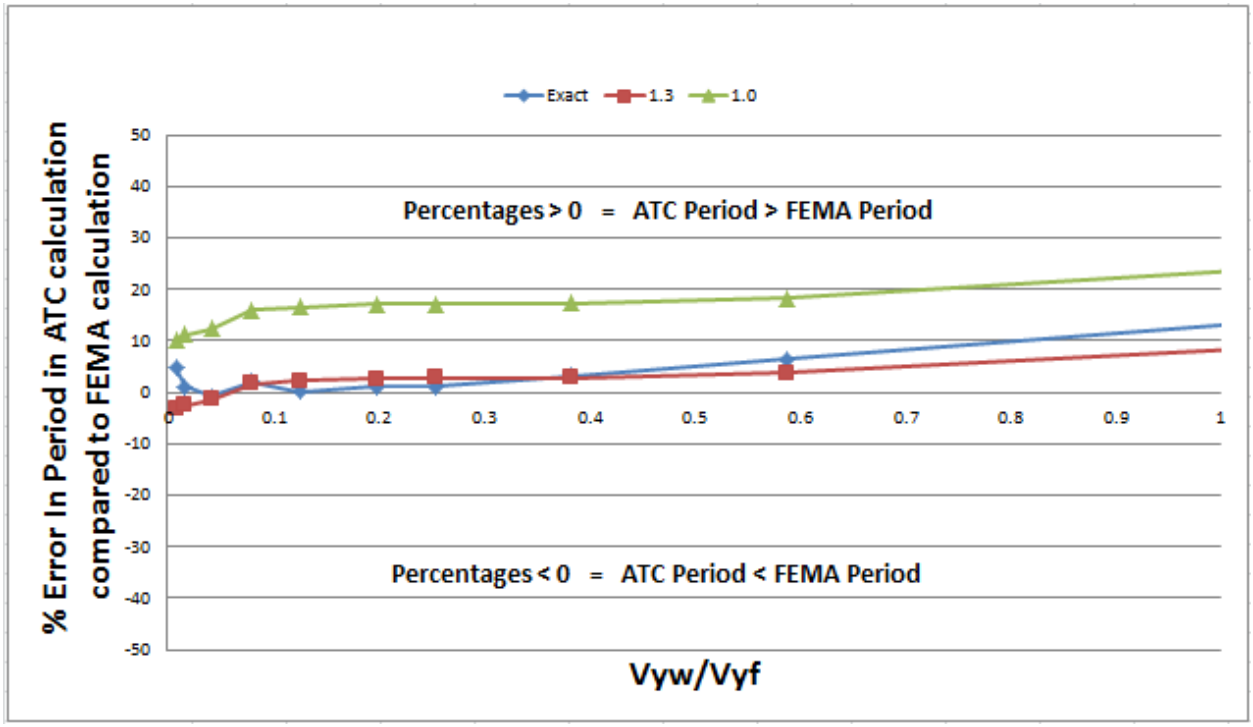

Figure 62: Error in Period of 6 Story Structure with .065% Roof Drift at Yielding

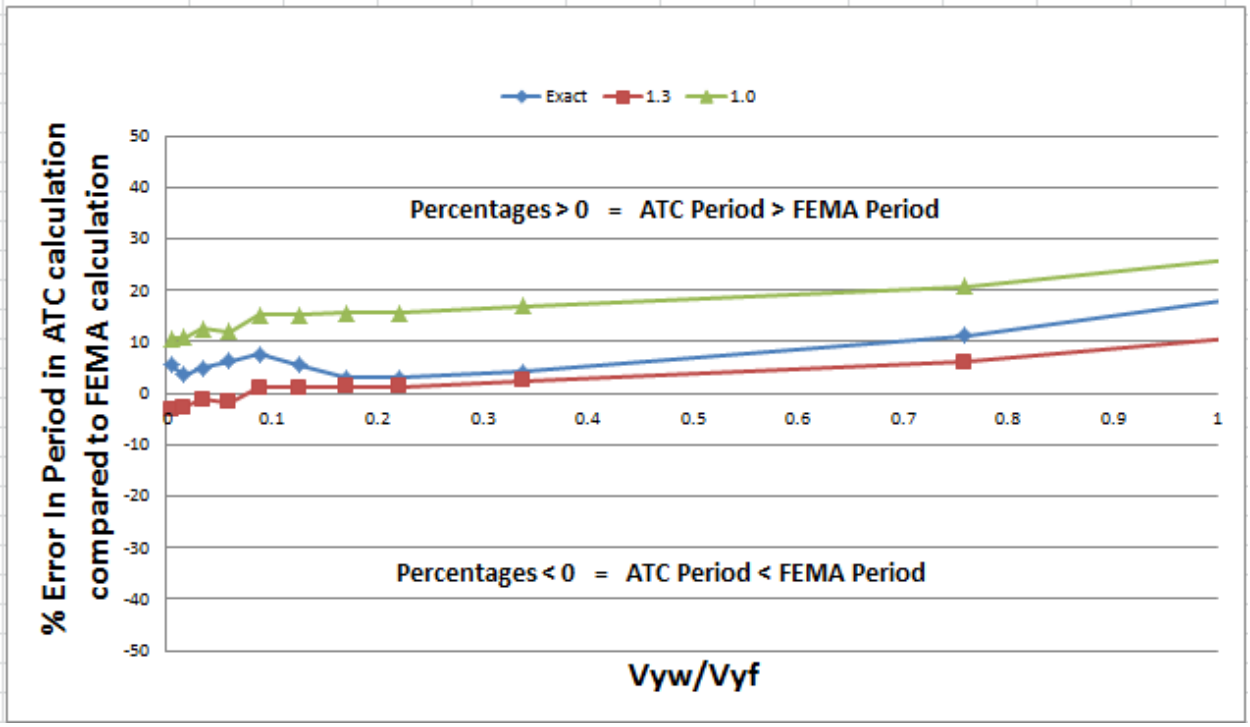

Figure 63: Error in Period of 9 Story Structure with .075% Roof Drift at Yielding

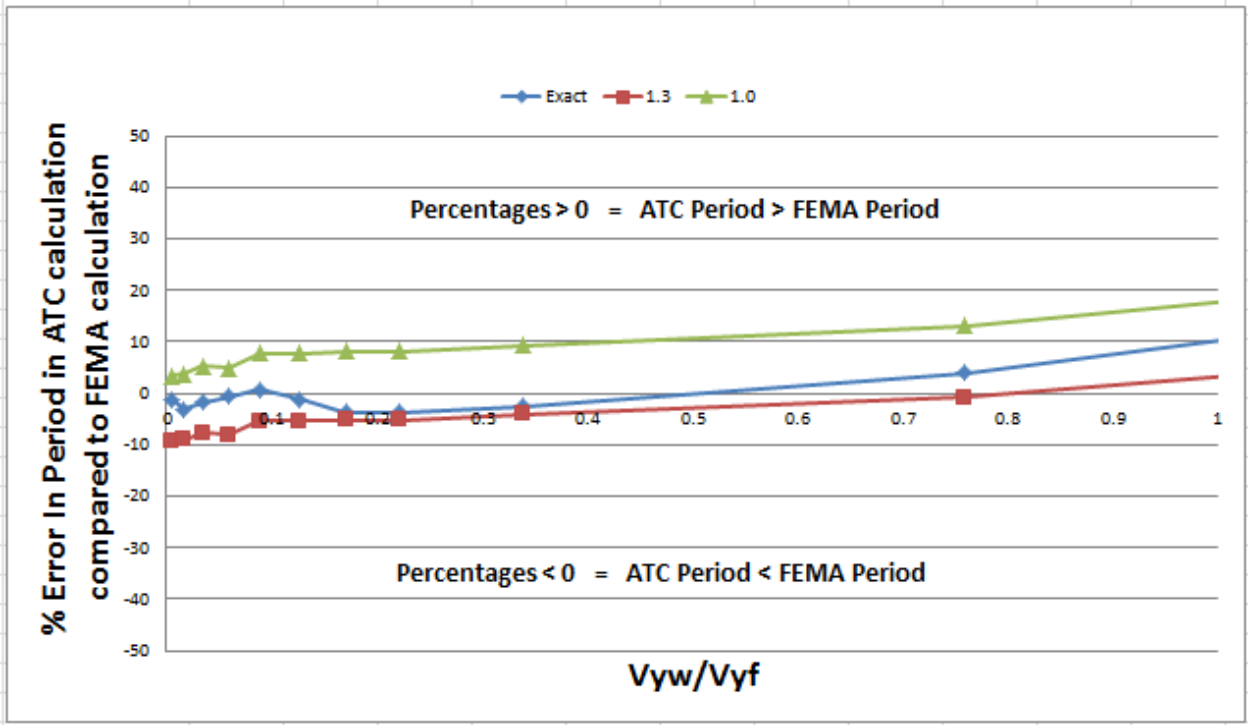

Figure 64: Error in Period of 9 Story Structure with .065% Roof Drift at Yielding

7. Conclusions, Limitations, and Future Work

Work produced for this thesis has led to the development of one possible solution for improving the existing ATC 78 RC frame methodology to include RC walls. A recommended procedure of how the methodology should be updated and organized, based on the findings in this body of work, is outlined in the following section.

7.1 Recommended Amended Procedure for Wall-Frame Period Calculations

- Step 1: Determine strength (V_{yf}) of columns using existing ATC 78 methodology.

- Step 2: Use simplified hand calculations to analyze the flexural strength ($V_{yw,flexure}$) of the wall, treating it like a cantilever beam and using an inverse triangular loading assumption as outlined in Section 4.2.

- Step 3: Determine shear strength of wall ($V_{yw,shear}$). (Method still being developed)

- Step 4: determine the strength of the wall (V_{yw}) using Equation 19, based on the governing failure mode

Equation 19: Determine Unmodified Strength of Shear Wall

$$V_{yw} = min(V_{yw,flexure}, V_{yw,shear})$$

- Step 5: Determine value of β based on results of Equation 19.
    - If *min* = $V_{yw,flexure}$ then β = 1.3, and if *min* = $V_{yw,shear}$ then β = 1.0.

- Step 6: Determine yield strength (V_y) of entire structure using Equation 20.

Equation 20: Yield Strength of Structure

$$V_y = \beta * (V_{yf} + V_{yw})$$

- Step 7: Determine effective period of the structure using Equation 21.

Equation 21: Calculate Effective Period of Structure

$$T_e = \alpha \sqrt{\frac{h_n W}{V_y}}$$

Where, h_n is the total height of the structure, W is the seismic weight, and α = .078 when $\frac{V_{yw}}{V_{yf}} \leq .15$ or α = .073 when $\frac{V_{yw}}{V_{yf}} > .15$

- Step 8: Use effective period to determine the demand on the structure and continue to use previously developed ATC 78 methodology.

7.2. Limitations and Future Work

This methodology is not yet complete due to uncertainties that arise from to different potential behaviors of RC walls that depend on their design and construct. These potential behaviors could include foundation rocking, bond slip, rebar yielding above and/or below the foundation, rebar de-bonding, out of plane bending, torsional effects, axial capacity, etc. Any one of these factors, and other factors not listed, can affect wall strength and drift values. The different effects that each of these potential behaviors will have on the system as a whole can lead to either conservative or non-conservative error in effective period approximation.

Another limitation to this research is that this body of work has only considered wall-frame systems where both the wall and the frame are designed to resist lateral forces. To better understand the behavior of wall only systems similar research should be conducted using a weaker frame, like those designed with thick beams and skinny columns. Frames that exhibit these characteristics are like those designed to resist gravity loads only and not lateral loads. Sometimes designers use this design tactic to achieve an architectural vision and thus making the structures especially prone to shear failure in the columns, which can then lead to building collapse. Additional research will better tell the story of systems that are dominated by wall strength as opposed to these systems that are dominated by frame strength.

Furthermore, all of the analyses used in this work only consider the effects of a 10" thick wall and all of the walls use the same rebar layout which does not include well confined regions or singly reinforced slender sections. It is unknown how thinner or thicker walls constructed using more or less reinforcement will affect these results. The ductility of the wall may also be important. Likewise, all of the work conducted only considers 3, 6, and 9 story tall structures. It is unknown how structures below or above these heights may behave differently.

The RC frames considered in this research are flexure dominated and not designed to experience shear or axial failure. In addition, the beam-column moment strength relations are set at $M_c/M_b = 1.0$. This means that failure is confined to the columns and is controlled by flexure do the $V_p/V_n = 0.6$. Further research into a shear controlled frame acting with a flexural dominated wall and a shear controlled frame acting with a shear controlled wall should also be conducted to determine how weaker frames are affected by the influence of the RC wall.

References

Arteta, C., Parra, P., & Moehle, J. (2015). *Modeling Criteria of Flexural Walls as Part of Frame-Wall Systems.* University of California, Civil and Environmental Engineering, Berkeley.

Arteta, C., Parra, P., & Moehle, J. (2015). *Modeling Criteria of Flexural Walls as Part of Frame-Wall Systems.* University of California, Civil and Environmental Engineering, Berkeley.

ASCE. (2010). *Minimum Design Loads for Buildings and Other Structures.* Reston, Virginia: American Society of Civil Engineers.

ASCE_41. (2013). *Seismic Rehabilitation of Existing Buildings.* Reston, Virginia: American Society of Civil Engineers.

ATC 78. (2014). *Seismic Evaluation of Older Concrete Frames for Collapse Potential.* Redwood City: FEMA.

Bond-slip Model to Capture Strain Penetration Effects. (s.d.). Tratto da Pantherfile: https://pantherfile.uwm.edu/jzhao/www/Bond_SP01_pages/Bond_models.html

Chopra, R. K. (1998, April). Period Formulas for Concrete Shear Wall Buildings. *Journal of Structural Engineering*, 426-433.

Elwood, K. J. (2004). Modeling Failures in Existing Reinforced Concrete Columns. *Canadian Journal of Civil Engineering*, 846-859.

FEMA_356. (2000). *356 Prestandard and Commentary for the Seismic Rehabilitation of Buildings.* Federal Emergency Management Agency. Reston: American Society of Civil Engineers.

Galanis, P. H., & Moehle, J. P. (2014, May 15). Development of Collapse Indicators for Risk Assessment of Older-Type Reinforced Concrete Buildings. *Earthquake Spectra*.

Hafiz. (2011, Oct. 29). *Difference Between Implicit and Explicit Solutions*. Tratto il giorno July 15, 2015 da Mathematics: http://math.stackexchange.com/questions/76902/difference-between-implicit-and-explicit-solutions

Haselton, C. B., & Wallace, J. (2009). *Simulating Seismic Structural Collapse of Reinforced Concrete Shear Wall Buildings: An Initial Pilot Study to Identify Modeling and Experimental Data Needs.* California State University, Chico.

Heidebrecht, A. C.-S. (1973, Februrary). Approximate Analysis of Tall-Wall Frame Structures. *Structural Division Proceedings of the American Society of Civil Engineers*, 199-221.

Kakavand, M. R. (2007). *Limit State Material manual.* School of Civil Engineering. Tehran, Iran: University of Tehran.

Lowes, L., Lehman, D., & Pugh, J. (1996). *Using OpenSees and Fiber Beam-Column Elements to Simulate the Earthquake Response to Simulate the Earthquake Response of Reinforced Concrete Walls.* Tratto da http://opensees.berkeley.edu/OpenSees/workshops/OpenSeesDays2012/A8_WallModelingWithBeams.pdf

Lu, X. (2015). *A Shear Wall Element for Nonlinear Seismic Analysis of Super-Tall Buildings Using OpenSees.* Beijing: Tsinghua University.

MacLeod, I. A. (1971). Equations for Deflection of Multistory Frames. *Building Science*, 25-31.

MacLeod, I. A. (1972). Simplified Analysis for Shear Wall-Frame Interaction. *Building Science*, 121-125.

Martinelli, P., & Filippou, F. C. (2009). Simulation of the Shaking Table Test of a Seven-Story Shear Wall Building. *Earthquake Engineering and Structural Dynamics*, 587-607.

Mckenna, F. (2014, August Friday). *OpenSees Wiki*. Tratto da The OpenSees Community: http://opensees.berkeley.edu/community/viewtopic.php?f=2&t=61755

Moehle, J. P., Mahin, S., & Yousef, B. (2010). *Modeling and Acceptance Criteria for Seismic Design and Analysis of Tall Buildings.* Redwood City: PEER/ATC.

Monti, G., & Spacone, E. (2000, June). Reinforced Concrete Fiber Beam Element with Bond-Slip. *Journal of Structural Engineering, 126*(6).

OpenSees Wiki. (2003). (C. a. Inc, Produttore) Tratto da Linear Elastic Planar Shear Walls: http://opensees.berkeley.edu/WebSVN/fil ... arWall.tcl

Orakcal, K., & Wallace, J. W. (2004). *Nonlinear Modeling of RC and SRC Structural Walls.* UCLA. Los Angeles: UCLA.

Orakcal, K., Massone, L. M., & Wallace, J. W. (2007). *Analytical Modeling of Reinforced Concrete Walls for Predicting Flexural and Coupled-Shear_Flexural Responses.* Los Angeles: Department of Civil and Environmental Engineering University of California.

Royal Commission. (2012). *Final Report: Volume 2 The Performance of Christchurch CBD Buildings.* Wellington, New Zealand: New Zealand Department of Building and Housing.

Saouma, V. E. (2014). *Non Linear Structural Analysis.* Boulder: University of Colorado.

Tang, Y., & Zhang, J. (2011, January). Probabilistic Seismic Demand Analysis of a Slender RC Shear Wall Considering Soil-Structure Interaction Effects. *Engineering Structures*, 218-229.

Taucer, F. F., Spacone, E., & Filippou, F. C. (1991). *A Fiber Beam-Column Element for Seismic Response Analysis of Reinforced Concrete Structures.* Berkeley: University of California.

Xiang, H. (2014). *Seismic Simulation of RC Wall-type Structures using Softened Shell Model.* Beijing Jiaotong University, School of Civil Engineering, Beijing.

Yassin, M. (1994). *Nonlinear Analysis of Prestressed Concrete Structures Under Monotonic and Cyclic loads.* Berkeley: University of California.

Appendix 1: Bilinear Approx. Pushovers for 9 Building Study

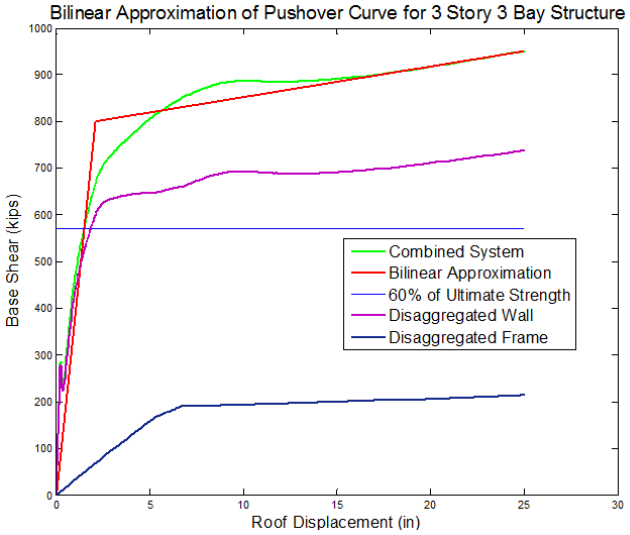

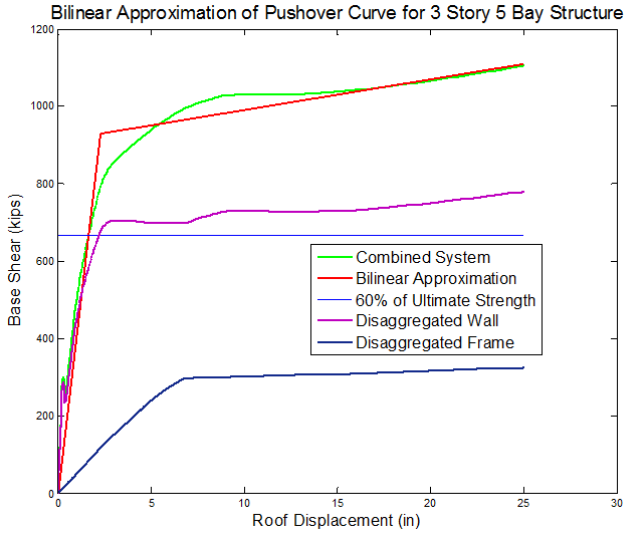

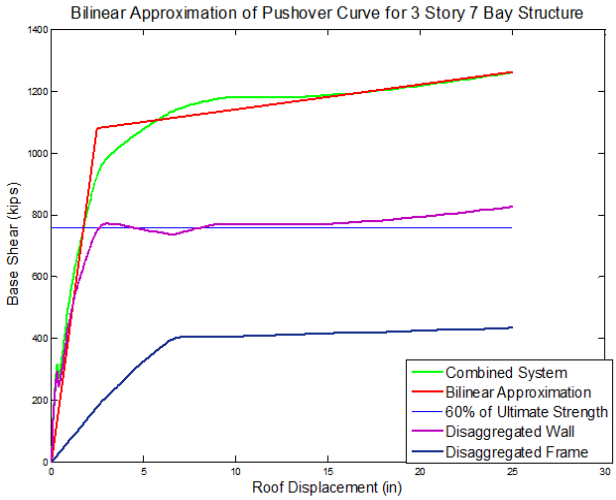

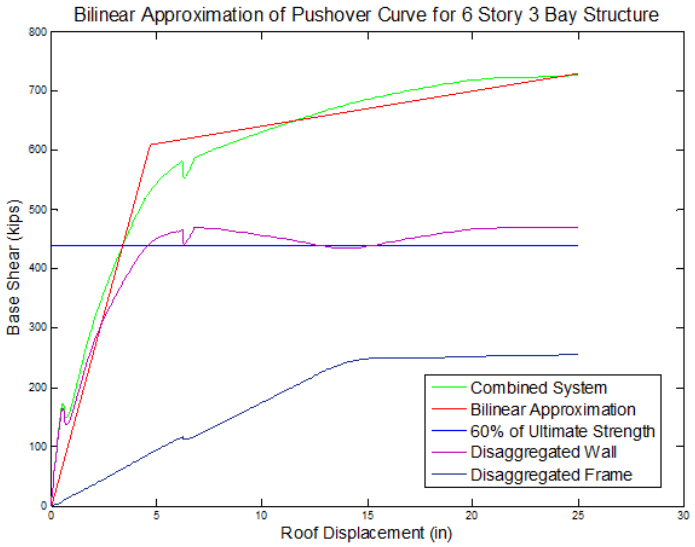
Bilinear Approximation of Pushover Curve for 6 Story 3 Bay Structure
Base Shear (kips)
Roof Displacement (in)
Combined System
Bilinear Approximation
60% of Ultimate Strength
Disaggregated Wall
Disaggregated Frame

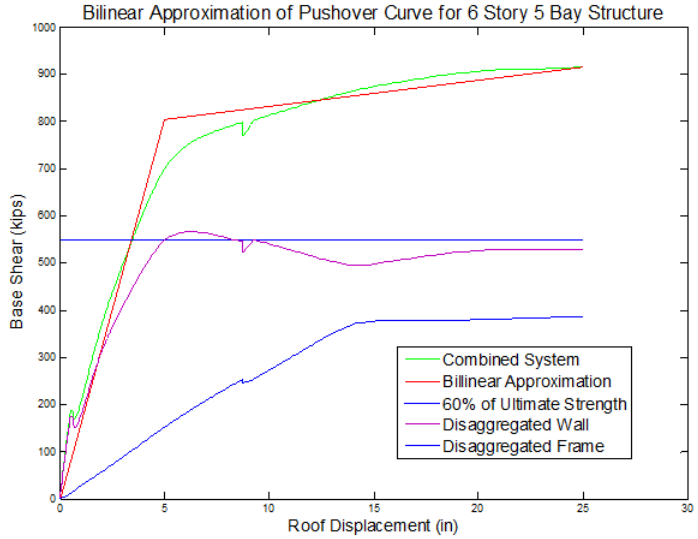
Bilinear Approximation of Pushover Curve for 6 Story 5 Bay Structure
Base Shear (kips)
Roof Displacement (in)
Combined System
Bilinear Approximation
60% of Ultimate Strength
Disaggregated Wall
Disaggregated Frame

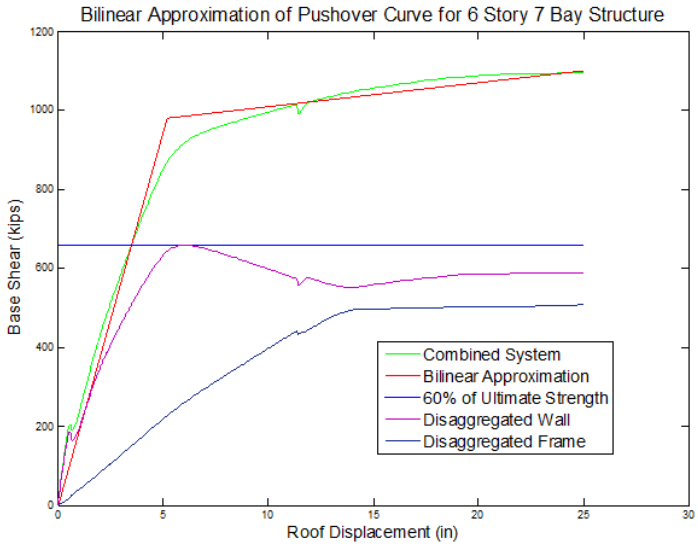
Bilinear Approximation of Pushover Curve for 6 Story 7 Bay Structure
Base Shear (kips)
Roof Displacement (in)
Combined System
Bilinear Approximation
60% of Ultimate Strength
Disaggregated Wall
Disaggregated Frame

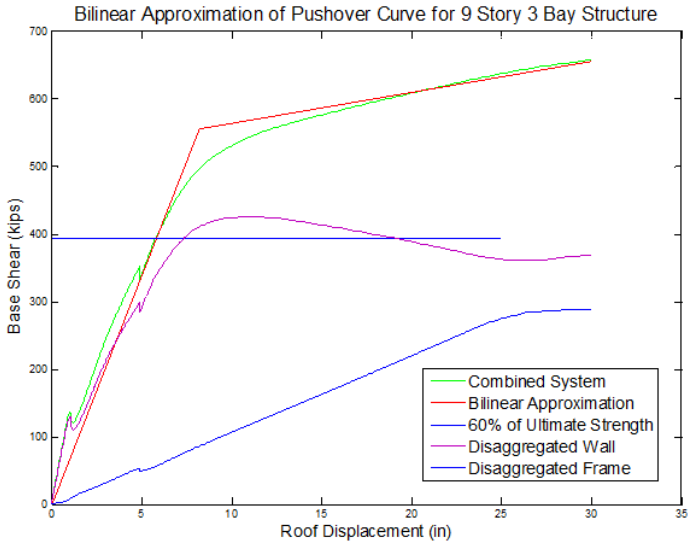
Bilinear Approximation of Pushover Curve for 9 Story 3 Bay Structure
Base Shear (kips)
Roof Displacement (in)
Combined System
Bilinear Approximation
60% of Ultimate Strength
Disaggregated Wall
Disaggregated Frame

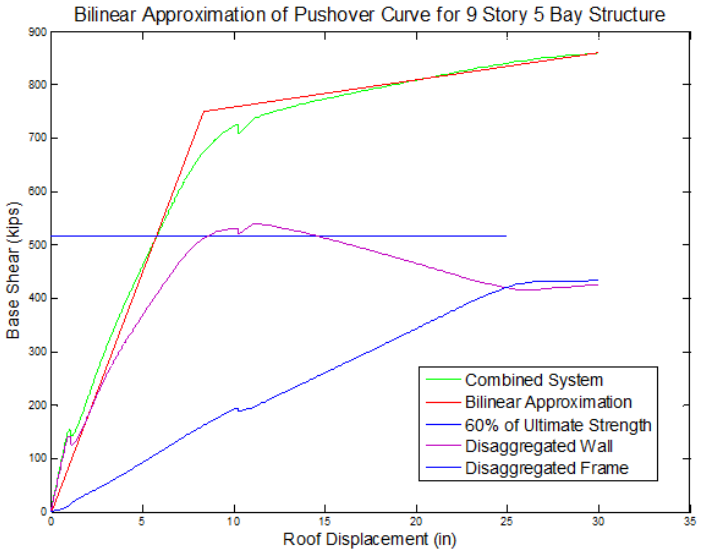
Bilinear Approximation of Pushover Curve for 9 Story 5 Bay Structure
Base Shear (kips)
Roof Displacement (in)
Combined System
Bilinear Approximation
60% of Ultimate Strength
Disaggregated Wall
Disaggregated Frame

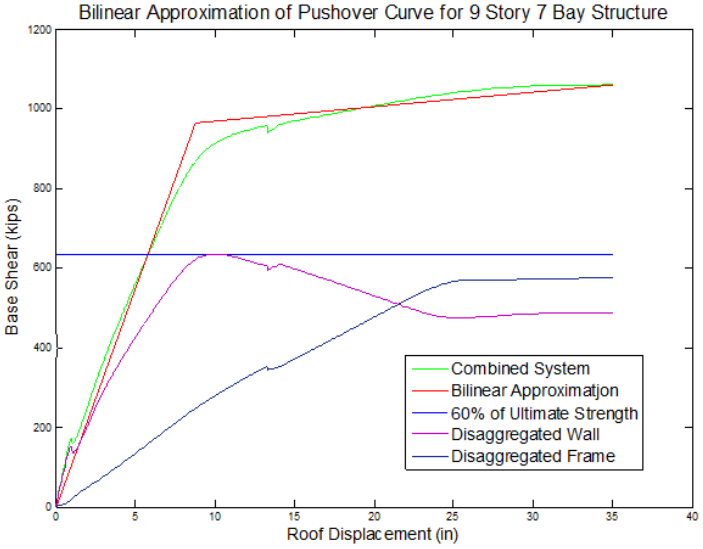
Bilinear Approximation of Pushover Curve for 9 Story 7 Bay Structure
Base Shear (kips)
Roof Displacement (in)
Combined System
Bilinear Approximatjon
60% of Ultimate Strength
Disaggregated Wall
Disaggregated Frame

Appendix 2: Bilinear Approx. Pushovers for 37 Building Study

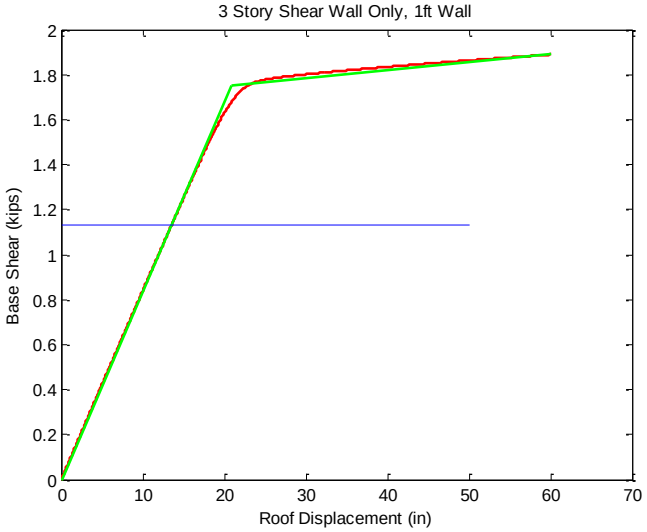

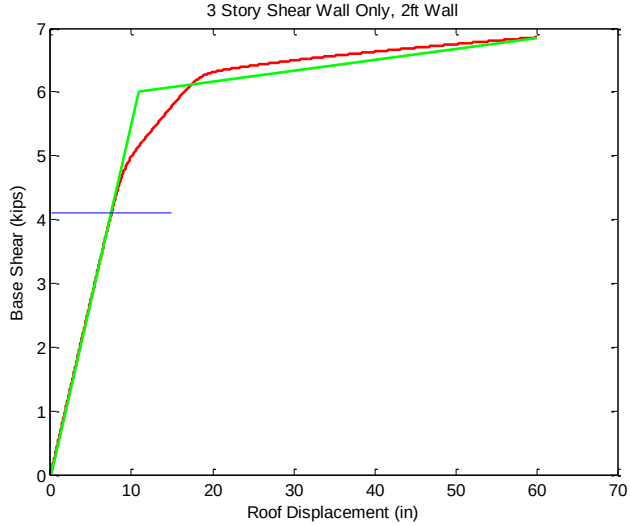

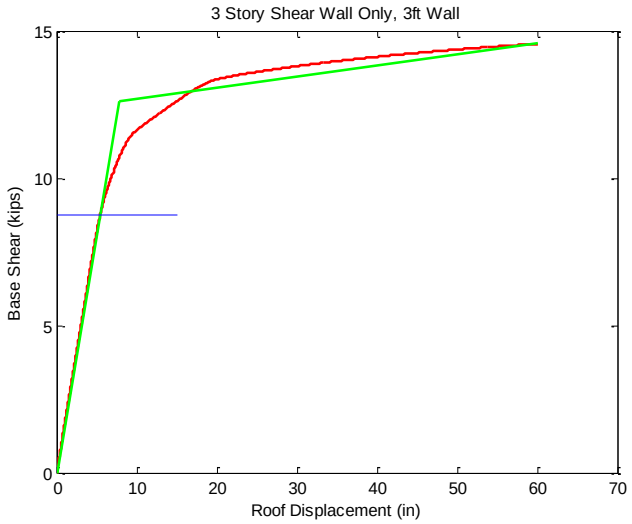

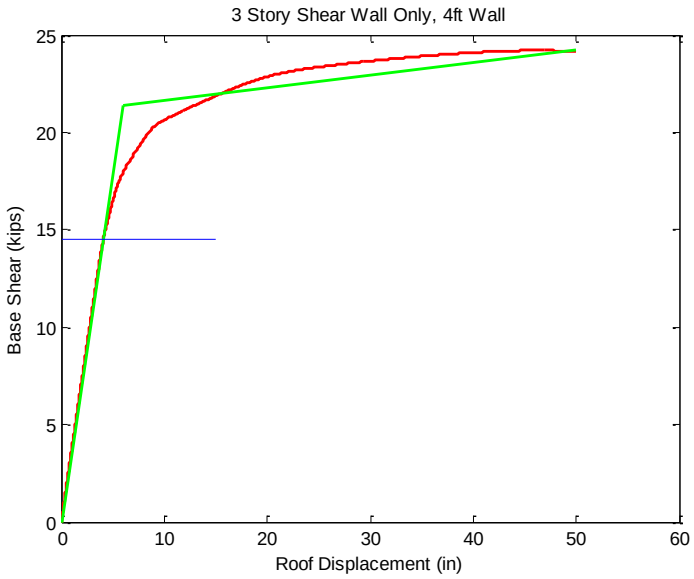
3 Story Shear Wall Only, 4ft Wall
Base Shear (kips)
Roof Displacement (in)
0
5
10
15
20
25
0
10
20
30
40
50
60

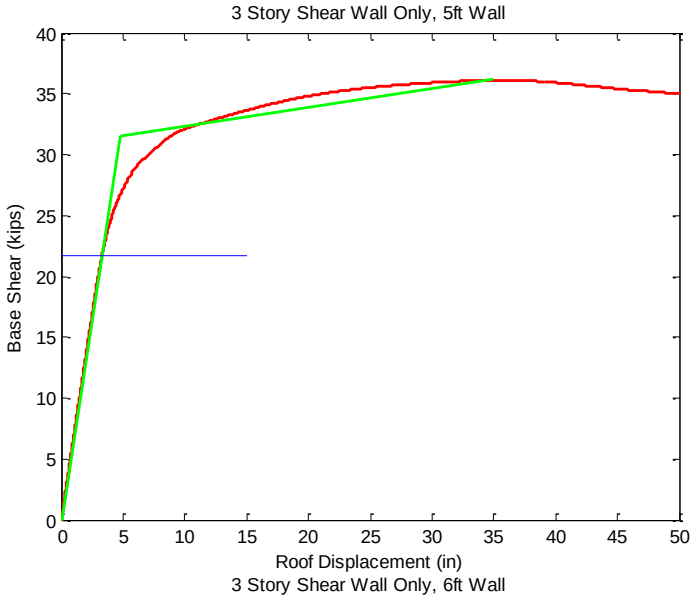
3 Story Shear Wall Only, 5ft Wall
Base Shear (kips)
Roof Displacement (in)
0
5
10
15
20
25
30
35
40
0
5
10
15
20
25
30
35
40
45
50

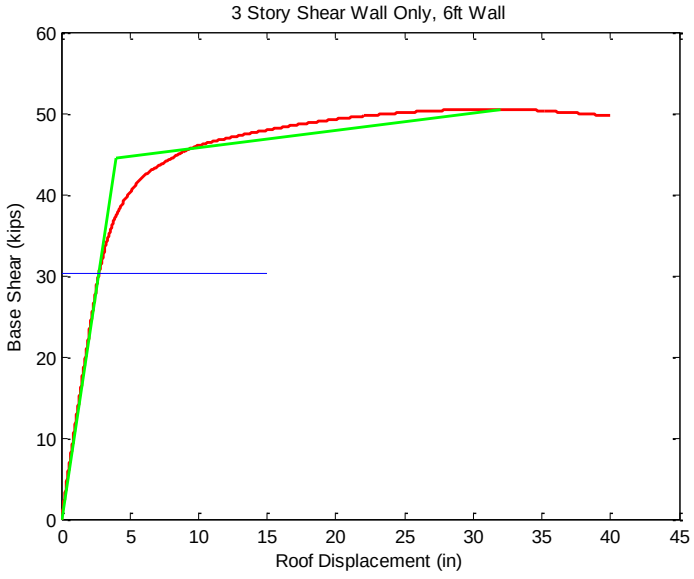
3 Story Shear Wall Only, 6ft Wall
Base Shear (kips)
Roof Displacement (in)
0
10
20
30
40
50
60
0
5
10
15
20
25
30
35
40
45

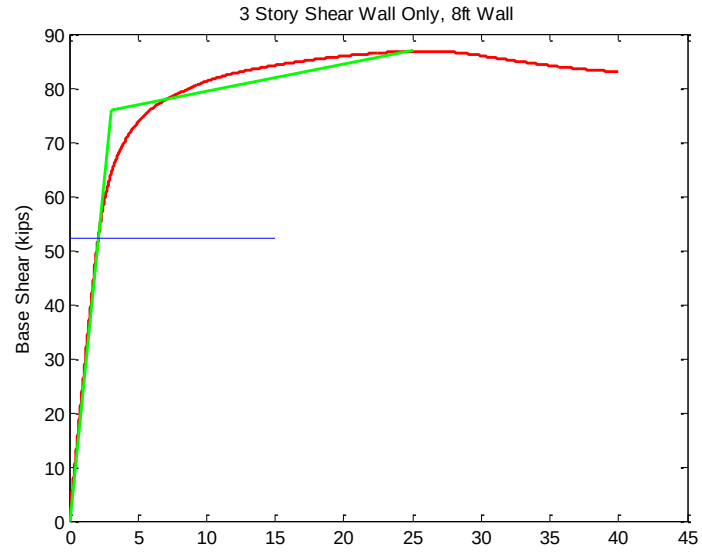
3 Story Shear Wall Only, 8ft Wall
Base Shear (kips)
Roof Displacement (in)
0
10
20
30
40
50
60
70
80
90
0
5
10
15
20
25
30
35
40
45

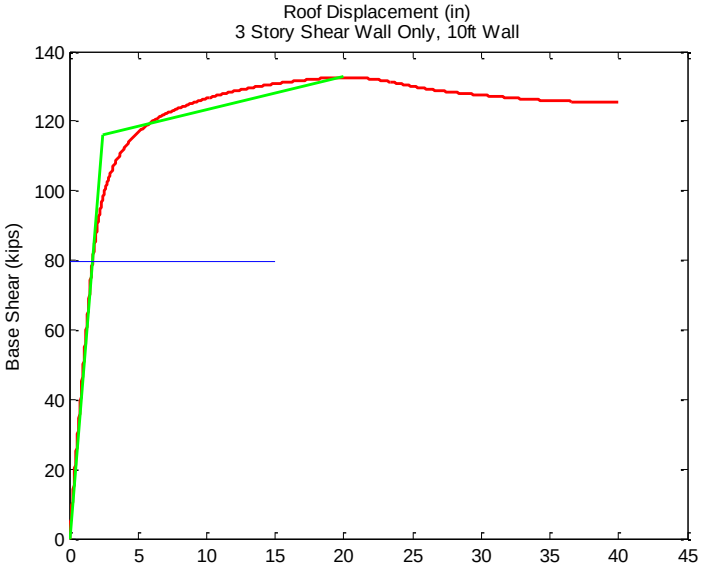
3 Story Shear Wall Only, 10ft Wall
Base Shear (kips)
Roof Displacement (in)
0
20
40
60
80
100
120
140
0
5
10
15
20
25
30
35
40
45

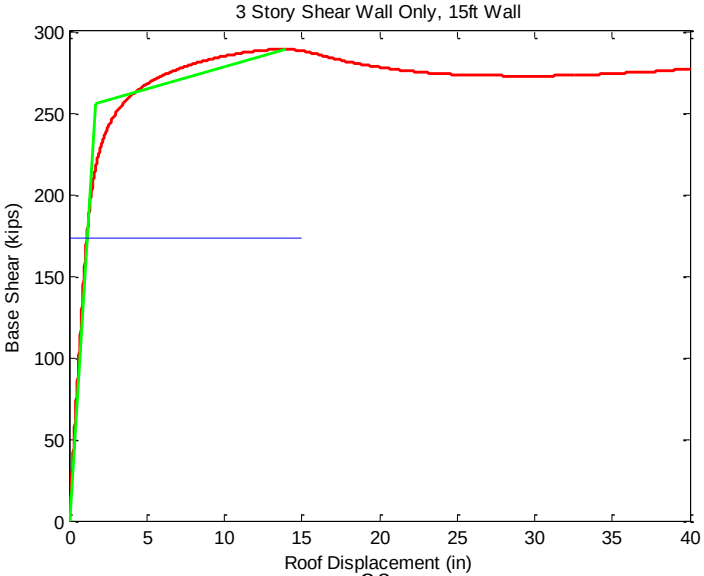
3 Story Shear Wall Only, 15ft Wall
Base Shear (kips)
Roof Displacement (in)
0
50
100
150
200
250
300
0
5
10
15
20
25
30
35
40

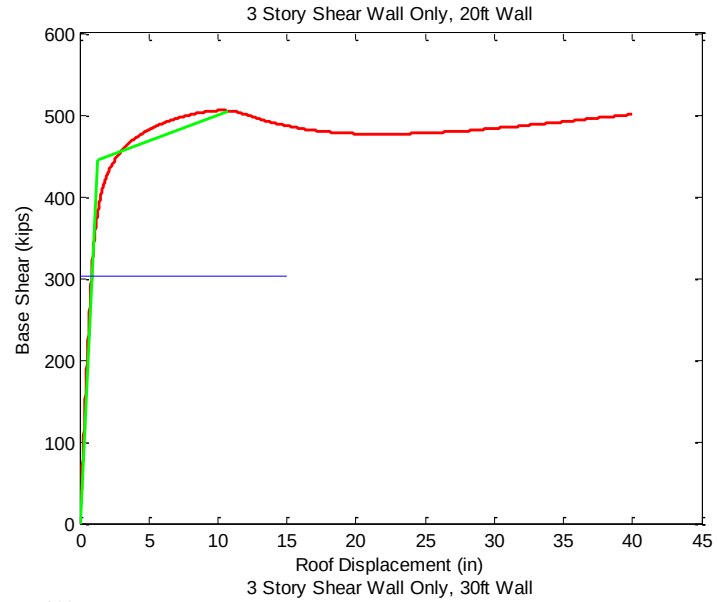
3 Story Shear Wall Only, 20ft Wall
Base Shear (kips)
Roof Displacement (in)
0
100
200
300
400
500
600
0
5
10
15
20
25
30
35
40
45

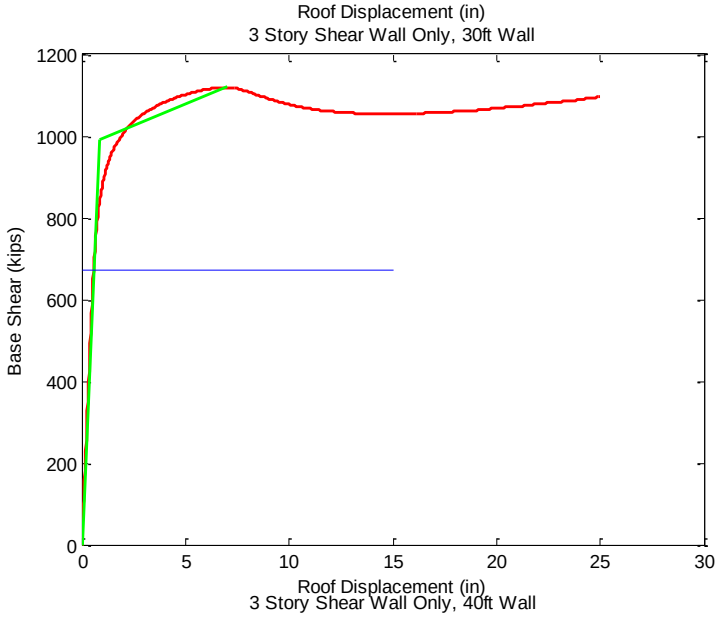
3 Story Shear Wall Only, 30ft Wall
Base Shear (kips)
Roof Displacement (in)
0
200
400
600
800
1000
1200
0
5
10
15
20
25
30

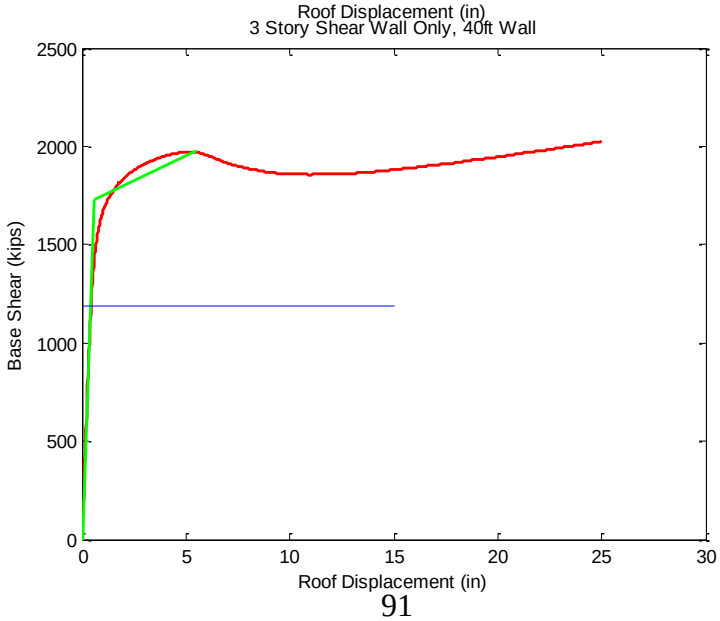
3 Story Shear Wall Only, 40ft Wall
Base Shear (kips)
Roof Displacement (in)
0
500
1000
1500
2000
2500
0
5
10
15
20
25
30

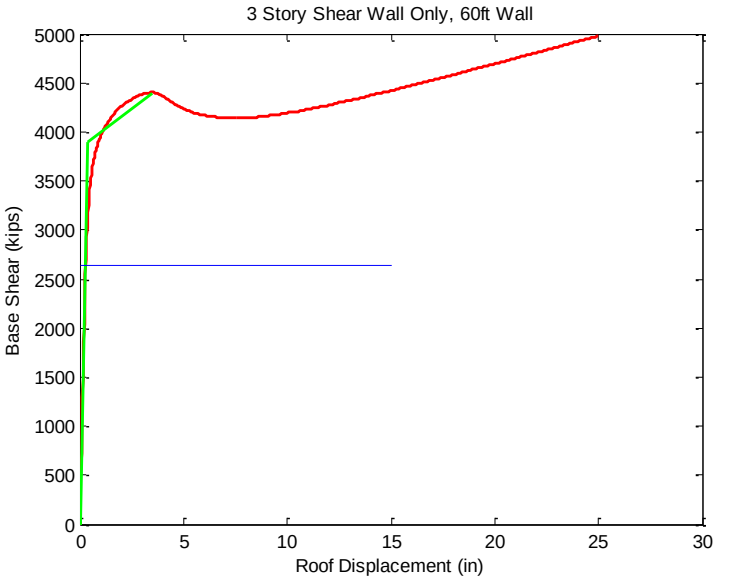
3 Story Shear Wall Only, 60ft Wall
Base Shear (kips)
Roof Displacement (in)

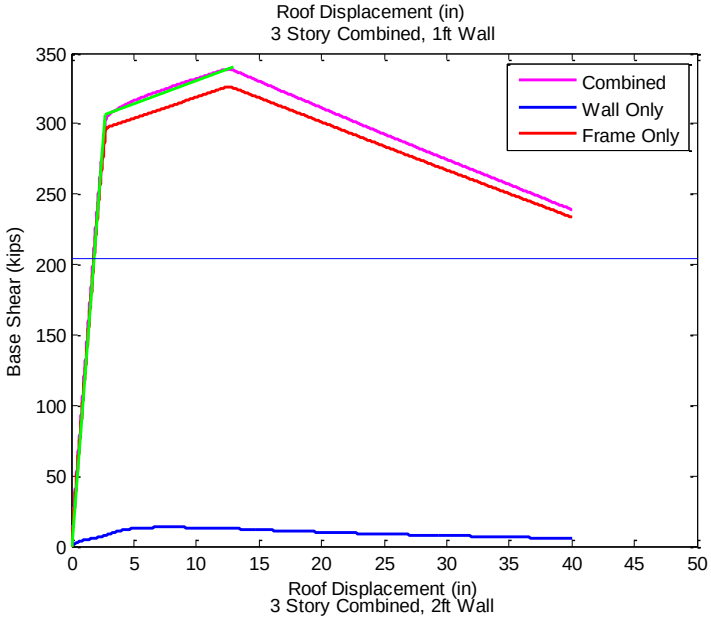
3 Story Combined, 1ft Wall
Combined
Wall Only
Frame Only
Base Shear (kips)
Roof Displacement (in)

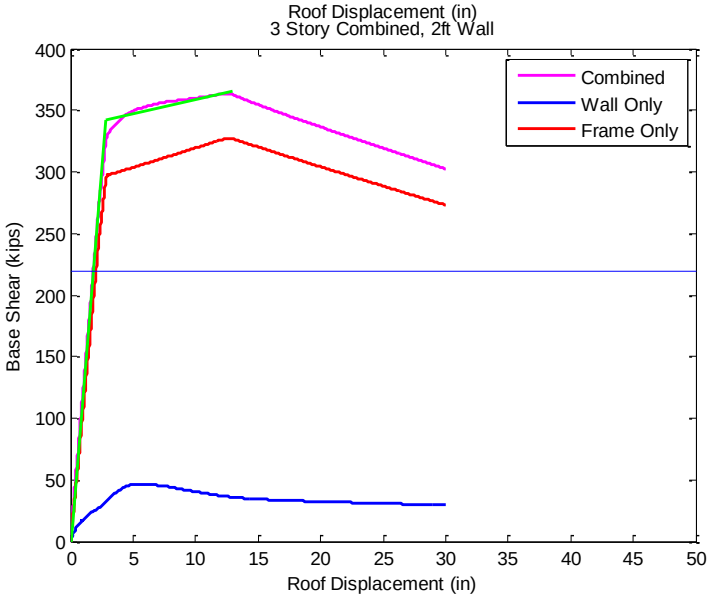
3 Story Combined, 2ft Wall
Combined
Wall Only
Frame Only
Base Shear (kips)
Roof Displacement (in)

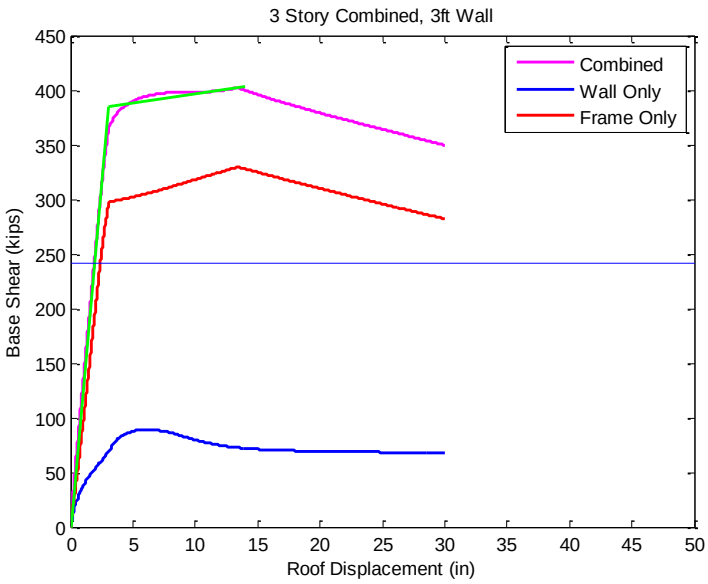
3 Story Combined, 3ft Wall
Combined
Wall Only
Frame Only
Base Shear (kips)
Roof Displacement (in)
0
50
100
150
200
250
300
350
400
450
0
5
10
15
20
25
30
35
40
45
50

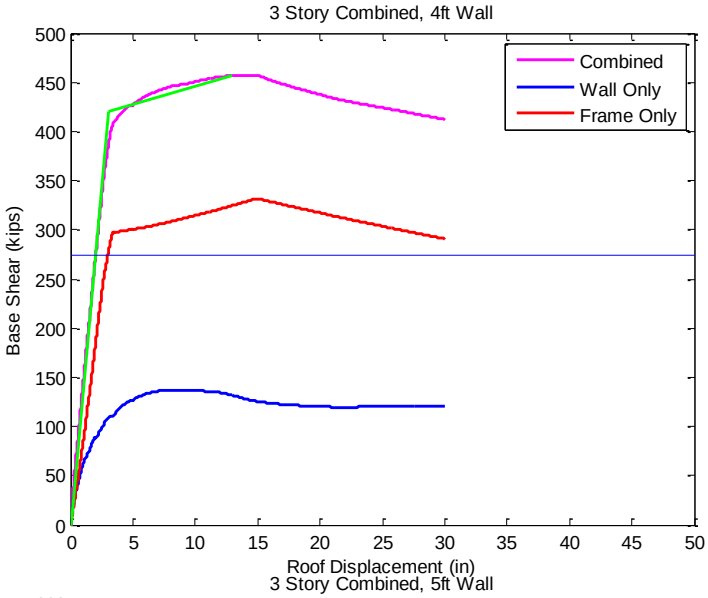
3 Story Combined, 4ft Wall
Combined
Wall Only
Frame Only
Base Shear (kips)
Roof Displacement (in)
0
50
100
150
200
250
300
350
400
450
500
0
5
10
15
20
25
30
35
40
45
50

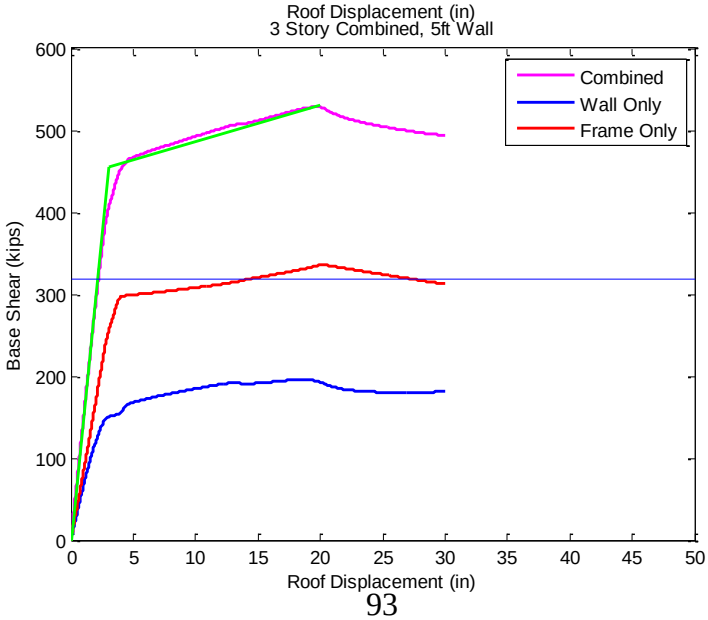
3 Story Combined, 5ft Wall
Combined
Wall Only
Frame Only
Base Shear (kips)
Roof Displacement (in)
0
100
200
300
400
500
600
0
5
10
15
20
25
30
35
40
45
50

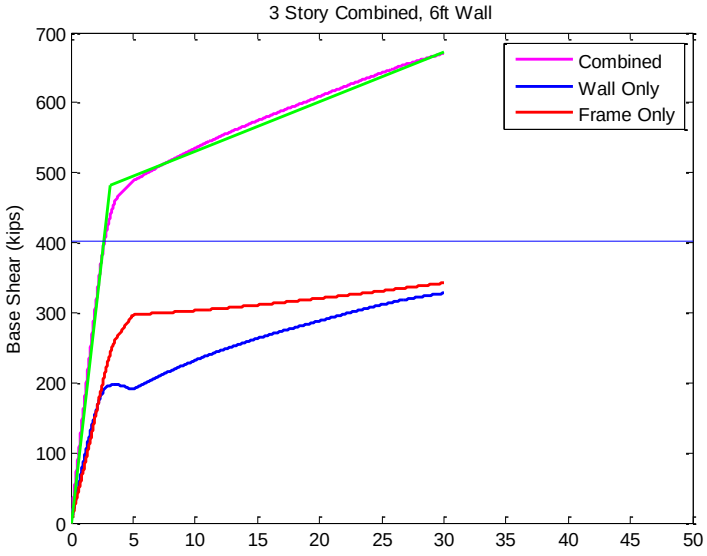
3 Story Combined, 6ft Wall
Combined
Wall Only
Frame Only
Base Shear (kips)
Roof Displacement (in)
0
100
200
300
400
500
600
700
0
5
10
15
20
25
30
35
40
45
50

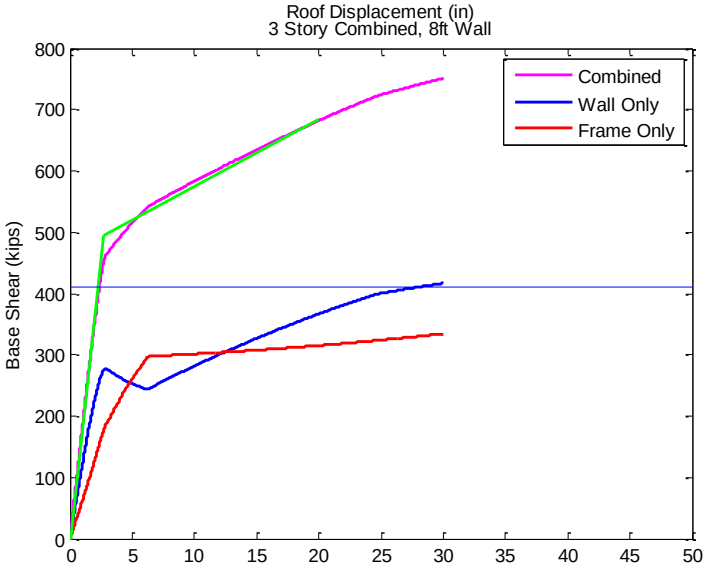
3 Story Combined, 8ft Wall
Combined
Wall Only
Frame Only
Base Shear (kips)
Roof Displacement (in)
0
100
200
300
400
500
600
700
800
0
5
10
15
20
25
30
35
40
45
50

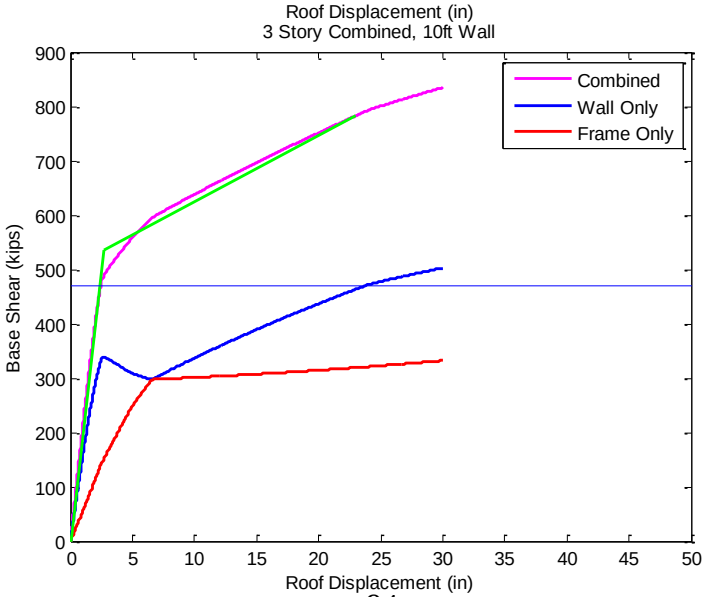
3 Story Combined, 10ft Wall
Combined
Wall Only
Frame Only
Base Shear (kips)
Roof Displacement (in)
0
100
200
300
400
500
600
700
800
900
0
5
10
15
20
25
30
35
40
45
50

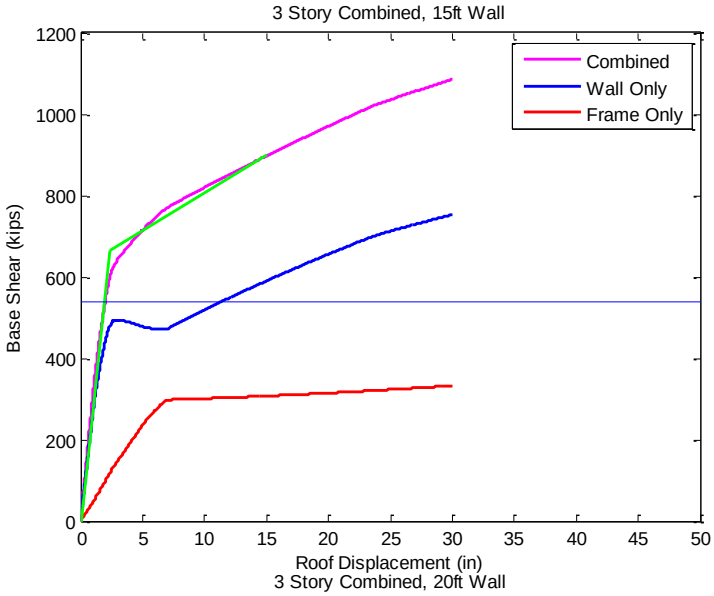
3 Story Combined, 15ft Wall
Combined
Wall Only
Frame Only
Base Shear (kips)
Roof Displacement (in)
0
200
400
600
800
1000
1200
0
5
10
15
20
25
30
35
40
45
50

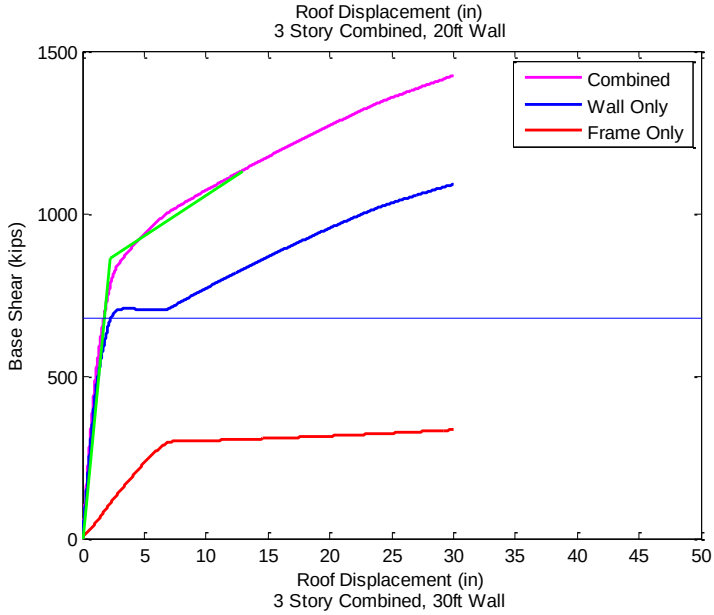
3 Story Combined, 20ft Wall
Combined
Wall Only
Frame Only
Base Shear (kips)
Roof Displacement (in)
0
500
1000
1500
0
5
10
15
20
25
30
35
40
45
50

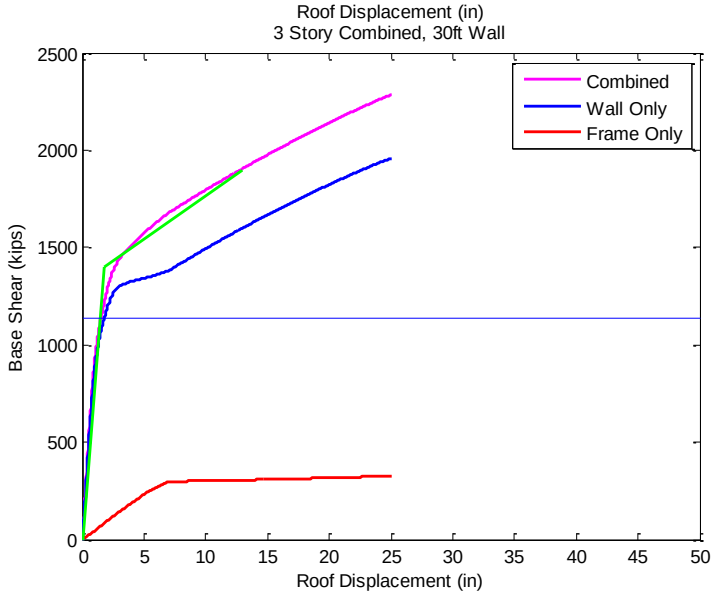
3 Story Combined, 30ft Wall
Combined
Wall Only
Frame Only
Base Shear (kips)
Roof Displacement (in)
0
500
1000
1500
2000
2500
0
5
10
15
20
25
30
35
40
45
50

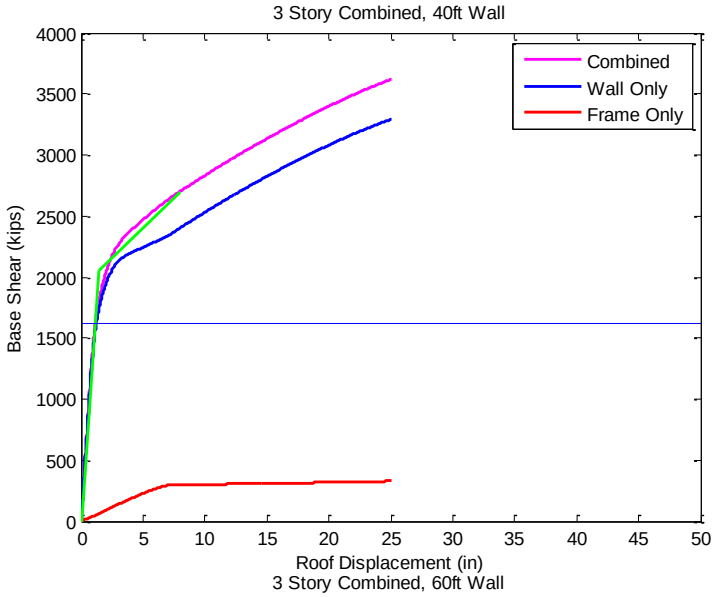
3 Story Combined, 40ft Wall
Combined
Wall Only
Frame Only
Base Shear (kips)
Roof Displacement (in)
0
500
1000
1500
2000
2500
3000
3500
4000
0
5
10
15
20
25
30
35
40
45
50

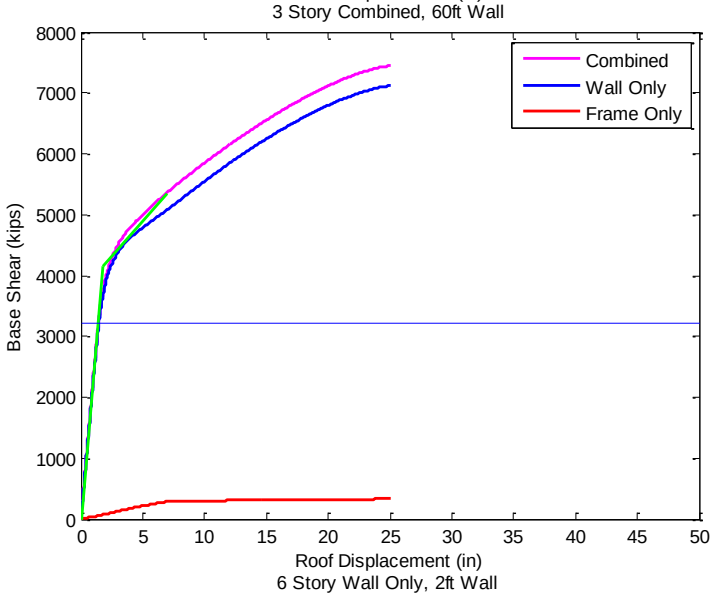
3 Story Combined, 60ft Wall
Combined
Wall Only
Frame Only
Base Shear (kips)
Roof Displacement (in)
0
1000
2000
3000
4000
5000
6000
7000
8000
0
5
10
15
20
25
30
35
40
45
50

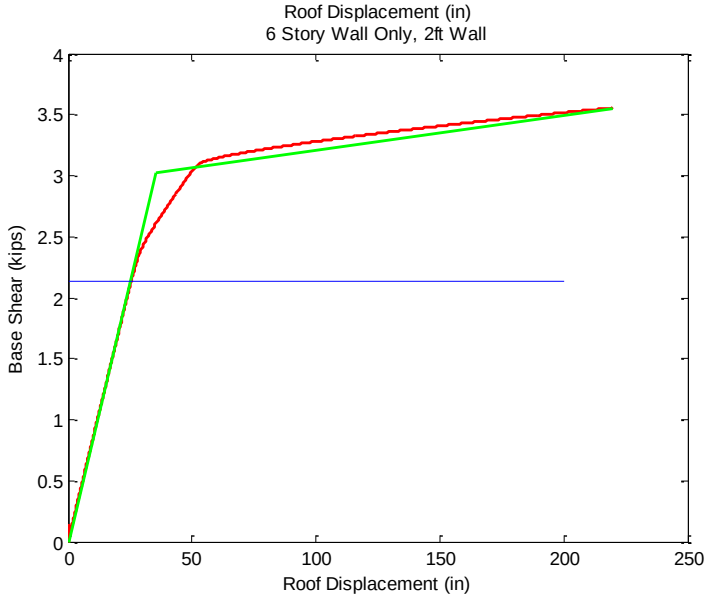
6 Story Wall Only, 2ft Wall
Base Shear (kips)
Roof Displacement (in)
0
0.5
1
1.5
2
2.5
3
3.5
4
0
50
100
150
200
250

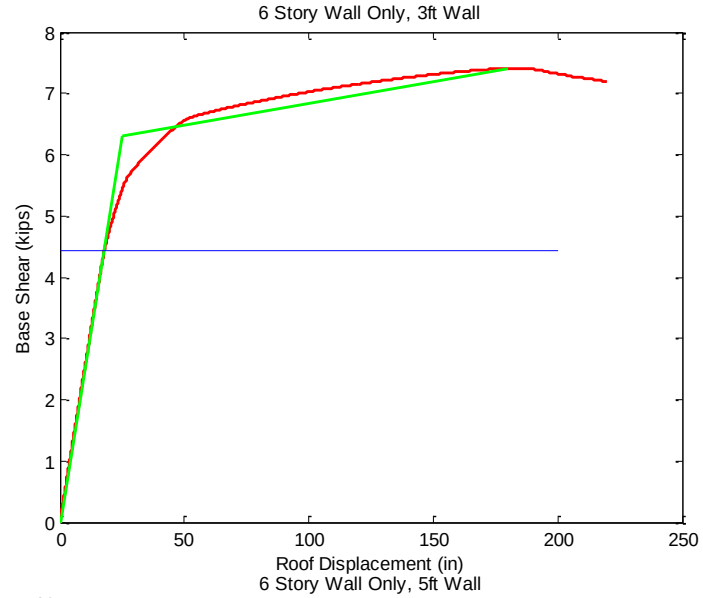
6 Story Wall Only, 3ft Wall
Base Shear (kips)
Roof Displacement (in)
0
1
2
3
4
5
6
7
8
0
50
100
150
200
250

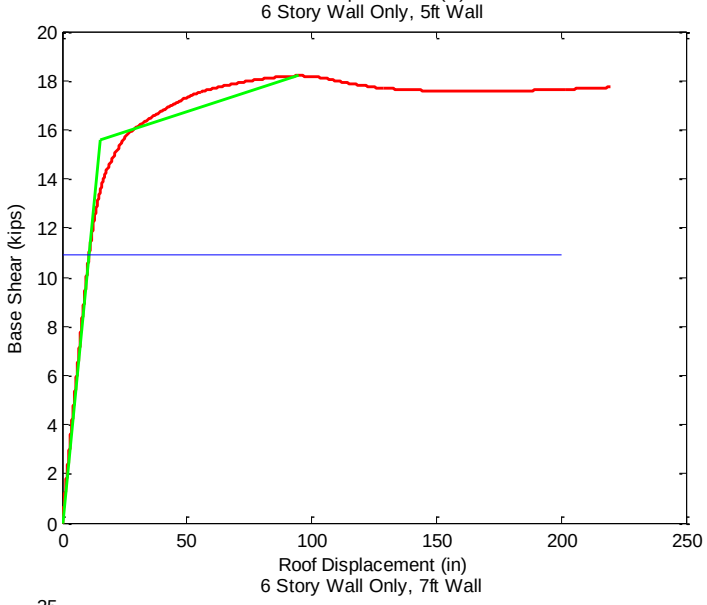
6 Story Wall Only, 5ft Wall
Base Shear (kips)
Roof Displacement (in)
0
2
4
6
8
10
12
14
16
18
20
0
50
100
150
200
250

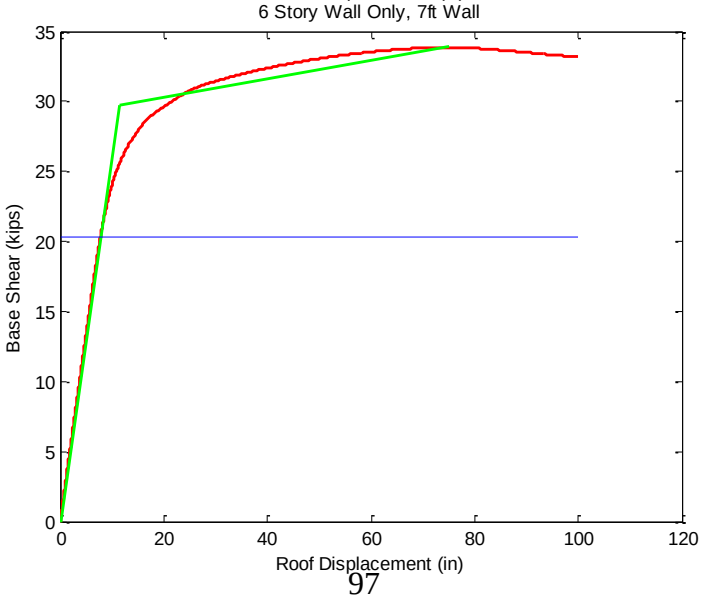
6 Story Wall Only, 7ft Wall
Base Shear (kips)
Roof Displacement (in)
0
5
10
15
20
25
30
35
0
20
40
60
80
100
120

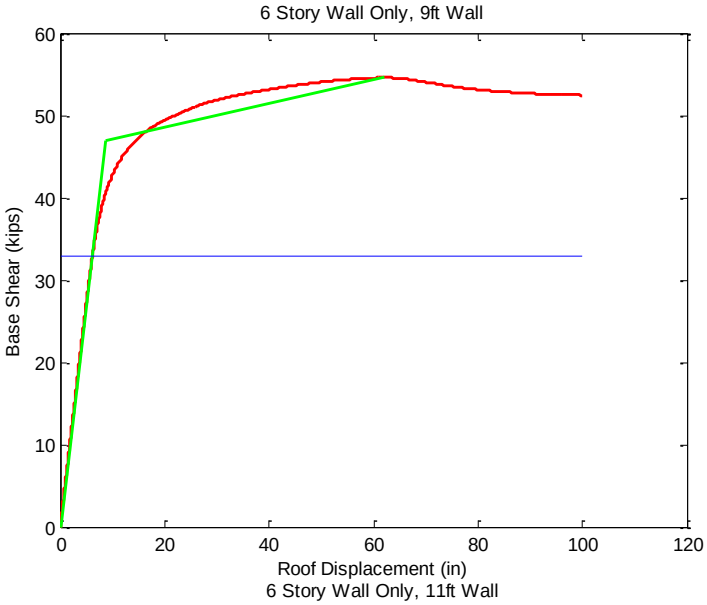
6 Story Wall Only, 9ft Wall
Base Shear (kips)
Roof Displacement (in)
0
10
20
30
40
50
60
0
20
40
60
80
100
120

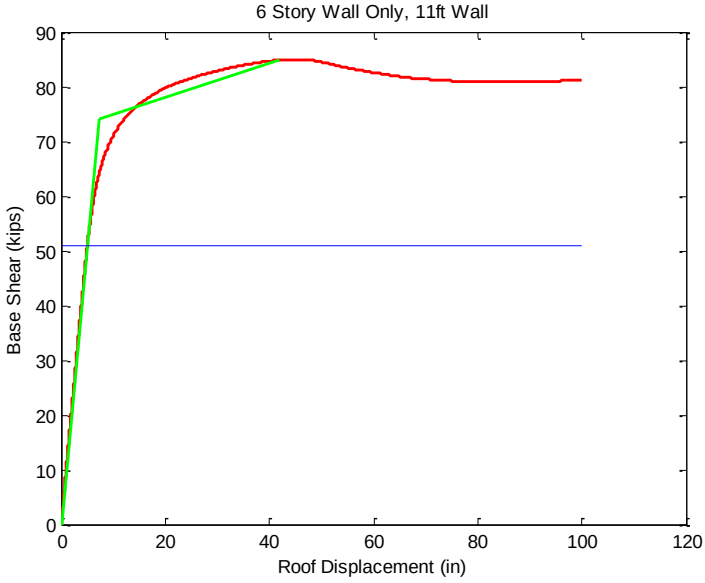
6 Story Wall Only, 11ft Wall
Base Shear (kips)
Roof Displacement (in)
0
10
20
30
40
50
60
70
80
90
0
20
40
60
80
100
120

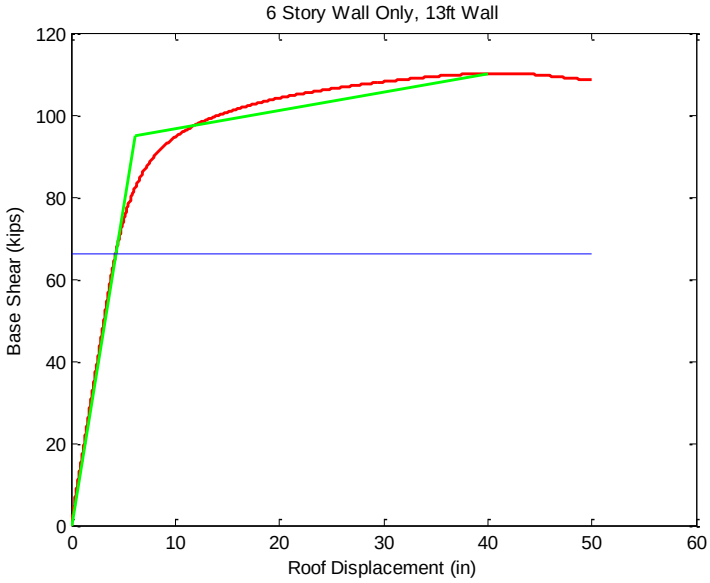
6 Story Wall Only, 13ft Wall
Base Shear (kips)
Roof Displacement (in)
0
20
40
60
80
100
120
0
10
20
30
40
50
60

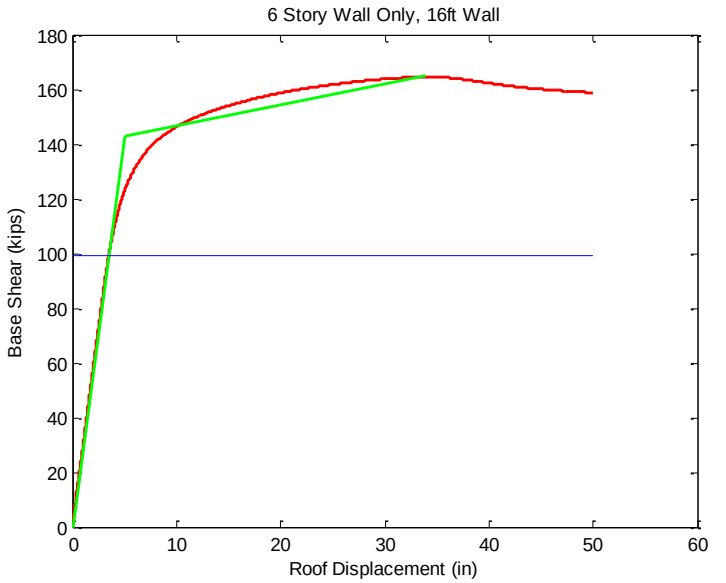
6 Story Wall Only, 16ft Wall
Base Shear (kips)
Roof Displacement (in)
0
20
40
60
80
100
120
140
160
180
0
10
20
30
40
50
60

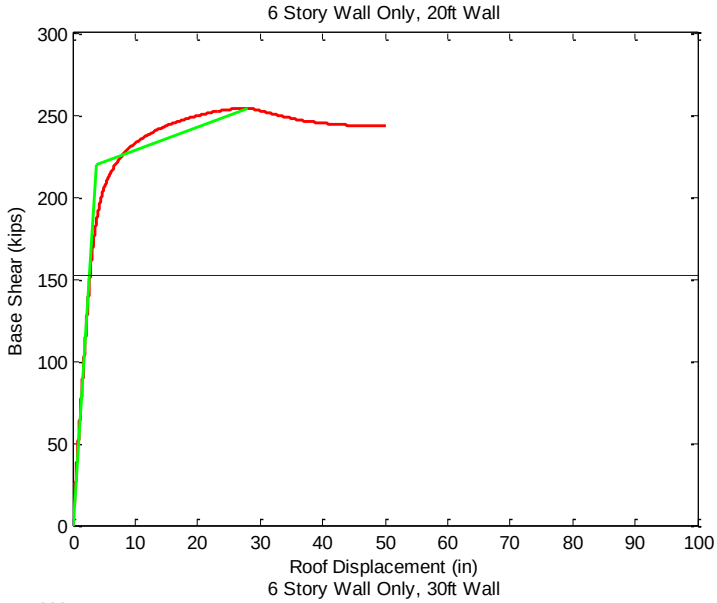
6 Story Wall Only, 20ft Wall
Base Shear (kips)
Roof Displacement (in)
0
50
100
150
200
250
300
0
10
20
30
40
50
60
70
80
90
100

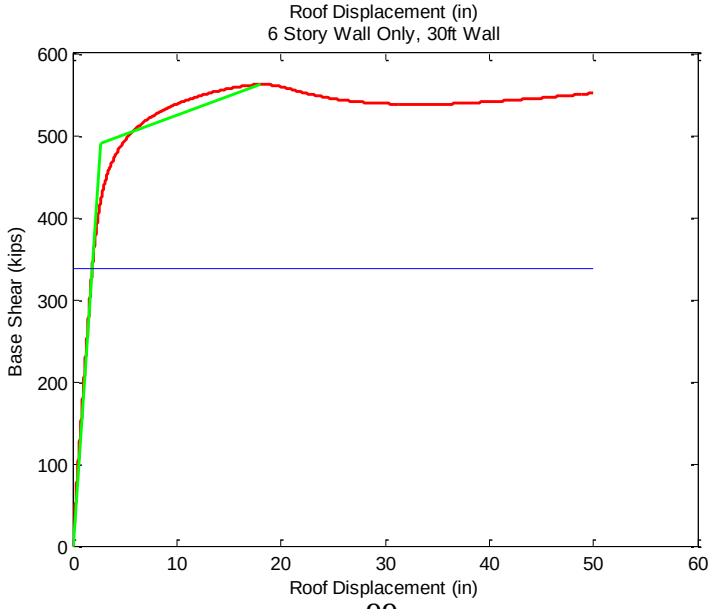
6 Story Wall Only, 30ft Wall
Base Shear (kips)
Roof Displacement (in)
0
100
200
300
400
500
600
0
10
20
30
40
50
60

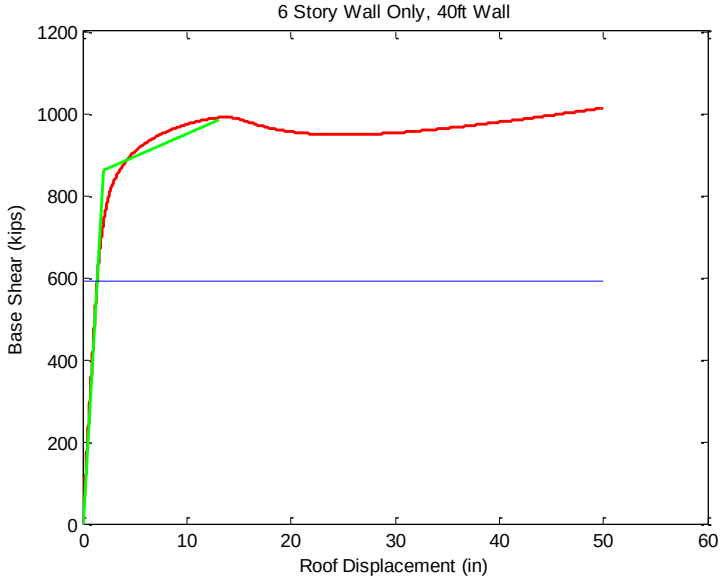
6 Story Wall Only, 40ft Wall
Base Shear (kips)
Roof Displacement (in)
0
200
400
600
800
1000
1200
0
10
20
30
40
50
60

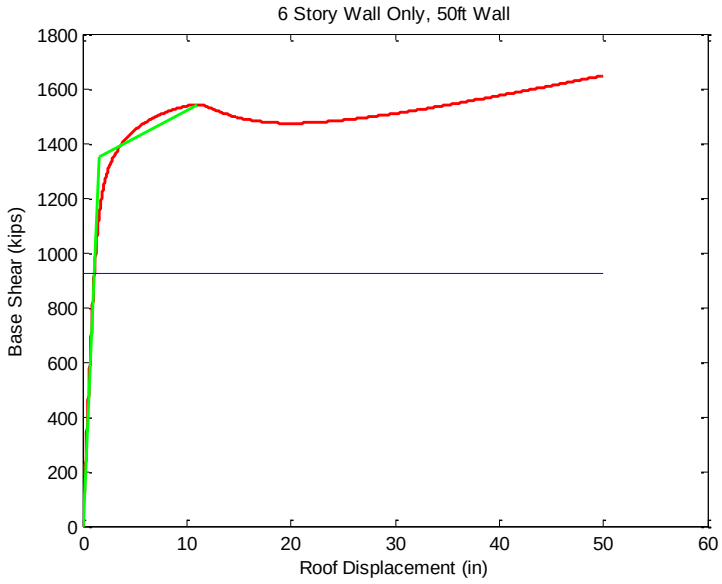
6 Story Wall Only, 50ft Wall
Base Shear (kips)
Roof Displacement (in)
0
200
400
600
800
1000
1200
1400
1600
1800
0
10
20
30
40
50
60

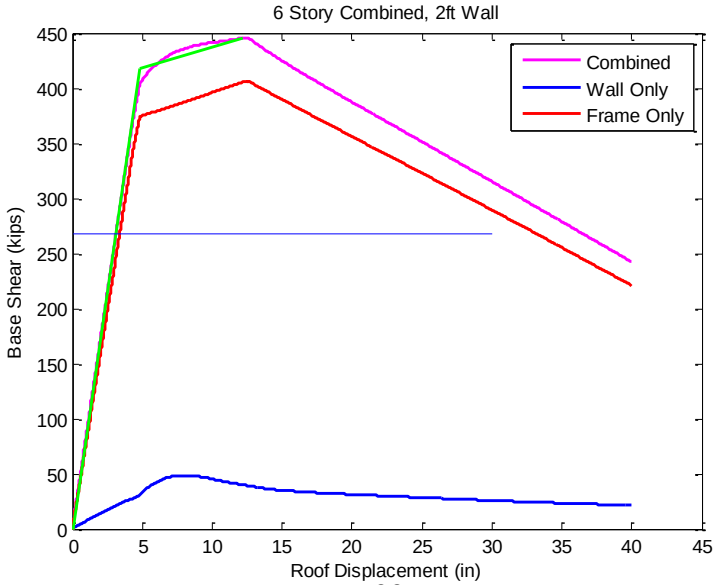
6 Story Combined, 2ft Wall
Combined
Wall Only
Frame Only
Base Shear (kips)
Roof Displacement (in)
0
50
100
150
200
250
300
350
400
450
0
5
10
15
20
25
30
35
40
45

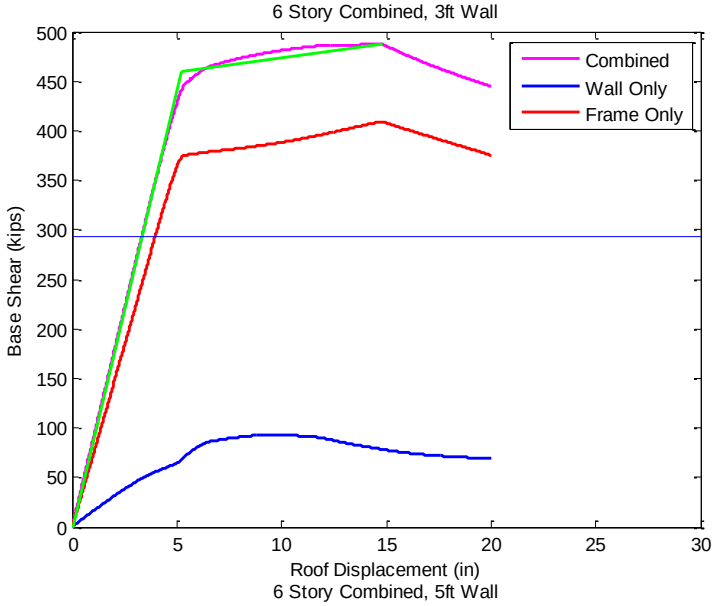
6 Story Combined, 3ft Wall
Combined
Wall Only
Frame Only
Base Shear (kips)
Roof Displacement (in)
0
50
100
150
200
250
300
350
400
450
500
0
5
10
15
20
25
30

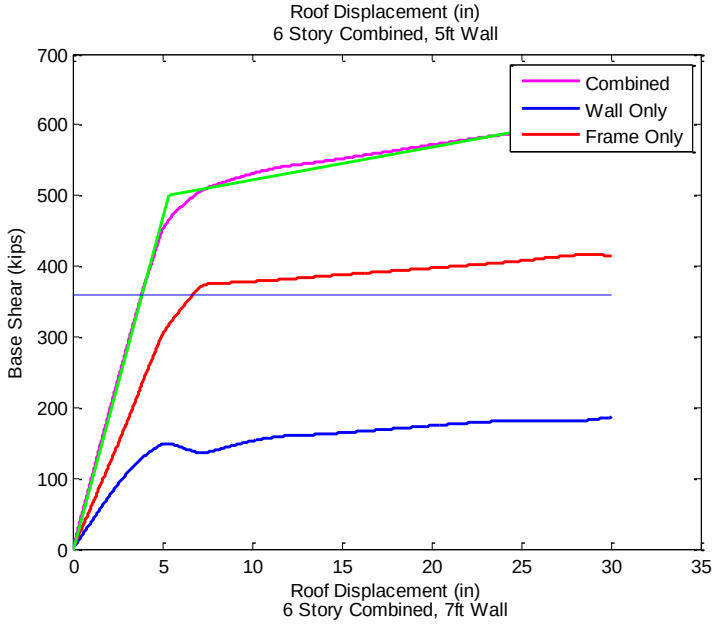
6 Story Combined, 5ft Wall
Combined
Wall Only
Frame Only
Base Shear (kips)
Roof Displacement (in)
0
100
200
300
400
500
600
700
0
5
10
15
20
25
30
35

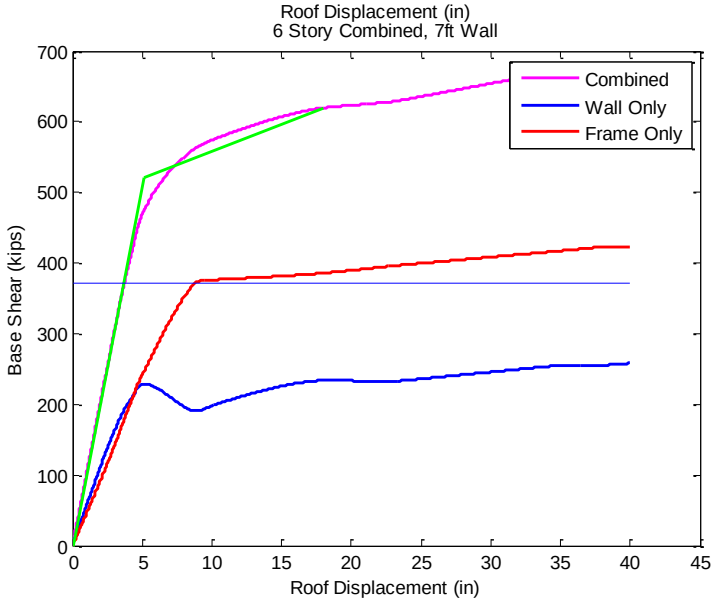
6 Story Combined, 7ft Wall
Combined
Wall Only
Frame Only
Base Shear (kips)
Roof Displacement (in)
0
100
200
300
400
500
600
700
0
5
10
15
20
25
30
35
40
45

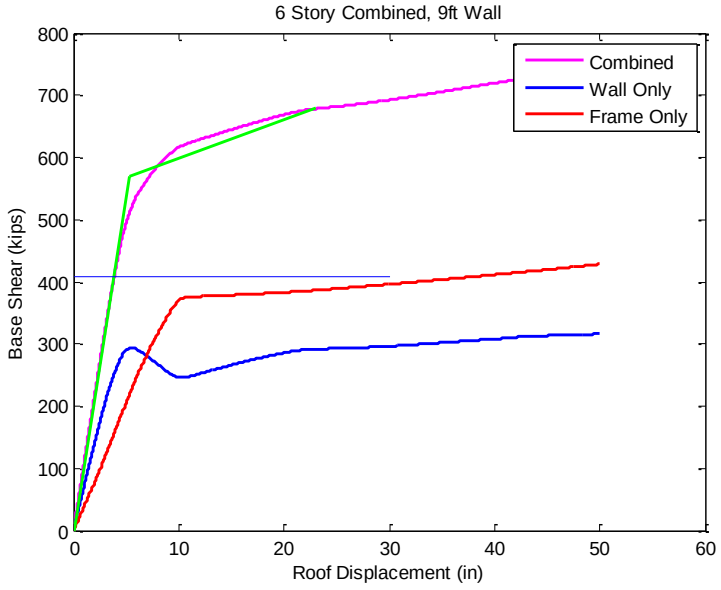
6 Story Combined, 9ft Wall
Combined
Wall Only
Frame Only
Base Shear (kips)
Roof Displacement (in)
0
100
200
300
400
500
600
700
800
0
10
20
30
40
50
60

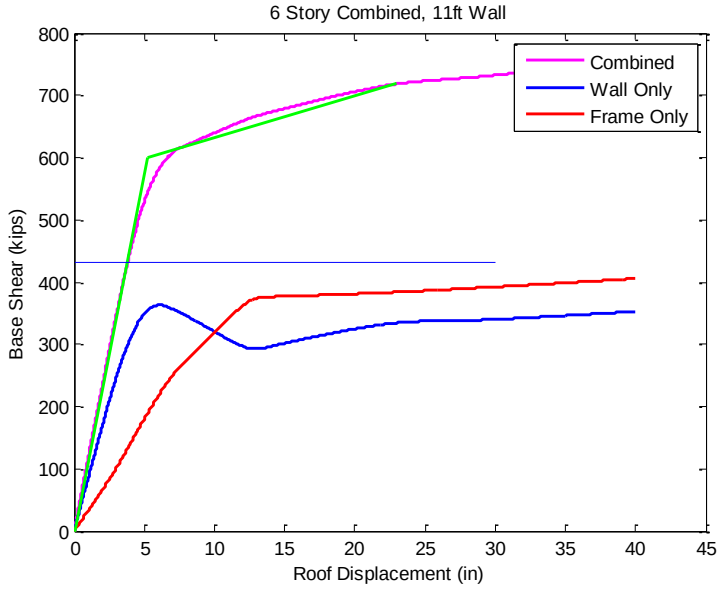
6 Story Combined, 11ft Wall
Combined
Wall Only
Frame Only
Base Shear (kips)
Roof Displacement (in)
0
100
200
300
400
500
600
700
800
0
5
10
15
20
25
30
35
40
45

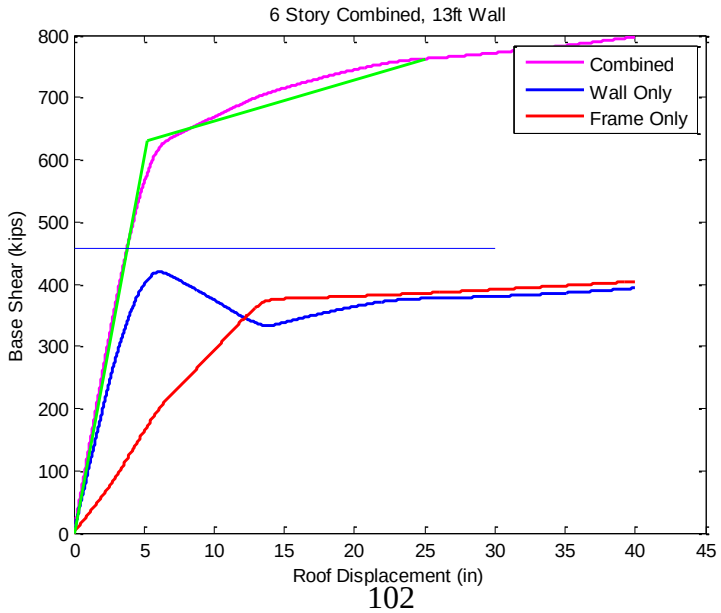
6 Story Combined, 13ft Wall
Combined
Wall Only
Frame Only
Base Shear (kips)
Roof Displacement (in)
0
100
200
300
400
500
600
700
800
0
5
10
15
20
25
30
35
40
45

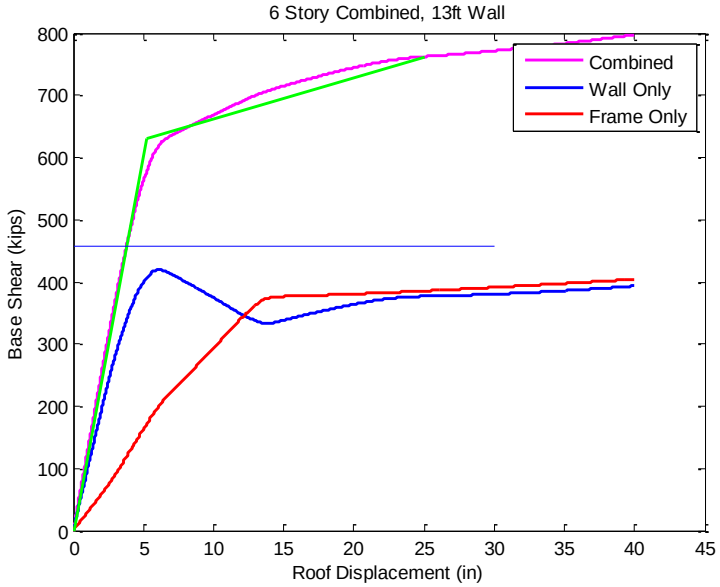
6 Story Combined, 13ft Wall
Combined
Wall Only
Frame Only
Base Shear (kips)
Roof Displacement (in)
0
100
200
300
400
500
600
700
800
0
5
10
15
20
25
30
35
40
45

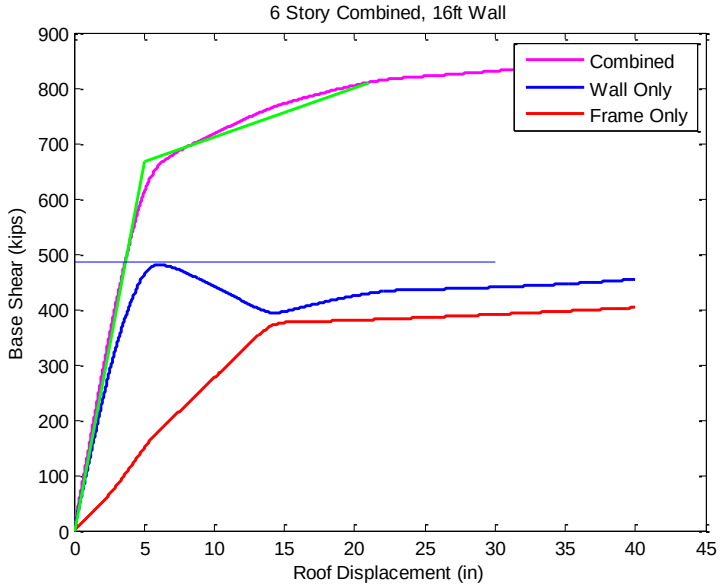
6 Story Combined, 16ft Wall
Combined
Wall Only
Frame Only
Base Shear (kips)
Roof Displacement (in)
0
100
200
300
400
500
600
700
800
900
0
5
10
15
20
25
30
35
40
45

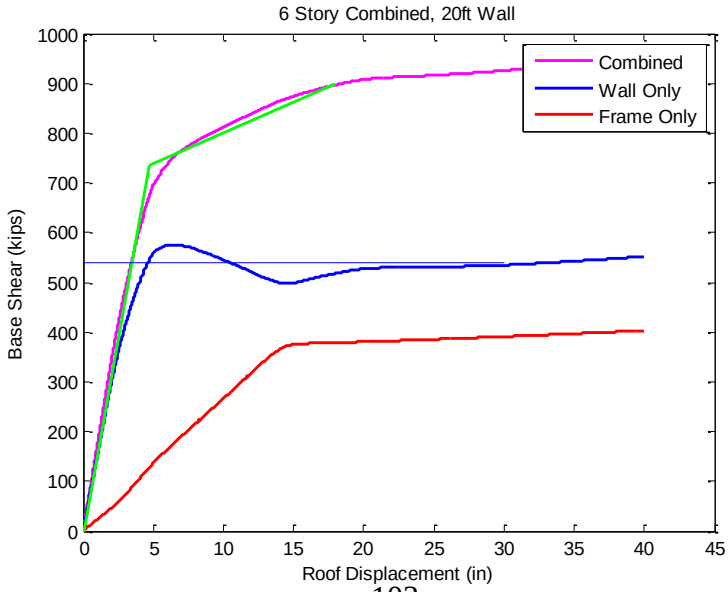
6 Story Combined, 20ft Wall
Combined
Wall Only
Frame Only
Base Shear (kips)
Roof Displacement (in)
0
100
200
300
400
500
600
700
800
900
1000
0
5
10
15
20
25
30
35
40
45

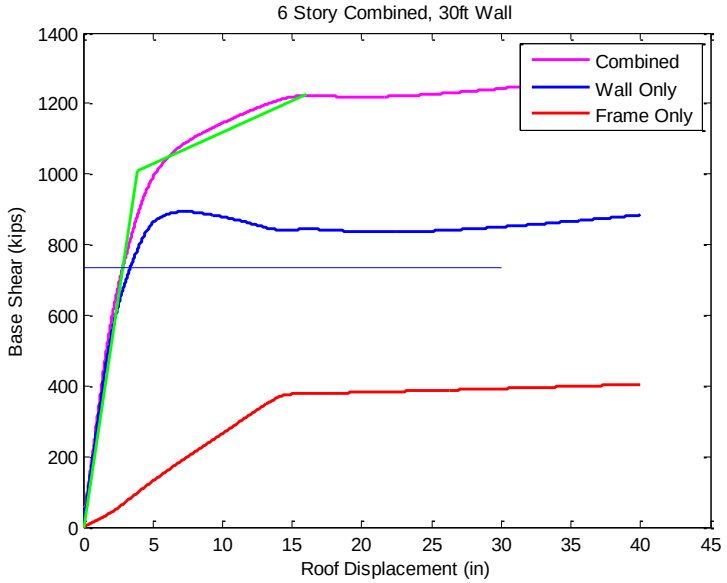
6 Story Combined, 30ft Wall
Combined
Wall Only
Frame Only
Base Shear (kips)
Roof Displacement (in)
0
200
400
600
800
1000
1200
1400
0
5
10
15
20
25
30
35
40
45

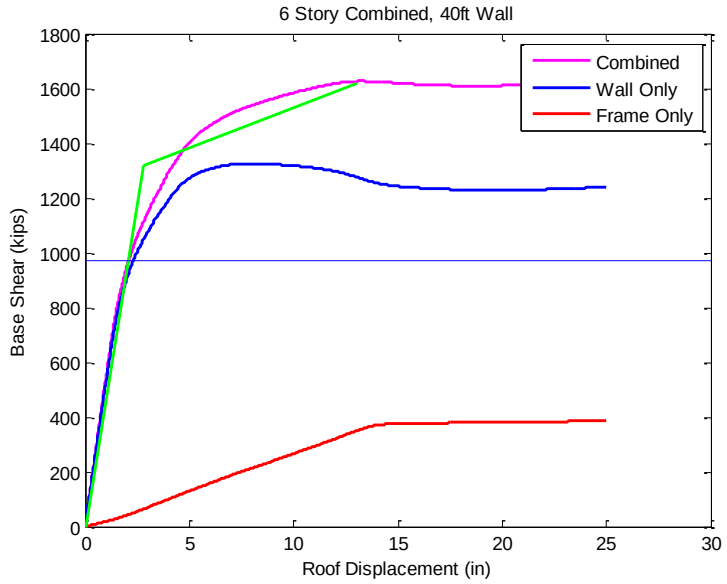
6 Story Combined, 40ft Wall
Combined
Wall Only
Frame Only
Base Shear (kips)
Roof Displacement (in)
0
200
400
600
800
1000
1200
1400
1600
1800
0
5
10
15
20
25
30

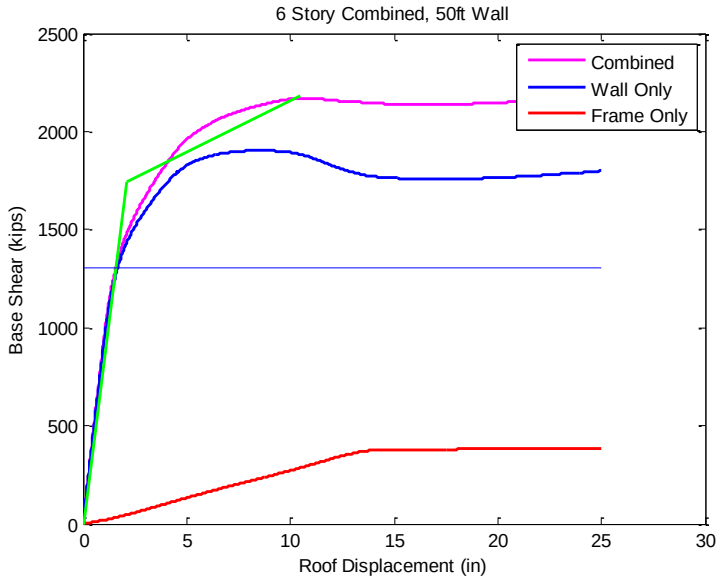
6 Story Combined, 50ft Wall
Combined
Wall Only
Frame Only
Base Shear (kips)
Roof Displacement (in)
0
500
1000
1500
2000
2500
0
5
10
15
20
25
30

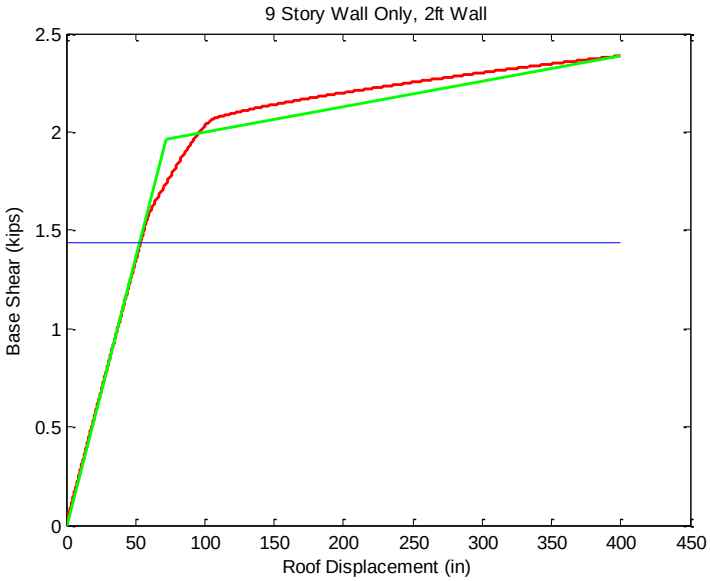
9 Story Wall Only, 2ft Wall
Base Shear (kips)
Roof Displacement (in)
0
0.5
1
1.5
2
2.5
0
50
100
150
200
250
300
350
400
450

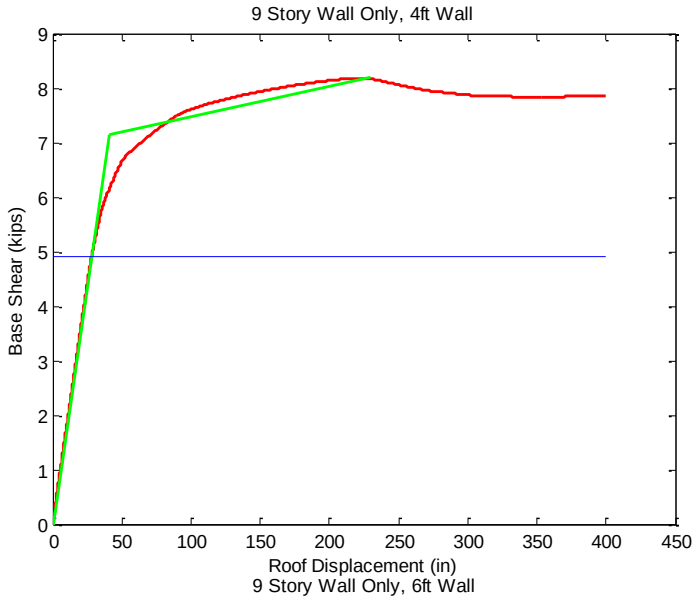
9 Story Wall Only, 4ft Wall
Base Shear (kips)
Roof Displacement (in)
0
1
2
3
4
5
6
7
8
9
0
50
100
150
200
250
300
350
400
450

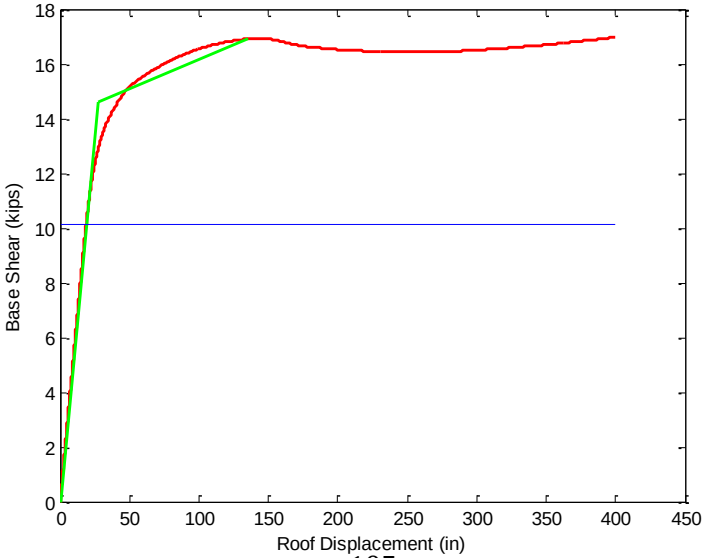
9 Story Wall Only, 6ft Wall
Base Shear (kips)
Roof Displacement (in)
0
2
4
6
8
10
12
14
16
18
0
50
100
150
200
250
300
350
400
450

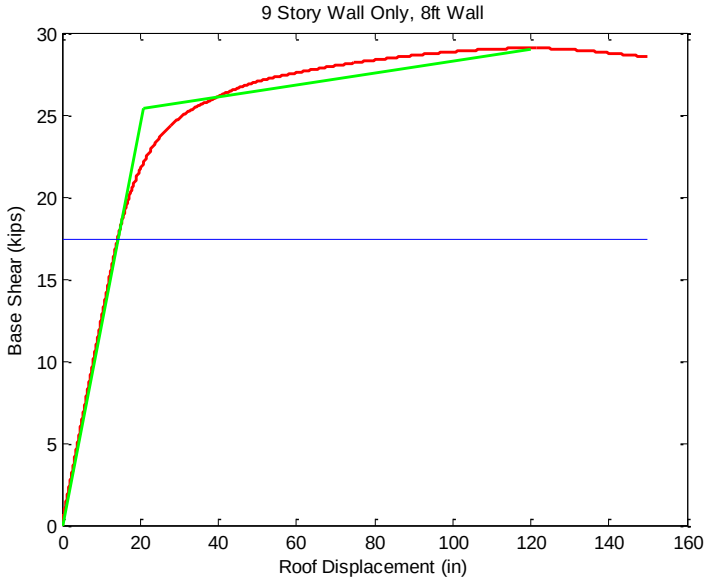
9 Story Wall Only, 8ft Wall
Base Shear (kips)
Roof Displacement (in)
0
5
10
15
20
25
30
0
20
40
60
80
100
120
140
160

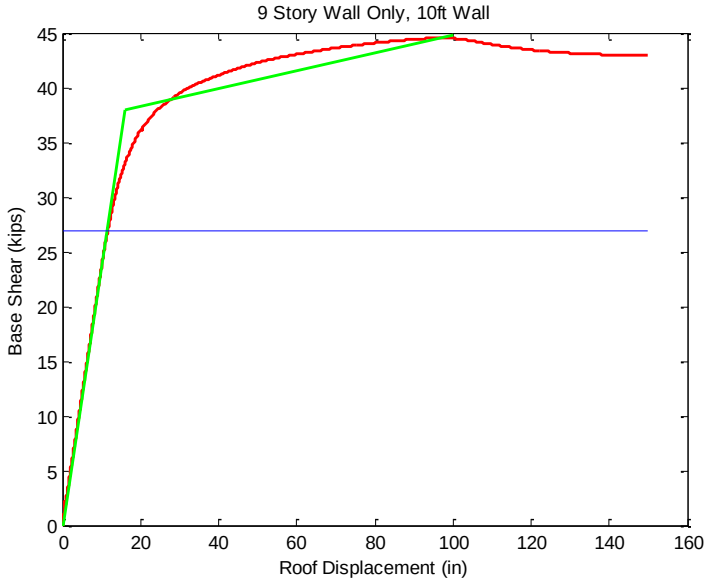
9 Story Wall Only, 10ft Wall
Base Shear (kips)
Roof Displacement (in)
0
5
10
15
20
25
30
35
40
45
0
20
40
60
80
100
120
140
160

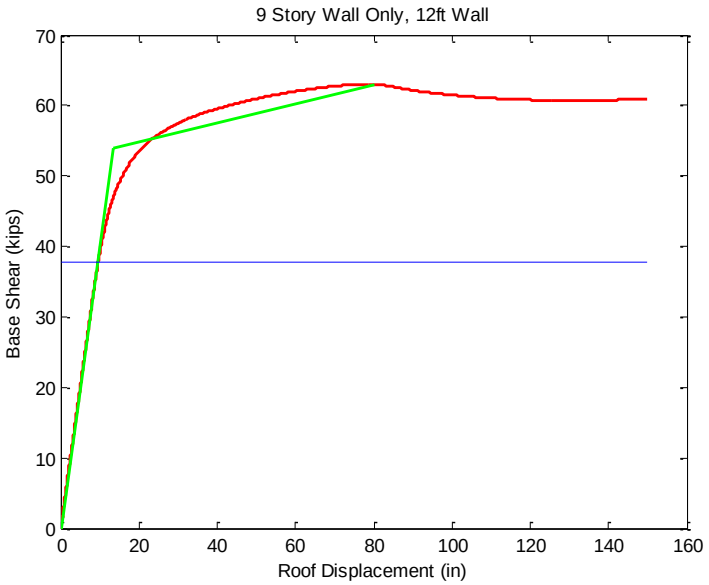
9 Story Wall Only, 12ft Wall
Base Shear (kips)
Roof Displacement (in)
0
10
20
30
40
50
60
70
0
20
40
60
80
100
120
140
160

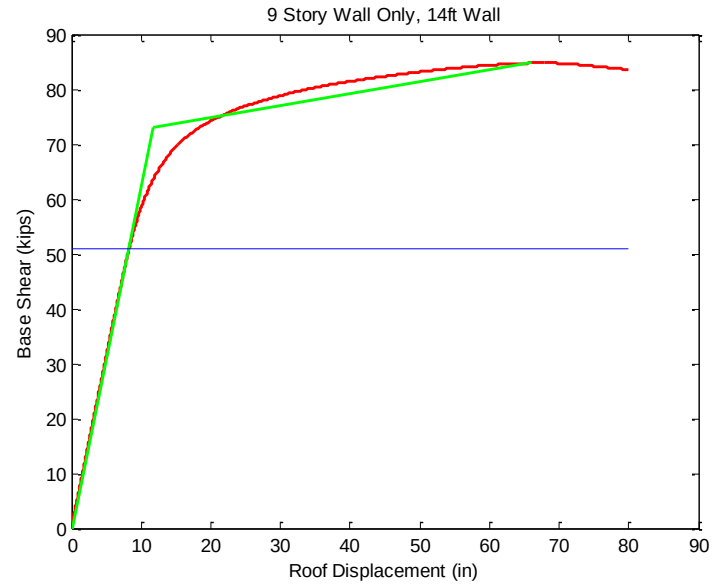
9 Story Wall Only, 14ft Wall
Base Shear (kips)
Roof Displacement (in)
0
10
20
30
40
50
60
70
80
90

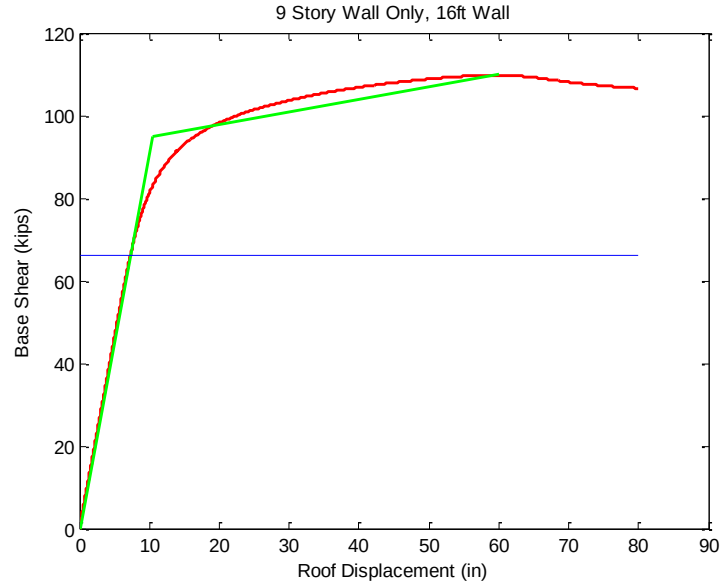
9 Story Wall Only, 16ft Wall
Base Shear (kips)
Roof Displacement (in)
0
20
40
60
80
100
120

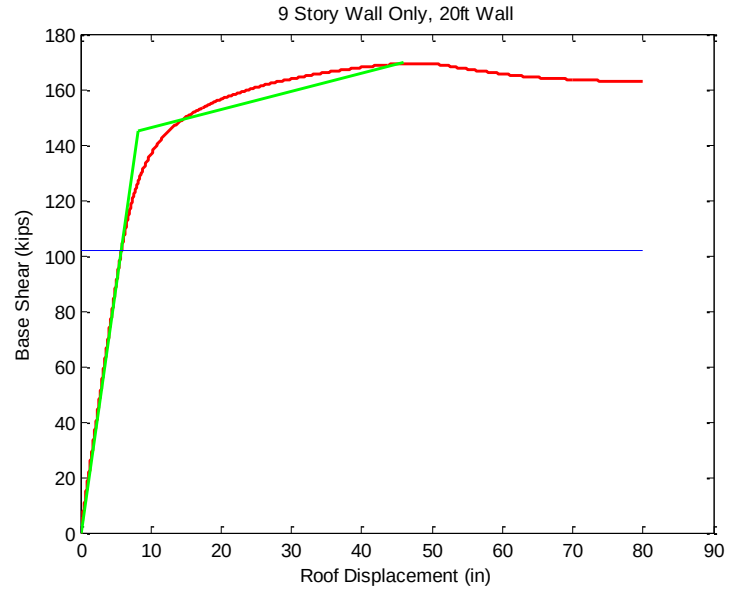
9 Story Wall Only, 20ft Wall
Base Shear (kips)
Roof Displacement (in)
0
20
40
60
80
100
120
140
160
180

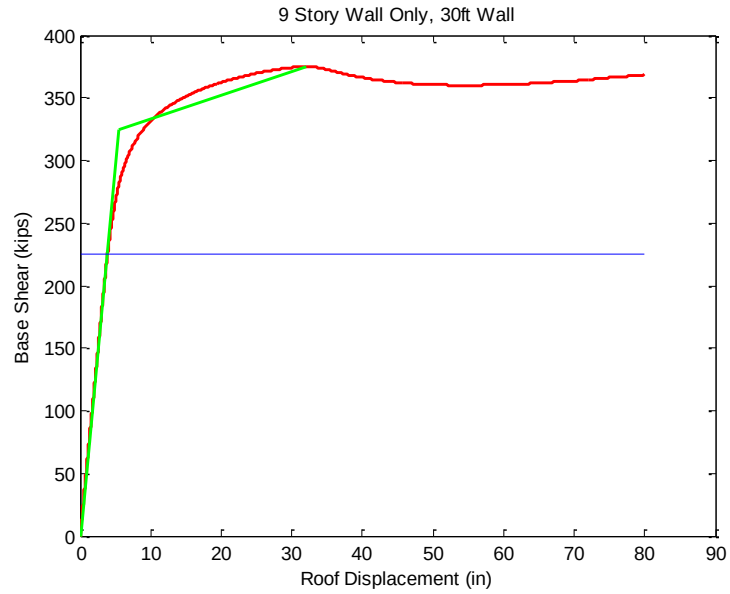
9 Story Wall Only, 30ft Wall
Base Shear (kips)
Roof Displacement (in)
0
50
100
150
200
250
300
350
400
0
10
20
30
40
50
60
70
80
90

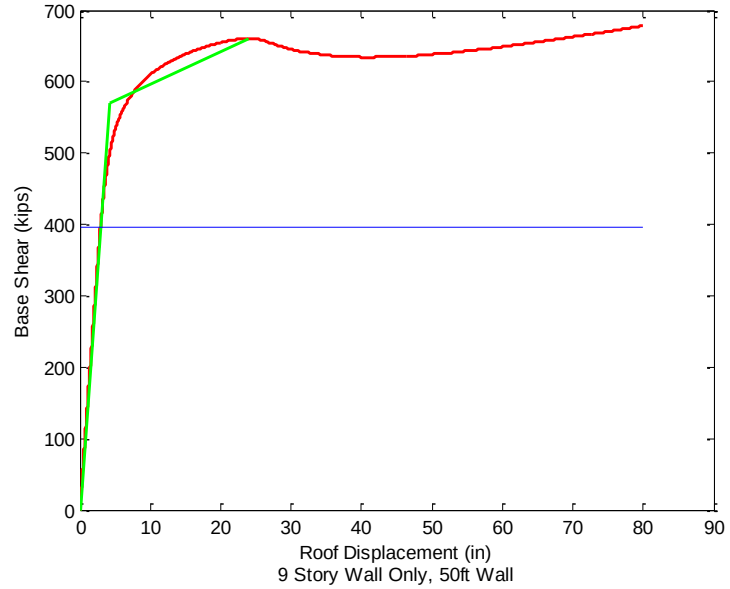
9 Story Wall Only, 40ft Wall
Base Shear (kips)
Roof Displacement (in)
0
100
200
300
400
500
600
700
0
10
20
30
40
50
60
70
80
90

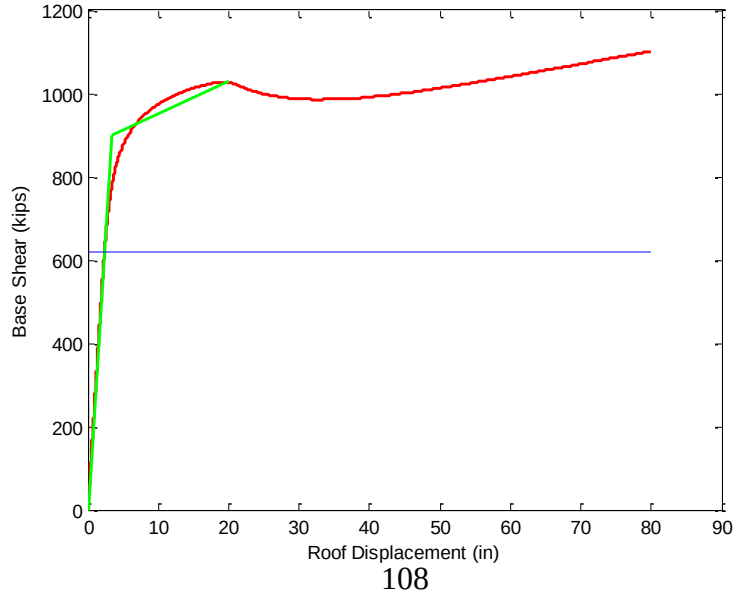
9 Story Wall Only, 50ft Wall
Base Shear (kips)
Roof Displacement (in)
0
200
400
600
800
1000
1200
0
10
20
30
40
50
60
70
80
90

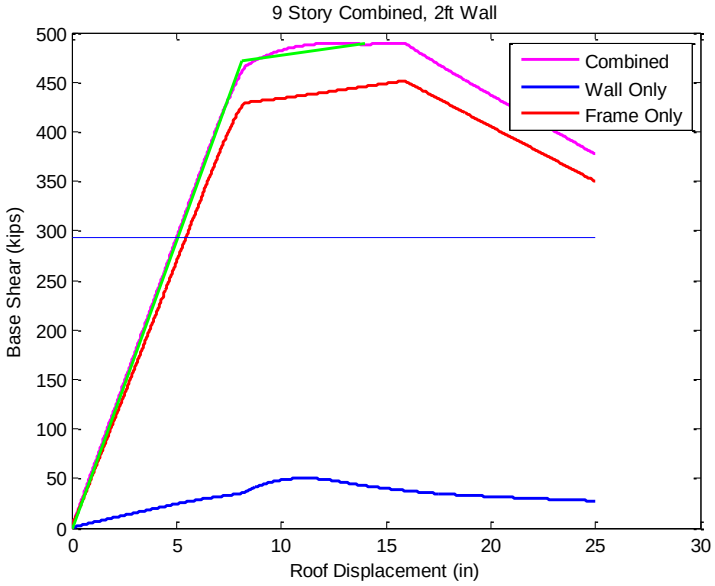
9 Story Combined, 2ft Wall
Combined
Wall Only
Frame Only
Base Shear (kips)
Roof Displacement (in)
0
50
100
150
200
250
300
350
400
450
500
0
5
10
15
20
25
30

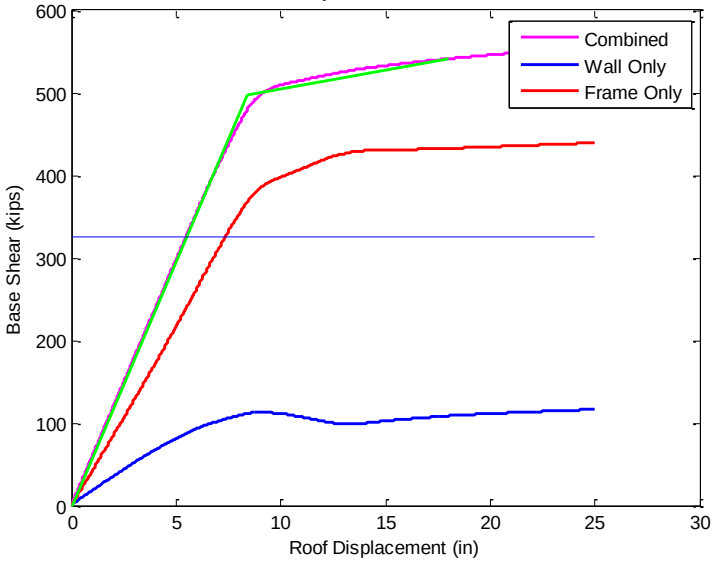
9 Story Combined, 4ft Wall
Combined
Wall Only
Frame Only
Base Shear (kips)
Roof Displacement (in)
0
100
200
300
400
500
600
0
5
10
15
20
25
30

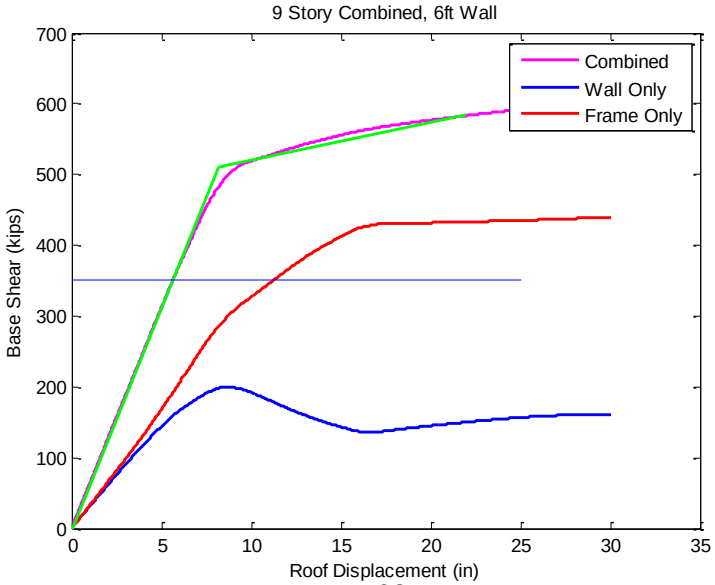
9 Story Combined, 6ft Wall
Combined
Wall Only
Frame Only
Base Shear (kips)
Roof Displacement (in)
0
100
200
300
400
500
600
700
0
5
10
15
20
25
30
35

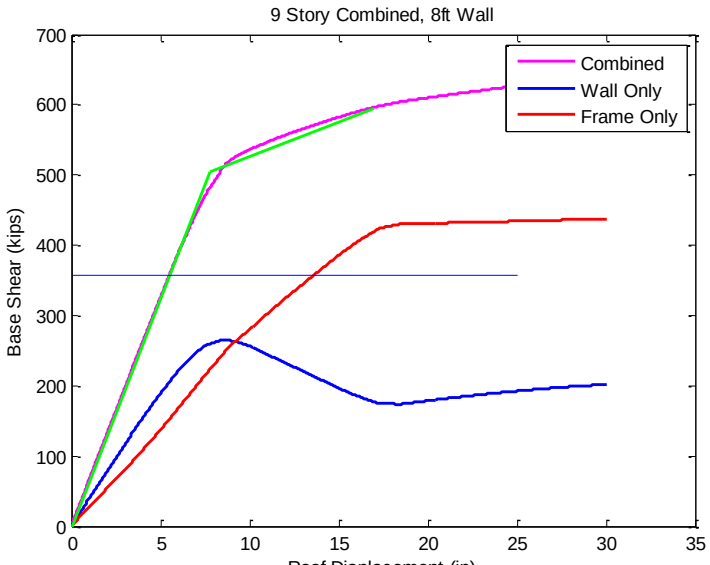
9 Story Combined, 8ft Wall
Combined
Wall Only
Frame Only
Base Shear (kips)
Roof Displacement (in)
0
100
200
300
400
500
600
700
0
5
10
15
20
25
30
35

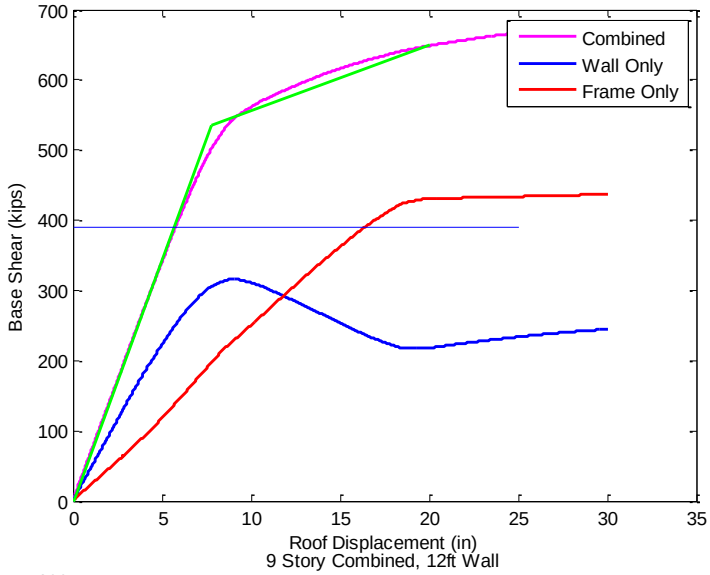
9 Story Combined, 10ft Wall
Combined
Wall Only
Frame Only
Base Shear (kips)
Roof Displacement (in)
0
100
200
300
400
500
600
700
0
5
10
15
20
25
30
35

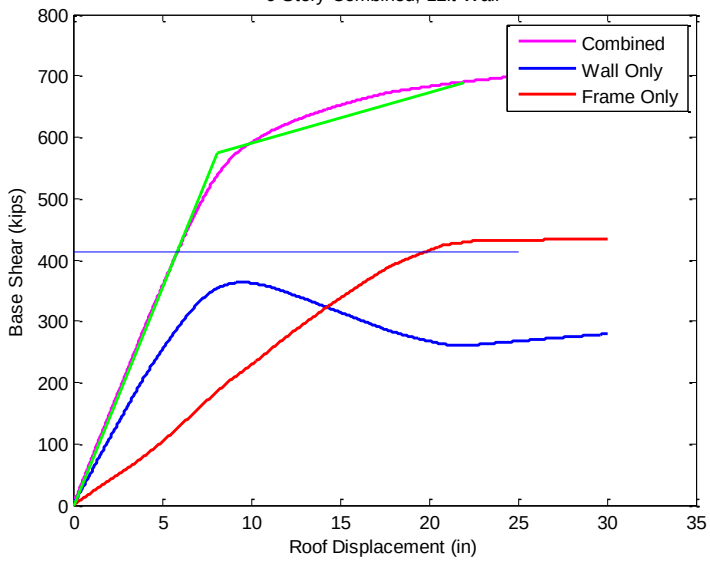
9 Story Combined, 12ft Wall
Combined
Wall Only
Frame Only
Base Shear (kips)
Roof Displacement (in)
0
100
200
300
400
500
600
700
800
0
5
10
15
20
25
30
35

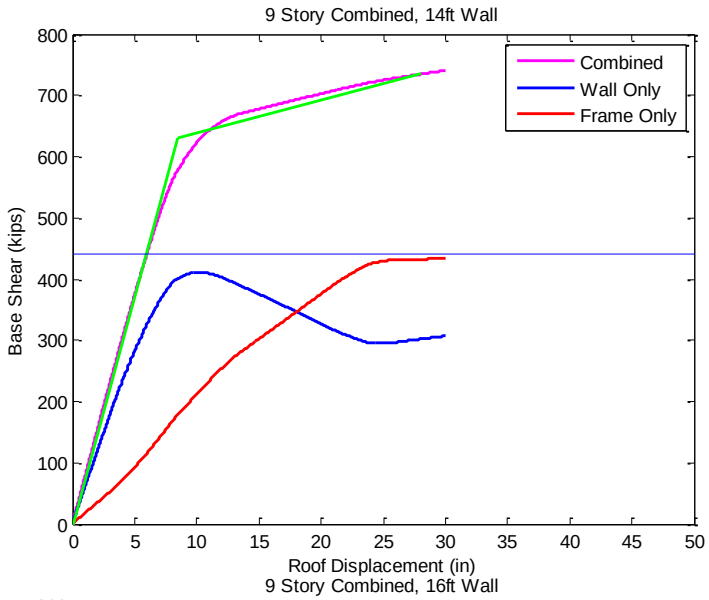
9 Story Combined, 14ft Wall
Combined
Wall Only
Frame Only
Base Shear (kips)
Roof Displacement (in)
0
100
200
300
400
500
600
700
800
0
5
10
15
20
25
30
35
40
45
50

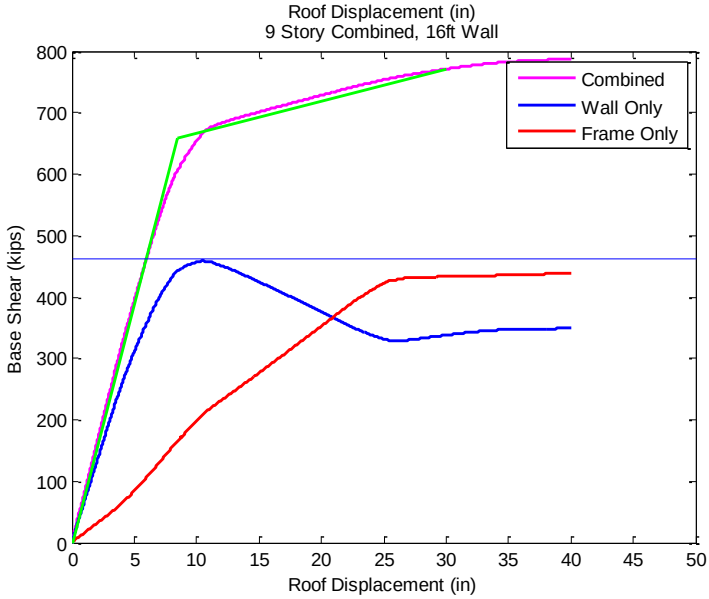
9 Story Combined, 16ft Wall
Combined
Wall Only
Frame Only
Base Shear (kips)
Roof Displacement (in)
0
100
200
300
400
500
600
700
800
0
5
10
15
20
25
30
35
40
45
50

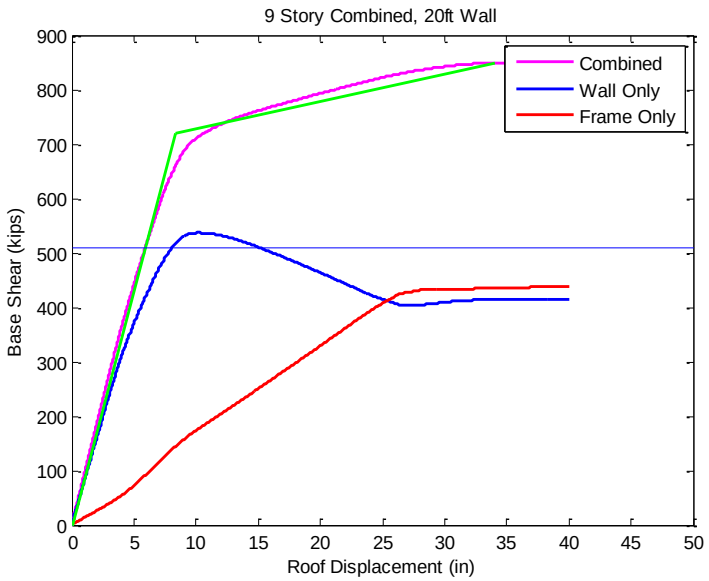
9 Story Combined, 20ft Wall
Combined
Wall Only
Frame Only
Base Shear (kips)
Roof Displacement (in)
0
100
200
300
400
500
600
700
800
900
0
5
10
15
20
25
30
35
40
45
50

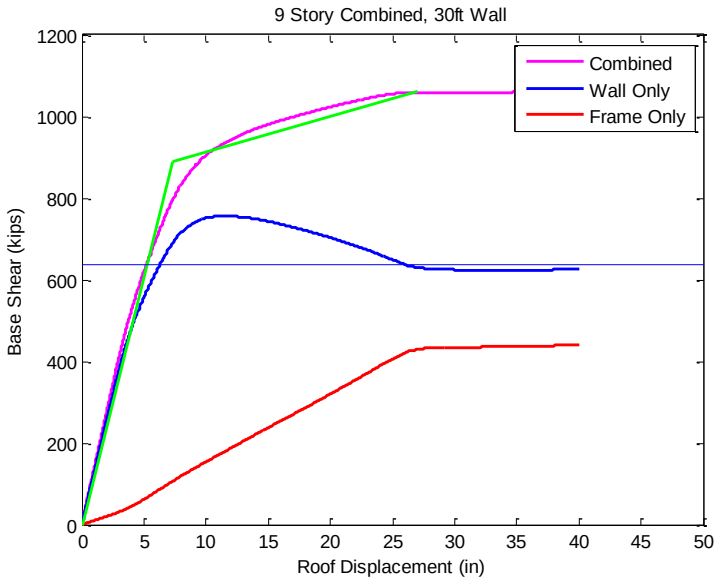
9 Story Combined, 30ft Wall
Combined
Wall Only
Frame Only
Base Shear (kips)
Roof Displacement (in)
0
200
400
600
800
1000
1200
0
5
10
15
20
25
30
35
40
45
50

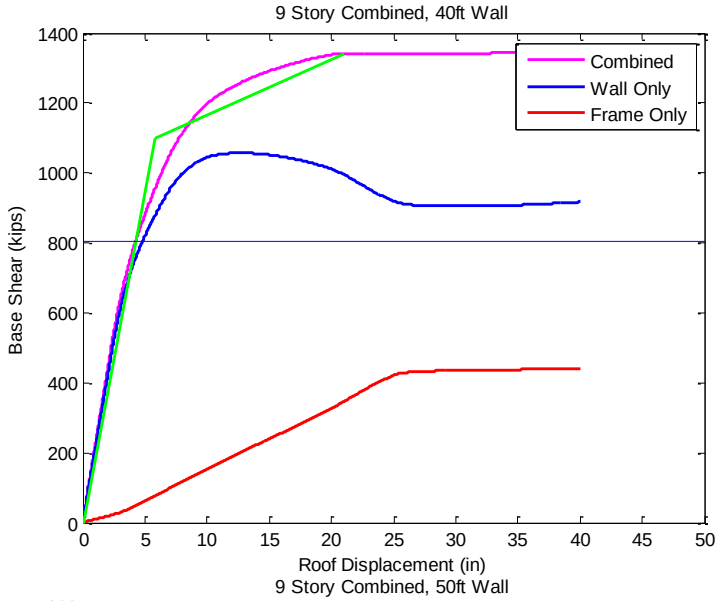
9 Story Combined, 40ft Wall
Combined
Wall Only
Frame Only
Base Shear (kips)
Roof Displacement (in)
0
200
400
600
800
1000
1200
1400
0
5
10
15
20
25
30
35
40
45
50

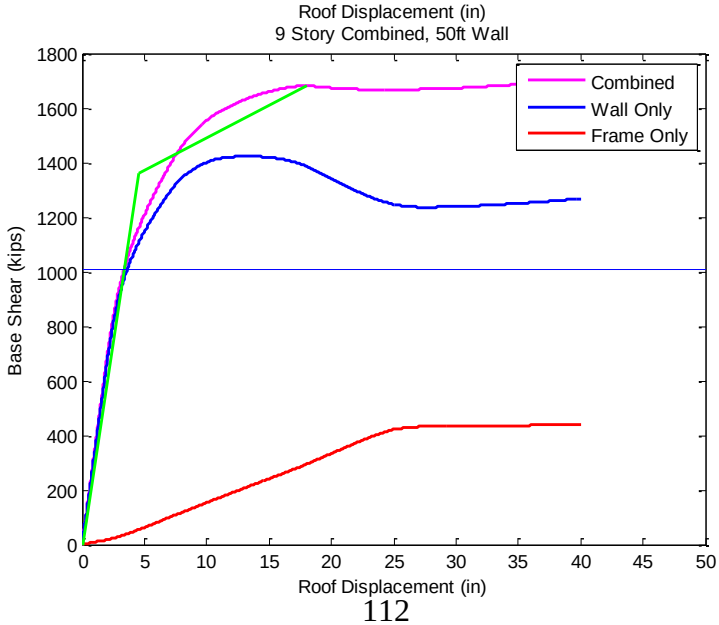
9 Story Combined, 50ft Wall
Combined
Wall Only
Frame Only
Base Shear (kips)
Roof Displacement (in)
0
200
400
600
800
1000
1200
1400
1600
1800
0
5
10
15
20
25
30
35
40
45
50